I&EC research
Industrial & Engineering Chemistry Research
pubs.acs.org/IECR
Review

Three-Dimensional MXene-Based Functional Materials for Water Treatment: Preparation, Functional Tailoring, and Applications

Yuekang Zhang, Guangfa Zhang,* Shuai Zhao, Ailin Gao, Jian Cui, and Yehai Yan*

Cite This: *Ind. Eng. Chem. Res.* 2023, 62, 7297−7335
Read Online

ABSTRACT: With the rapid development of economics and society, the water pollution and water shortage problem is becoming more and more severe. Excellent 3D separation functional materials for efficient water purification are highly required, but their design and fabrication still remain a big challenge at present. Benefiting from distinct advantages, such as 2D nanolamellar structure, high hydrophilicity, abundant functional groups, and desirable mechanical strength, 2D transition metal carbide/nitride materials, MXenes, have afforded a new platform for the creation of 3D water treatment functional materials. This review summarizes recent progress in 3D MXene-based functional materials toward wastewater treatment and water reclamation. In this review, common fabrication approaches for 3D MXene structures are emphatically summarized and recent developments of 3D MXene functional materials focused on the capacitive deionization (CDI), solar desalination, adsorption, and photocatalytic degradation of pollutants are critically reviewed. Besides, the impact of the structural design on their material performance is outlined. The critical challenges of 3D MXene materials in the aforementioned fields are also highlighted. Finally, we provide a brief perspective on the future development of 3D MXene materials toward practical effluent treatments.

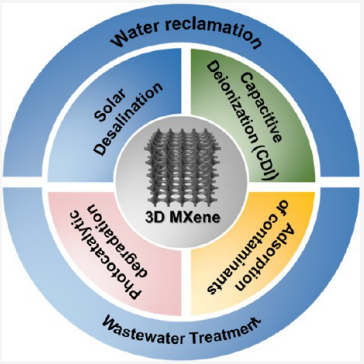

1. INTRODUCTION

Owing to the distinct advantages of 2D nanomaterials, including large specific surface areas, high surface free energies, and unique physical and chemical properties, 2D nanomaterials are regarded as the ideal material types for aqueous environmental remediation through adsorption, catalysis, and water environment monitoring.[1−3] MXenes are emerging two-dimensional nanomaterials whose excellent physicochemical properties have been gradually explored since they were first discovered in 2011.[4] The large specific surface areas,[5] excellent electrical properties,[6,7] hydrophilicities,[8] tunable surface groups, and environmental compatibility make MXenes promising for wastewater treatment applications such as adsorption of pollutants in water,[9] desalination, and photocatalytic degradation.[10,11]

In recent years, many efforts have been devoted to developing novel water treatment functional materials based on the MXene building unit. Despite these advances, there are still some obstacles to the construction and application of MXene-based functional materials. For example, (1) due to the presence of interlayer interactions, MXenes tend to easily form agglomerates in water, which severely damages the active surface of the materials, and (2) it is difficult to recycle the nanomaterials dispersed in the water body, which not only increases the cost but also may endanger human health. Therefore, by assembling 2D nanosheets into three-dimensional (3D) porous structures (such as aerogels, hydrogels, and foams), researchers can effectively avoid the restacking of 2D MXene nanosheets and thus achieve highly efficient surface utilization, obtaining MXene composites with excellent comprehensive properties.[12−14]

Three-dimensional MXene-based porous materials can not only retain the vital structural merits of nanosheets but also exhibit the following distinct advantages: First, a rational 3D assembled structure can avoid the restacking of nanosheets, providing a larger available surface area and more active sites, which greatly improves the adsorption efficiency and capacitance.[15,16] Second, the interconnected porous structure provides rich fast channels for water transportation.[8,17] Third, the highly interconnected conductive MXene network offers a variety of avenues for electron transfer, which greatly enhances the photocatalytic efficiency.[18,19] Consequently, the assembly of two-dimensional MXene nanosheets into three-dimensional porous structures is all-important to overcoming the drawbacks of the nanomaterials themselves and to expanding the applications of MXenes in wastewater treatment as well as water reclamation.

To date, numerous methods have been developed for constructing three-dimensional MXene-based functional materials toward water restoration and water resource regener-

Received: February 1, 2023
Revised: April 12, 2023
Accepted: April 13, 2023
Published: May 5, 2023

https://doi.org/10.1021/acs.iecr.3c00306
Ind. Eng. Chem. Res. 2023, 62, 7297−7335

ation.[13,14] However, to our knowledge, there is almost no comprehensive review that summarizes the fabrication strategy and application advantages of 3D MXene-derived structures for wastewater treatment as well as water reclamation. Based on this, a timely and comprehensive review is required to highlight the progress of 3D MXene-based structures in this field. This review outlines the current classical synthesis methods of MXenes; highlights the commonly used assembly strategies of 3D MXene materials; summarizes their current advanced research progress in wastewater treatment fields such as solar desalination, capacitive deionization (CDI), adsorption of pollutants, and photocatalytic degradation (Figure 1); and discusses the future prospects of 3D MXene materials for wastewater treatment and water resource regeneration.

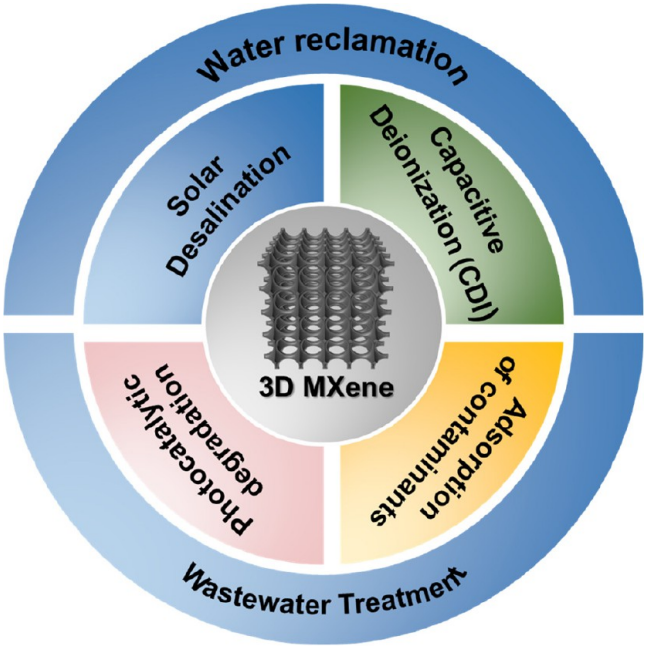

Figure 1. Schematic diagram of the application of 3D MXene assembly structures in wastewater treatment (adsorption and photocatalytic degradation of pollutants in water) and water reclamation (solar water desalination and CDI).

2. AN OVERVIEW OF MXenes

2.1. Structure of MXenes. MXenes are a class of transition metal carbides, nitrides, or carbon nitrides with two-dimensional layered structures. The microstructure is uniquely "accordion-like". It is generally synthesized through the selective etching of the A atomic layer from the corresponding precursor MAX phase. The general formula of the structure of this precursor MAX phase is $M_{n+1}AX_n$ (n = 1, 2, 3, 4), as shown in Figure 2a; "M" in the formula represents the transition metal part of the genus element, "A" represents an element of the third and fourth main groups, and "X" represents a carbon or nitrogen element.[20−22]

It has been demonstrated in numerous studies that M−A bonds are far more aggressive than M−X bonds in the MAX phase.[25] Therefore, it is likely to selectively break the M−A bond by setting suitable experimental conditions, thus removing the A atomic layer to obtain MXenes (Figure 2b).[26,27] As shown in Figure 2c, MXenes have the structural general formula $M_{n+1}X_nT_x$ (n = 1, 2, 3, 4) where M and X are inherited from the precursor MAX phase and T_x represents the functional groups (mainly −OH, −F, O, etc.) which are bound to the outermost M layer. Due to the diversity of MAX phases, MXenes exist in many configurations, including M_2XT_x, $M_3X_2T_x$, $M_4X_3T_x$, and $M_5X_4T_x$. Different configurations of MXenes can be composed of different elements, so MXenes are a large family of two-dimensional materials.[24]

To date, the most widely studied MXene remains $Ti_3C_2T_x$, which was first discovered in 2011 and has become a typical representative of MXene materials.[4] As mentioned earlier, $Ti_3C_2T_x$ is a nanomaterial with an accordion-like structure obtained by selective etching of the aluminum atomic layer in the three-dimensional precursor Ti_3AlC_2, which is later delaminated by exfoliation means such as ultrasound or ion stripping to obtain single-layer or layer-less two-dimensional nanosheets.

MXene nanosheets have a morphology similar to that of conventional (2D) nanomaterials, and the theoretical layer thicknesses of single-layer MXene nanosheets are all less than 1 nm, often with transverse dimensions of several tens of micrometers.[28]

2.2. Synthesis of MXenes. Various preparation strategies have been developed for the production of MXenes from the MAX phase, as shown in Figure 3.[11,29−35]

It is worth noting that the prepared MXenes often have different end-group functional groups due to different etchants and etching conditions.[36] Also, whether the corresponding MXenes can be obtained from the corresponding MAX phases depends on many factors, such as precursors, etchants, suitable etching conditions, and intercalation processes. So far, tremendous efforts have been made to find new ways to prepare MXenes, and various etchants have been developed, such as HCl−LiF,[37] NH_4HF_2,[38] and NH_4F.[39] Table S1 briefly summarizes the advantages and disadvantages of various MXene preparation methods. Several typical strategies for the preparation of MXenes are described in detail below.

2.2.1. Direct HF Etching Method. Hydrofluoric acid etching is a method that was used for the first time to prepare MXenes, and it is one of the more used etching methods at present. As shown in Figure 4a, this method uses a strong corrosive hydrofluoric acid solution to etch the aluminum atoms in Ti_3AlC_2 to obtain $Ti_3C_2T_x$.[4] The etching mechanism takes advantage of the fluorophilic nature of aluminum atoms, and after the etching reaction, the Al atoms are replaced by −OH, −F, −O, etc. groups. In recent years, the HF etching mechanism of Ti_3AlC_2 has been investigated using density functional theory (DFT), showing that the exfoliation of the Ti_3C_2-MXene is carried out by HF insertion into the edge of the Ti_3AlC_2-MAX phase.[40] First is the spontaneous dissociation of HF, which etches from the edges; then the H/F groups at the edges weaken the interlayer forces, leading to the opening of the interlayer interstices, allowing HF to enter the interlayer and further etch the Al atomic layer to form fluorinated MXenes. The material obtained here is not layered, but has an "accordion-like" multilayer structure. The absence of Al atoms greatly weakens the force between $M_{n+1}X_n$ layers, making them easier to separate, so they can be peeled into fewer layers using mechanical means such as conventional ultrasound, but with lower yields. In order to obtain more monolayer nanosheets, it is generally necessary to introduce an intercalator for intercalation in parallel with sonication.

This method is applicable to almost all Al-containing MAX phases used to prepare the corresponding MXenes, but it is

https://doi.org/10.1021/acs.iecr.3c00306
Ind. Eng. Chem. Res. 2023, 62, 7297−7335

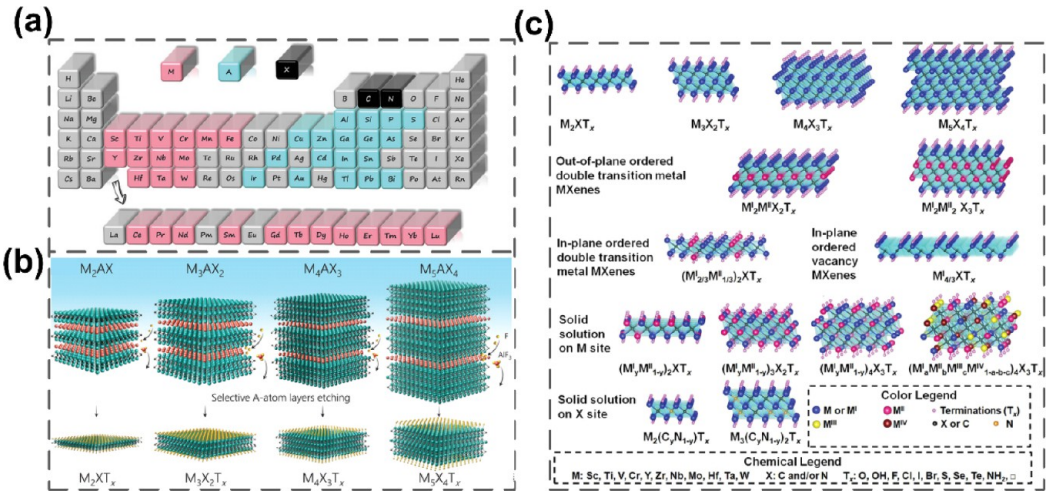

Figure 2. Structure and elemental composition of MXenes. (a) Elements represented by "M", "A", and "X" in the general formula of MAX phase structure. (Reproduced with permission from ref 22. Copyright 2021 Wiley-VCH GmbH & Co.) (b) Schematic diagram of a typical process for the preparation of MXenes from the counterpart MAX phase. (Reproduced with permission from ref 23. Copyright 2021 Wiley-VCH GmbH & Co.) (c) Typical MXene structures and compositions. (Reproduced with permission from ref 24. Copyright 2021 Wiley-VCH GmbH & Co.)

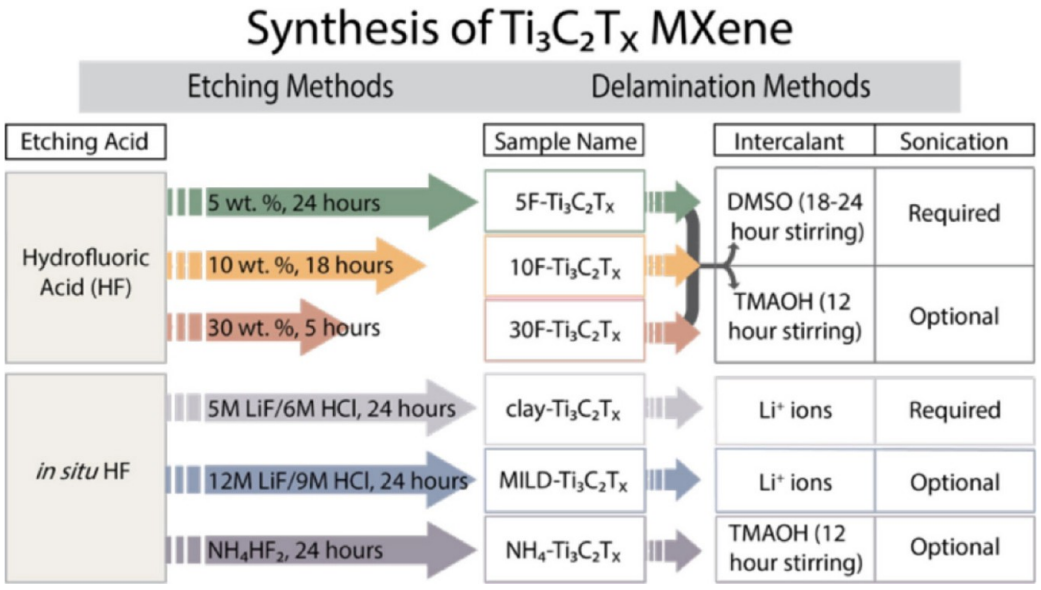

Figure 3. Etching process and interlayer stripping process conditions for the direct HF method as well as the in situ HF method. (Reproduced from ref 29. Copyright 2017 American Chemical Society.)

worth noting that the etching conditions required for different kinds of MAX phases often vary. In general, the larger the value of n and the atomic number of the M element in the $M_{n+1}AlX_n$ phase, the more drastic the etching conditions required.

2.2.2. In Situ HF Etching Method. At present, direct HF etching has been extensively used for the preparation of MXenes, but it still has many unavoidable drawbacks of its own: (i) the use of hydrofluoric acid in large quantities will lead to environmental pollution; (ii) hydrofluoric acid is highly corrosive, which is not conducive to maintaining the structural integrity of $M_{n+1}X_n$ and will seriously damage the excellent properties of the MXene itself;[38,41] (iii) the multilayer MXenes made by the direct hydrofluoric acid method are not easy to peel off, and it is difficult to obtain monolayer nanosheets, which requires subsequent steps such as intercalation and peeling, and the process is tedious.

In order to find a simpler and more effective etching method, a combination of LiF and HCl aqueous solution has been explored in recent years to etch the MAX phase instead of HF, and quite good results have been achieved.[37] In this method, a mixture of LiF and HCl is used to etch Ti_3AlC_2, and after several centrifugal washes, it is possible to obtain a swollen clay-like material as a result of the insertion of Li^+ into the layers of $Ti_3C_2T_x$ during the etching process and its stripping into a single layer or few layers.

This method actually uses relatively mild conditions to etch MXenes, and the HCl solution and the HF generated in situ from LiF remain in play during the etching process. The etching process is accompanied by the spontaneous intercalation of Li^+, thus avoiding the subsequent tedious intercalation step of the direct HF etching method, and can be directly used to produce 2D nanosheets. The minimum intensity layer delamination (MILD) method reported in one

https://doi.org/10.1021/acs.iecr.3c00306
Ind. Eng. Chem. Res. 2023, 62, 7297−7335

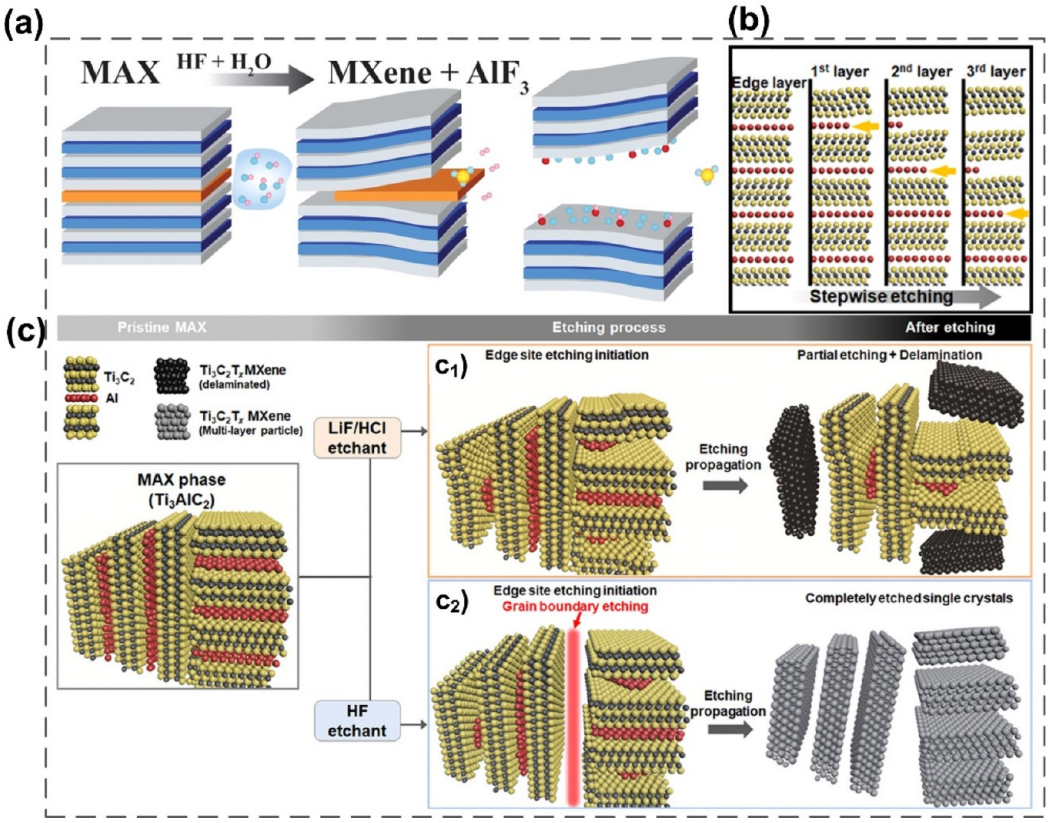

Figure 4. Direct HF method and in situ HF method. (a) Schematic diagram of the direct HF etching method. (Reproduced from ref 40. Copyright 2016 American Chemical Society.) (b) Schematic of the stepwise etching process. (c) Schematic diagram of etching mechanism of HF etchant and LiF/HCl etchant. (c_1) LiF/HCl and (c_2) HF solutions. (Reproduced from ref 42. Copyright 2021 American Chemical Society.)

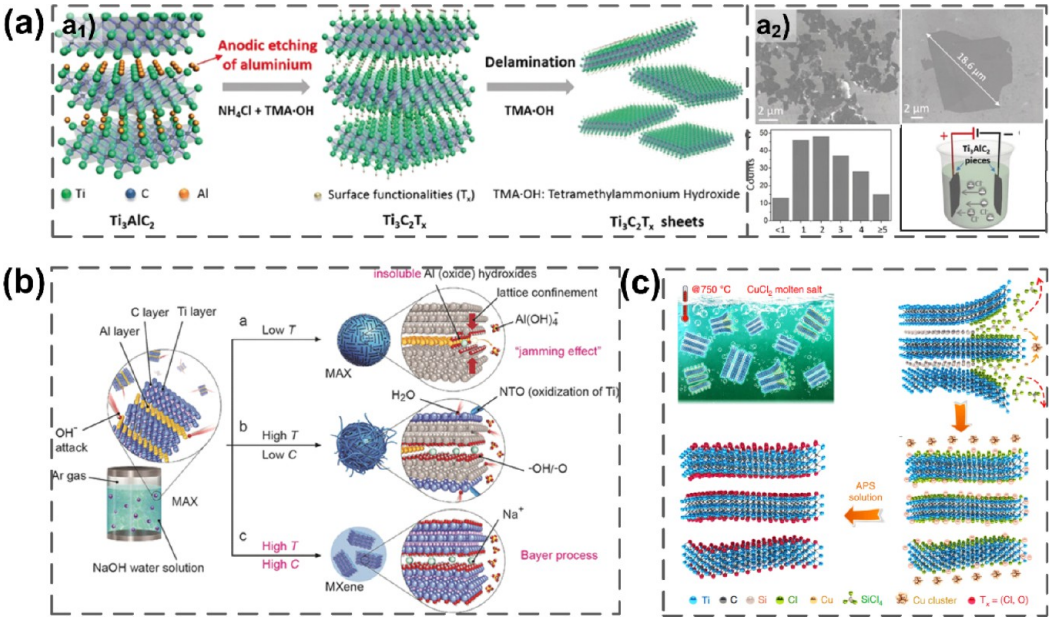

Figure 5. Fluorine-free etching process. (a) Electrochemical etching method. (a_1) Schematic diagram of the electrochemical etching and layering process. (a_2) SEM images of the electrochemical cell formulation as well as the prepared $Ti_3C_2T_x$ and the distribution of statistical values. (Reproduced with permission from ref 43. Copyright 2018 Wiley-VCH GmbH & Co.) (b) Effect of temperature and concentration of aqueous NaOH solution on etching reaction. (Reproduced with permission from ref 45. Copyright 2018 Wiley-VCH GmbH & Co.) (c) Schematic diagram of the process of $Ti_3C_2T_x$ preparation from Lewis molten salt. (Reproduced with permission from ref 47. Copyright 2020 Nature.)

study was able to achieve $Ti_3C_2T_x$-MXene delamination into monolayer 2D nanosheets by simple manual shaking using an optimal ratio of LiF to HCl.[39] Because strenuous exfoliation means such as ultrasound are avoided, MXene nanosheets can be prepared in as large a size as possible, which offers a foundation for studying the excellent properties of MXene

https://doi.org/10.1021/acs.iecr.3c00306
Ind. Eng. Chem. Res. 2023, 62, 7297−7335

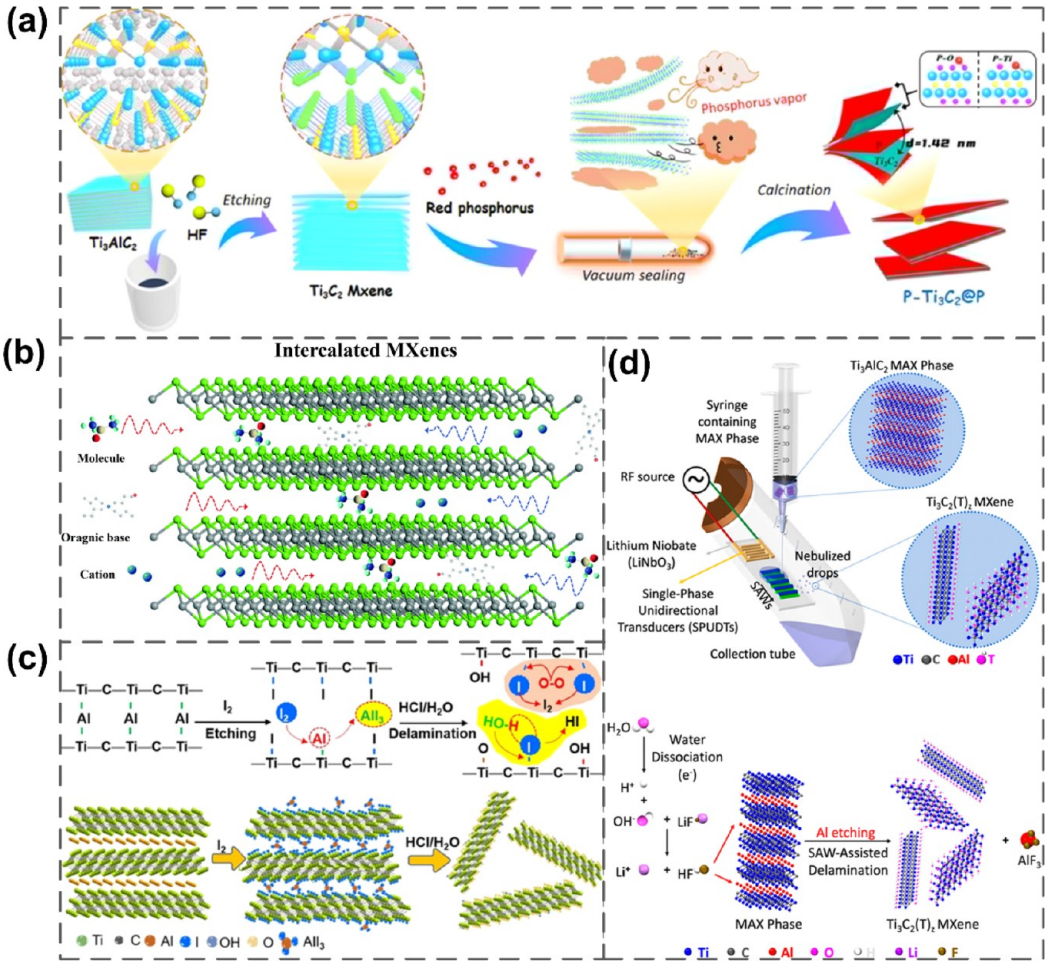

Figure 6. Exfoliation process as well as emerging preparation methods. (a) Schematic diagram of phosphorus vapor delamination and embedding of Ti_3C_2 MXene. (Reproduced from ref 60. Copyright 2021 American Chemical Society.) (b) Different kinds of intercalating agents for MXenes. These include molecular, cationic, and organic bases. (Reproduced with permission from ref 52. Copyright 2022 Royal Society of Chemistry.) (c) Schematic diagram of the process of preparing 2D-$Ti_3C_2T_x$ by etching and layering Ti_3AlC_2 using iodine under anhydrous conditions. (Reproduced with permission from ref 61. Copyright 2021 Wiley-VCH GmbH & Co.) (d) Schematic diagram of the experimental setup and potential physicochemical mechanisms for surface acoustic wave (SAW) promotion of $Ti_3C_2T_z$ MXene derivatization. Specifically, the rapid dissociation of water molecules under the action of SAW generates hydroxyl radicals and protonated material, which generates localized "in situ HF" in the presence of LiF. The Al in the Ti_3AlC_2-MAX phase is selectively etched away, and the MXene sheet is subsequently delaminated by the strong mechanical vibrations associated with SAW. (From ref 62. CC BY 4.0.)

nanosheets themselves. More importantly, because it avoids the use of strongly corrosive HF, the preparation process is safe, the operation steps are simple, and the exfoliation effect is good, which is one of the most commonly used synthetic routes at present.

A recent study has further elaborated the differences in etching mechanisms of different etchants.[42] The authors found that the etching of the MAX phase was performed in a stepwise etching manner for both HF etchant and HCl/LiF etchant (Figure 4b). Therefore, it can be expected that HF etchant can prepare an accordion-like multilayer MXene faster and more efficiently, while LiF/HCl etchant etches relatively gently and does not break polycrystalline MAX into single crystals, and is accompanied by Li^+ intercalation during etching, so that a portion of monolayer MXene nanosheets with relatively larger lateral dimensions can be obtained during washing (as shown in Figure 4c).

2.2.3. Fluorine-Free Preparation of MXenes. The strong corrosiveness of HF and its defect of easily causing damage to the environment and human body have been troubling, so the preparation of MXenes by fluorine-free etching is of important research value.

2.2.3.1. Electrochemical Etching. Electrochemical etching is a green etching method that does not require the use of HF or fluoride salts as the etchant. As shown in Figure 5a$_1$, in an alkaline solution consisting of tetramethylammonium hydroxide (TMA-OH) and NH_4Cl, with MAX-Ti_3AlC_2 as the anode, the Al in MAX is rapidly etched by the negative chloride ions in the electrolyte due to the stronger Al−Cl bond than the Al−Ti bond during the etching process, and at the same time, NH_4^+ is continuously inserted into the layer, which provides for the anodic edge etching and the inner layer of the material further etching of the interior of the material. Above 90% of the MXene prepared by this method is monolayer or bilayer nanosheets with an average lateral size larger than 2 μm (as indicated in Figure 5a$_2$), which is much better than the conventional HF method etching. In addition, the produced MXene nanosheets do not contain any fluorine groups, and it is also confirmed that the capacitors prepared by the MXene nanosheets prepared by this method have much better

https://doi.org/10.1021/acs.iecr.3c00306
Ind. Eng. Chem. Res. 2023, 62, 7297−7335

capacitive performances than the conventional fluorine-containing MXene.[43]

2.2.3.2. Alkali Etching. Due to the strong reactivity between alkaline substances and Al elements, the development of using alkaline substances as etchants to prepare MXenes has been a focus of research. Li et al.[44] used a high concentration of aqueous KOH solution to react with the Al layer. As Al was continuously etched, −OH performed chemisorption on the surface of the prepared nanosheet M layer, and the reaction equations are as follows:

$$Ti_3AlC_2 + KOH + H_2O = Ti_3C_2 + KAlO_2 + 3/2H_2 \quad (1)$$

$$Ti_3C_2 + 2H_2O = Ti_3C_2(OH)_2 + H_2 \quad (2)$$

However, the reaction conditions of alkali treatment are crucial for the preparation of MXenes. Li et al.[45] reported the hydrothermal etching of Al in Ti_3AlC_2 with 27.5 M NaOH at 270 °C under an argon atmosphere to obtain high purity (∼92 wt %) multilayer $Ti_3C_2T_x$. More importantly, they systematically investigated the effects of different reaction conditions on MXene formation, as shown in Figure 5b. It is pointed out that the reaction temperature is the key to inducing the formation of MXenes rather than other metal oxides, while the concentration of NaOH solution is crucial to controlling the MXene product with high purity.

In summary, compared with the direct HF etching method, the preparation conditions of alkaline etchants are relatively safe and the prepared materials show superior performance in some fields. However, alkali etching often requires high-temperature and high-pressure preparation conditions, which are not conducive to large-scale production and are prone to oxidative degradation of the materials, and the quality of the prepared nanosheets needs to be further optimized.

2.2.3.3. Lewis Acid Molten Salt Etching Method. Li et al.[46] reported the successful preparation of $Ti_3C_2T_x$ by Lewis acid molten salt etching, but several etching methods including those mentioned above were limited to the Al-containing MAX phase.

In recent years, a study has further investigated and proposed a more general Lewis acid molten salt etching method that expands the selection of the MAX phase.[47] As shown in Figure 5c, MS-$Ti_3C_2T_x$-MXene can be successfully prepared using Ti_3SiC_2-MAX phase as the precursor. This breaks through the limitation that only an Al-containing MAX phase can be selected as the precursor, and it makes an important contribution to the expansion of the preparation methods of MXenes.

In addition to the aforementioned precursor MAX phase based etching methods, methods such as chemical vapor deposition (CVD)[48−50] are also options for the synthesis of MXenes. Compared with etching methods, CVD enables the preparation of larger size and higher quality 2D nanosheets, and the 2D morphology of the crystals can be tuned by changing the synthesis reaction conditions. For example, it is possible to change the growth direction of the crystal (lateral or longitudinal) by controlling the temperature. However, at present, this method can only be used to produce a few specific MXenes, such as α-Mo_2C crystals,[50] and the production conditions are harsh and only suitable for laboratory production.

2.2.4. Interpolation and Layering. For better exploration of the properties of MXene nanosheets and to broaden their application directions, it is necessary to exfoliate the accordion-like multilayer MXenes obtained by etching into monolayer nanosheets, and many exfoliation methods have been developed.

First, it was found that mechanical means such as ultrasound can effectively suppress the formation of interlayer stabilization forces and produce single-layer or few-layer nanosheets.[51] However, the efficiency is often low and causes structural defects in the material. In multilayer MXenes, adjacent nanosheets are kept together by various interactions, but such interactions do not prevent the intercalation of organic molecules caused by the negative charge on the MXene surface as well as other cations. Therefore, intercalation agents can be used to widen the layer spacing of multilayer MXene nanosheets and weaken the interlayer forces to induce their separation into single-layer nanosheets with much higher peeling efficiency than direct mechanical methods.[52] As shown in Figure 6b, a variety of intercalating agents, including polar organic molecules (DMSO, hydrazine, urea, etc.),[53,54] organic base molecules,[35,55] and metal ions,[56−59] have been reported for more efficient exfoliation of MXene nanosheets.

It is worth noting that not many metal ions were allowed to enter the interlayer after the Al was removed by HF etching of the MAX phase.[58] Thus, spontaneous intercalation of metal ions is significantly more efficient than subsequent intercalation of additional metal ions when etching with a combination of fluoride and hydrochloric acid solutions, and the relatively larger hydration diameter of lithium ions makes their delamination much more efficient than that of other metal ions.[59] Of course, people have not stopped exploring easier ways to strip. Recently, Yuan et al.[60] reported a facile method to prepare layered MXenes using phosphorus vapor precipitated from commercial red phosphorus. As shown in Figure 6a, in this method, the stacked Ti_3C_2-MXene is blown away by phosphorus vapor, which is eventually deposited on the surface and partially embedded in the sandwich of a small number of exfoliated layered Ti_3C_2 nanosheets, thus directly obtaining novel two-dimensional RP/Ti_3C_2 nanocomposites. This simple direct gas-phase-assisted stripping is certainly a more attractive approach.

2.2.5. Emerging Synthetic Methods. In addition to the classical MXene synthetic pathways described above, various emerging pathways have been also proposed in recent years. First, Xue et al.[63] prepared Ti_3C_2 with a unique structure by a fluorine-free chemical combination ball-milling method. This ball-milling method is simpler and more environmentally friendly than other etching methods. Moreover, the prepared Ti_3C_2 has a larger specific surface area due to its unique layered porous structure. This contributes to increased ion storage and accelerated ion spreading and fast electron transport, which yields excellent electrochemical properties and extraordinary potential for other applications.

In 2014, Halim et al.[38,64] proposed the use of ammonium bis(fluoride) (NH_4HF_2) to prepare MXene instead of the hazardous HF. Recently, Natu et al.[65,66] found that MXene could also be prepared by etching MAX using NH_4HF_2 in an anhydrous organic polar solvent environment. Specifically, the etching is accomplished by the decomposition of NH_4HF_2 into NH_4F and HF in a polar solvent. Although this method leads to residues during etching, it also broadens the application of MXenes in anhydrous systems. This has also stimulated the development of various methods for the preparation of MXenes in anhydrous systems. Recently, Shi et al.[61]

https://doi.org/10.1021/acs.iecr.3c00306
Ind. Eng. Chem. Res. 2023, 62, 7297−7335

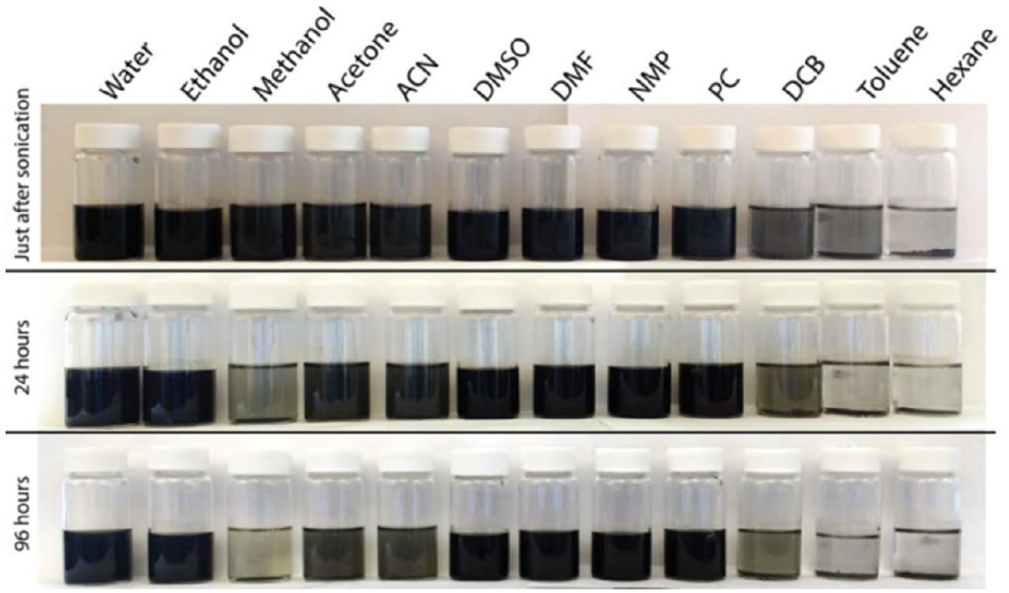

Figure 7. Dispersion and stability of $Ti_3C_2T_x$ in typical solvents. (Reproduced from ref 71. Copyright 2017 American Chemical Society.)

successfully etched the Al layer in Ti_3AlC_2 using I_2 in anhydrous ACN as the solvent environment. However, since the etching byproduct AlI_3 particles would adhere to the layers of the etched product, a low concentration of HCl solution was required to remove the impurities. In this process, the weaker Ti−I is replaced by Ti−OH, Ti−O, etc. during the washing process. The specific etching as well as washing and layering processes are shown in Figure 6c.

The long time and low yield of traditional etching methods have also been a major concern. An ultrafast acoustic synthesis method based on salt solutions has been recently reported.[62] As shown in Figure 6d, this method is performed by exposing a water mixture of LiF and MAX phases to surface acoustic waves (SAW), and under megahertz frequency acoustic excitation, the water molecules dissociate to generate protons and combine with the ions generated by LiF to selectively etch the MAX phase. The vibration of the acoustic wave is more helpful for the delamination of MXene. In conclusion, this method transforms the synthesis of MXene from the conventional minimum of 24 h to an ultrafast synthesis in milliseconds with objective yields.

The emergence of these emerging methods avoids the use of environmentally harmful fluorides, and these methods are greener and more efficient than the conventional HF-based etching methods. More importantly, these methods often offer unique advantages while simplifying the preparation process based on traditional etching methods, for example, the preparation of MXenes with larger specific surface areas or excellent water resistance. This makes it possible to tailor the physical and chemical properties of the material by modulating the MXene surface groups. Moreover, with the continuous efforts of researchers, the green and efficient preparation of MXenes with different structural properties has become a reality, and such tunable properties make them promising for applications and promote their industrialization.

2.2.6. Large-Scale Preparation of MXenes. At present, MXenes have been used in various fields of research work due to their excellent physical and chemical properties, and how to realize the large-scale industrial production of MXene materials has been the focus of research. Among the main reasons limiting batch production are the following: first, the fabrication of the precursor MAX phase is generally sintering expensive high-purity elemental powders with low yields. This is also the main factor contributing to the high price of MXenes. Recently, a preparation method with the use of molten salt shielding synthesis/sintering has been reported, which has more achievable reaction conditions and simpler process steps, and batch (>1 kg) manufacturing is possible. This offers the possibility of industrial production of MXenes.[67]

Second, the tedious and complicated preparation process is difficult to transfer from the laboratory to the factory. Although there have been studies reporting the synthesis of $Ti_3C_2T_x$ scaled up to 50 g without any quality degradation, the classical etching method has not only safety hazards but also very serious environmental pollution, which is not in line with the current concept of green development. Emerging preparation processes such as electrochemical etching require complex and expensive equipment.[68]

Third, the easy oxidation of MXene material causes great trouble for manufacturing and storage. The most researched and widely used MXene material is mainly $Ti_3C_2T_x$, whose environmental instability has been a painful point that is difficult to solve. Although there are a few studies that can improve the oxidation resistance by preparing MXene materials with specific functional groups, it they are difficult to replicate with industrial production.

2.3. Physicochemical Properties of MXenes. MXenes exhibit high specific surface areas, good electrical and thermal conductivities, controlled hydrophilicities, surface active functional groups for graft modification, and adjustable structures, which give them a series of unique physicochemical properties. In recent years, MXenes and their derivatives have also shown excellent potential in the fields of wastewater treatment and water reclamation. The following will discuss the excellent properties of MXenes used for wastewater treatment.

2.3.1. Surface Wettability and Solution Processability. MXene nanosheets exhibit good hydrophilicity and can form stable aqueous dispersions, which is the basis for the good aqueous processability of MXene materials. Based on this,

https://doi.org/10.1021/acs.iecr.3c00306
Ind. Eng. Chem. Res. 2023, 62, 7297−7335

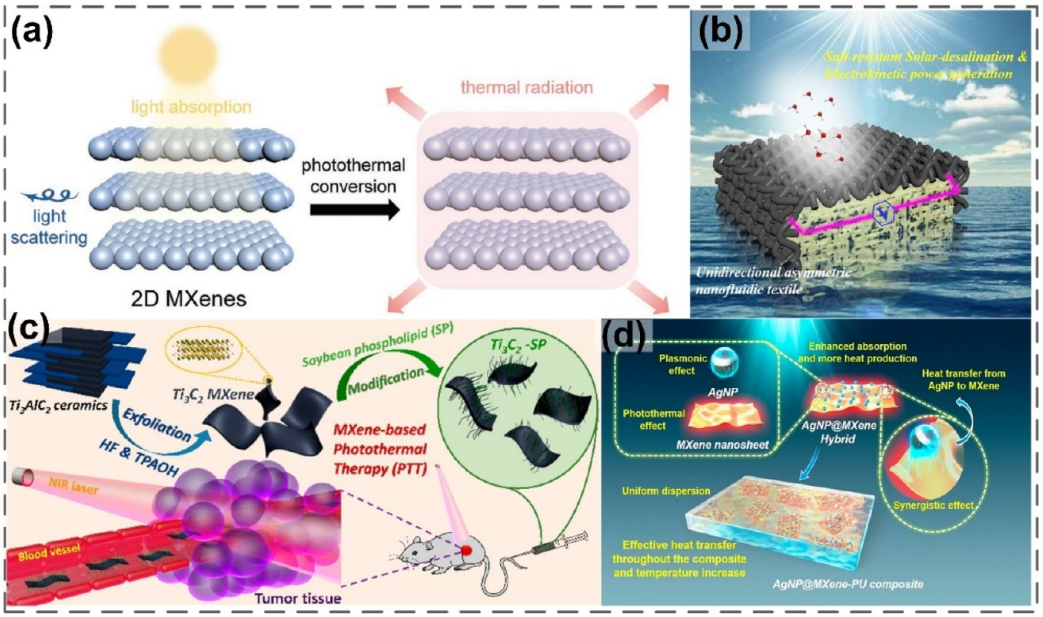

Figure 8. (a) Schematic diagram of the photothermal conversion of MXene materials. (Reproduced with permission from ref 83. Copyright 2020 Wiley-VCH GmbH & Co.) (b) Schematic diagram of an asymmetrically deposited MXene fabric. Also applied to solar-powered desalination and electrokinetic power generation. (Reproduced from ref 84. Copyright 2021 American Chemical Society.) (c) Schematic diagram of Ti_3C_2 nanosheets used as photothermal therapy (PTT) tumor reagent to induce tumor ablation under NIR irradiation. (Reproduced from ref 75. Copyright 2017 American Chemical Society.) (d) Transparent MXene hybrid coating with light-driven self-healing for smart wearable devices. (Reproduced from ref 76. Copyright 2019 American Chemical Society.)

some researchers have designed aqueous inks based on large-size MXene nanosheets that can be directly used for 3D printing.[69] The inherent hydrophilicities of MXene-based materials stem from a variety of negatively charged groups introduced to their surfaces during the preparation process. Notably, the $Ti_3C_2T_x$ nanosheets exhibit higher O/F ratios when synthesized using the method of mixed HCl and LiF solutions.[70] This results in better hydrophilicity of the macroscopic components constructed.[8] The surface functional groups on MXene and the negative charge they provide not only enable its application for the attachment of contaminants in water but also provide the possibility of surface modification of MXenes by electrostatic interactions or chemical modification.

In addition, a study reported the dispersibility of MXenes in different organic solvents. Ti_3C_2 was dispersed in three different types of solutions under the same conditions, and the results showed that Ti_3C_2 could form stable suspensions in H_2O, PC, DMF, NMP, DMSO, and ethanol,[71] as shown in Figure 7. By analyzing the characteristics of each solvent and the experimental results, it was found that the dispersion of Ti_3C_2 in each solvent was mainly related to the surface tension of the solvent, and Ti_3C_2 was able to form a stable suspension in the solvent with a large surface tension.

In summary, MXene materials have good solution processing properties and are easily coblended with other materials, which lays the foundation for their subsequent assembly into 3D macrostructures.

2.3.2. Electrical Properties. The most attractive property of MXene materials is undoubtedly their superior electrical properties. The electrical conductivity of MXene films has been reported to be as high as 15 100 S cm^{-1} and can be tuned by adjusting the surface functional groups.[7] The inherent hydrophilicity of a MXene coupled with its ultrahigh electrical conductivity makes it promising for applications in wastewater treatment. For example, its two-dimensional structure and high electron transfer properties make it suitable for trapping photogenerated electrons, thus facilitating efficient separation of photogenerated carriers, making a MXene an ideal cocatalyst material for photocatalytic applications.[72]

In addition, MXene materials exhibit ultrahigh energy storage capacities. The rapid embedding of ions between the atomic layers of MXene materials results in high-capacity capacitance,[6] and notably, MXenes are capable of forming free-standing electrodes that exhibit high measurement capacitances (>300 F cm^{-3}) due to the avoidance of binders.[73] In recent years, it has been realized that MXene materials are well-suited for use as CDI electrodes, with high-capacity capacitance resulting in large salt storage capacity, rapid embedding of ions leading to outstanding salt electrosorption capacity, and effective avoidance of the disadvantages of conventional carbon material electrodes limited by available specific surface areas.

2.3.3. Photothermal Conversion Performance. The MXene $Ti_3C_2T_x$ intrinsically possesses great electromagnetic wave absorption properties, and some studies have reported that the final fate of electromagnetic waves absorbed by $Ti_3C_2T_x$ is reflected internally through the lattice structure of $Ti_3C_2T_x$ and eventually consumption in the form of heat. This inspired the study of the interactions between MXenes and the most common electromagnetic waves—sunlight.

MXenes have excellent photothermal conversion properties, but their specific mechanisms have not been fully revealed. However, a series of studies have been conducted to explore the specific mechanism. Wang et al.[74] designed a droplet laser heating system and determined that a MXene has an internal photothermal conversion efficiency close to 100%. It was reported that this excellent photothermal conversion efficiency may be related to the semimetallic-like energy band structure of the MXene, which gives it a localized plasmon resonance

https://doi.org/10.1021/acs.iecr.3c00306
Ind. Eng. Chem. Res. 2023, 62, 7297−7335

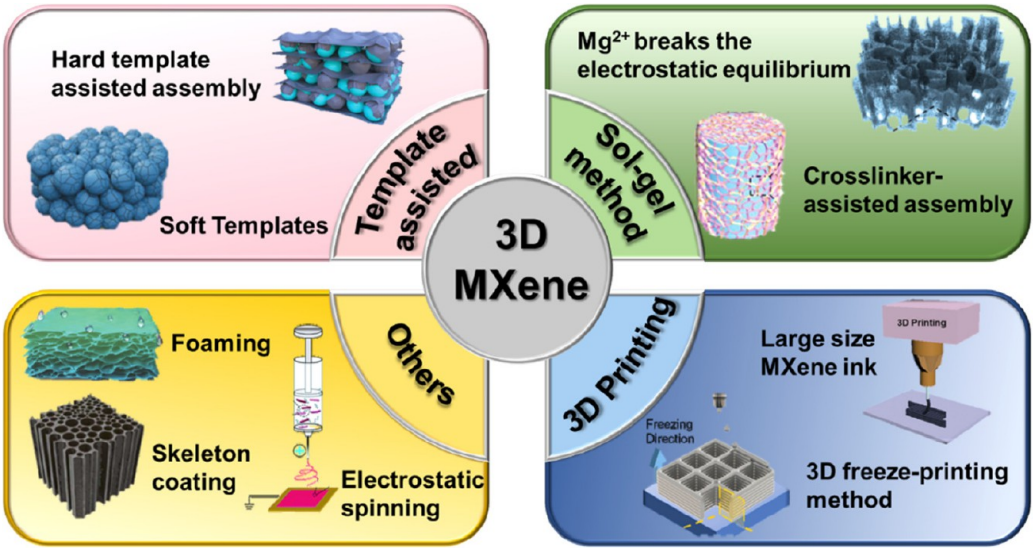

Figure 9. Schematic diagram of various preparation methods for 3D MXene structures. Image for "template assisted". (left) Reproduced with permission from ref 88. Copyright 2019 Wiley-VCH GmbH & Co. (right) Reproduced with permission from ref 89. Copyright 2021 Wiley-VCH GmbH & Co. Image for "sol−gel method". (left) Reproduced with permission from ref 90. Copyright 2019 Wiley-VCH GmbH & Co. (right) Reproduced with permission from ref 91. Copyright 2021 Wiley-VCH GmbH & Co. Image for "3D printing". (left) Reproduced with permission from ref 92. Copyright 2022 Wiley-VCH GmbH & Co. (right) Reproduced with permission from ref 69. Copyright 2019 Wiley-VCH GmbH & Co. Image for "others". Foaming: Reproduced with permission from ref 93. Copyright 2017 Wiley-VCH GmbH & Co. Skeleton coating method: Reproduced with permission from ref 94. Copyright 2022 Elsevier. Electrostatic spinning: Reproduced with permission from ref 95. Copyright 2019 Royal Society of Chemistry.

effect (LSPR). Lin et al.[75] measured the UV−vis−NIR absorption spectra of ultrathin $Ti_3C_2T_x$ nanosheets and found that they have a high absorption at 750−850 nm in the near-infrared region, which is similar to some expensive metal nanoparticles such as gold nanoparticles. This absorption property is not observed in other two-dimensional nanomaterials; thus MXenes have unparalleled advantages in the field of photothermal conversion.

Currently, MXene materials have been widely used in various fields due to their high photothermal conversion capabilities. For example, Ti_3C_2 nanosheets were used as an efficient photothermal therapy (PTT) tumor reagent, and outstanding NIR-light-induced tumor ablation without recurrence could be achieved by intravenous injection of Ti_3C_2, demonstrating the potential of MXenes in the biomedical field (Figure 8c).[76] In addition, as shown in Figure 8a,b,d, MXene materials are often seen in cutting-edge research in fields such as smart wear[76−79] and solar-powered desalination.[80−82]

Because of the above excellent physicochemical properties, MXenes have been widely used in the direction of wastewater treatment, such as solar water desalination and photocatalytic degradation of pollutants. In practical applications, by loading MXene nanosheets into 3D components with reasonable structures, they can not only retain their intrinsic excellent properties but also have many advantages, which are of great research value.

2.3.4. Functionalization or Post-treatment of MXenes. So far, MXenes have shown many fascinating properties and have been widely used in various fields. However, it is clear that researchers should not be satisfied with this, as the richness of the MXene surface and its unique structure open the door for research into its functional modification to impart new functionalities. On the one hand, the surface functional groups of MXenes can be used as the reaction platforms to chemically modify the MXene materials. For example, Chen et al. synthesized novel Janus MXene nanosheets through manipulation of the MXene surface chemistry by asymmetrically grafting polystyrene onto the MXene nanosheets.[85] The modified MXene nanosheets achieve hydrophilicity on one side and hydrophobicity on the other. Hence, this fascinating asymmetric wettability enables stable dispersion of the Janus MXene in various organic solvents ranging from polar to nonpolar, effectively expanding the application area of MXenes, especially in nonaqueous systems. On the other hand, structural changes in the material can be achieved by specific means to modulate its properties. One study used low-energy ion implantation to achieve functionalization of a 2D MXene.[86] The results show that the Mn doping distribution and a series of structural changes are introduced in the two-dimensional MXene by ion implantation, forming a large number of reactive defects and oxygen suspension bonds at the C and Ti sites and changing their electronic structures, which is beneficial to modulating the carrier types in the material as well as the optical response, promoting the application of MXenes in various fields such as photocatalysis and energy storage.[86]

More than that, simple post-treatment of a MXene is also effective enough to improve its properties. For instance, Zhang et al. employed a simple natural oxidation and calcination strategy to chemically modify MXene nanosheets and successfully introduced Ti^{3+}−TiO_2 nanoparticles and amorphous carbon on the surface, which led to a significant enhancement of the absorption of the modified nanosheets in the whole solar wavelength band.[87] All these examples show that the post-treatment of MXene can further expand the applications of MXene materials in various fields. The modification can be targeted to give MXene materials some specific functionalities to achieve material customization, which will also become one of the main directions of future research.

https://doi.org/10.1021/acs.iecr.3c00306
Ind. Eng. Chem. Res. 2023, 62, 7297−7335

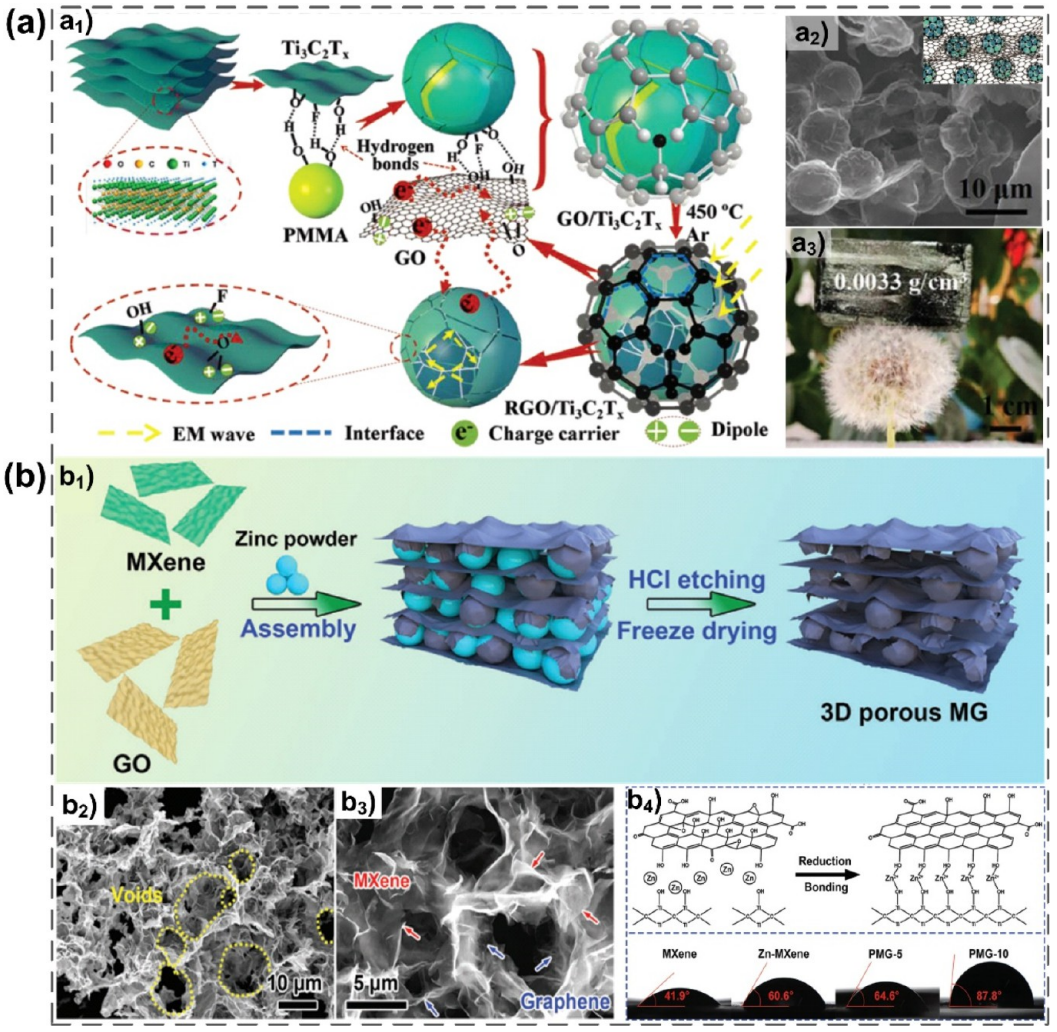

Figure 10. Hard template assisted assembly of MXene 3D structure. (a) PMMA microsphere template. (a_1) Schematic diagram of the preparation of $Ti_3C_2T_x$ spheres as well as $Ti_3C_2T_x$/rGO composite foam. (a_2) Microscopic morphology. (a_3) Macroscopic schematic diagram of the ultralight composite foam. (Reproduced with permission from ref 96. Copyright 2018 Wiley-VCH GmbH & Co.) (b) Zn particles used as template. (b_1) Schematic diagram of the preparation of $Ti_3C_2T_x$/rGO composite. (b_2, b_3) Microscopic morphology of the composite porous structure. (b_4) Proposed mechanism for inhibiting oxidation and variation of water contact angle with rGO content composites. (Reproduced with permission from ref 89. Copyright 2021 Wiley-VCH GmbH & Co.)

3. PREPARATION OF 3D MXene STRUCTURES

Similar to other low-dimensional nanomaterials, MXenes have a severe tendency to restack during application, which means they greatly lose their chemically active surfaces, leads to the loss of surface-active sites, and severely hinders electron conduction. In addition, it greatly limits the compounding of MXenes with other functional materials, which directly affects the application performance of MXene materials. Fortunately, the assembly of MXenes into three-dimensional porous structures, such as aerogels and foams, is an effective way to solve the above problems.

The weak gelation ability of MXenes themselves has been the main factor limiting the assembly of MXenes into macroscopic structures.[13] In recent years, various MXene-based 3D assembly methods have been developed, for example, the template method, frame assist method, sol−gel/self-assembly method, foaming method, and 3D printing. Through these methods, 2D MXene nanosheets can be effectively assembled into various three-dimensional structures, which greatly expands their application in the fields of wastewater treatment and water reclamation. In this section, we summarize in detail the current manufacturing methods and morphological structures of various 3D MXene assembly architectures (Figure 9).

3.1. Template Assisted Assembly. At present, the template method is the most direct and effective method to construct 3D nanocomposites, which can precisely regulate the pore structure of 3D materials by selecting template materials with different morphologies and sizes. Generally speaking, the template method is to deposit nanomaterials on the surface of the template through the interaction between nanomaterials and the template and then remove the template by various ways to obtain 3D porous structures based on nanomaterials. The presence of many functional groups on the surfaces of MXenes and the negative charges of these groups provide the basis for the interaction between MXenes and the template. The template method can be divided into the hard template method and the soft template method depending on the material being used as the template.

3.1.1. Hard Templates. A hard template is usually a solid material with good shape retention. Currently, various polymer

https://doi.org/10.1021/acs.iecr.3c00306
Ind. Eng. Chem. Res. 2023, 62, 7297−7335

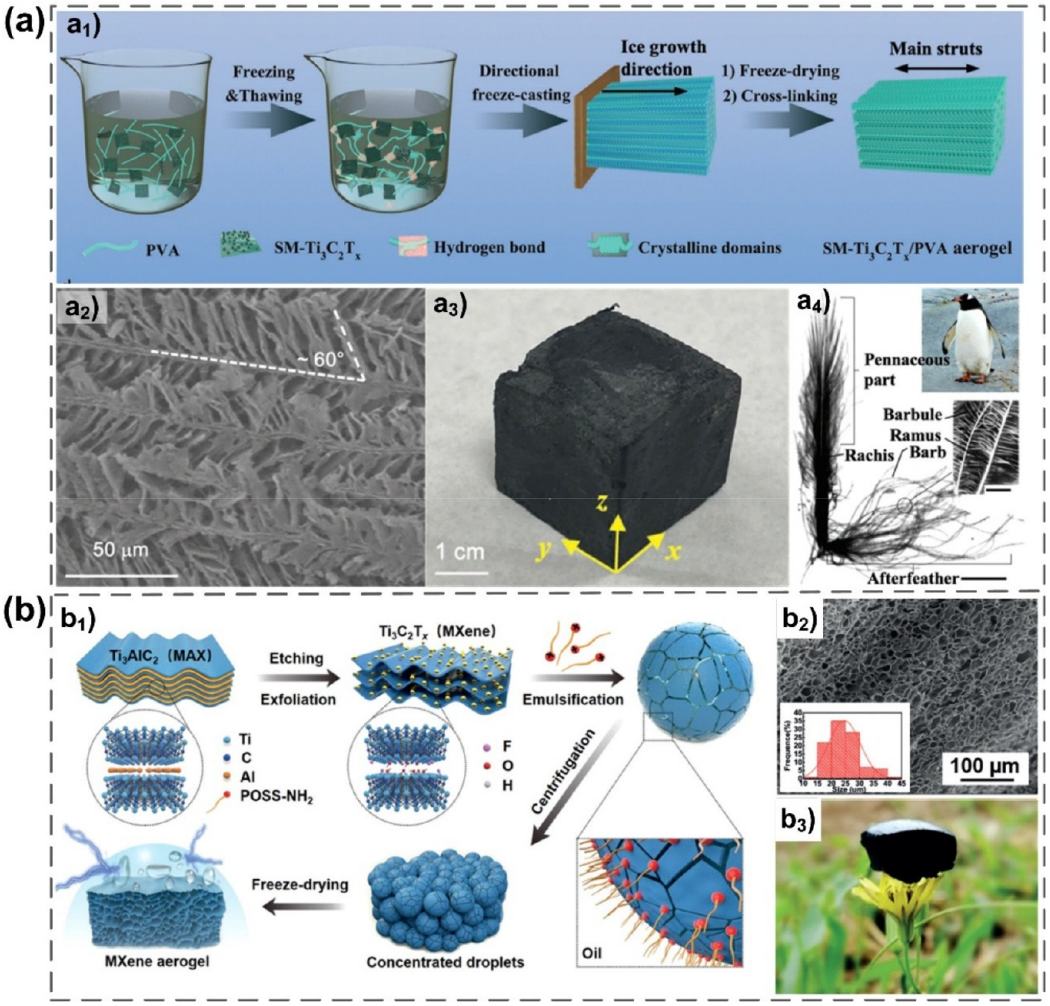

Figure 11. Ice template method as well as soft template method. (a) Preparation of PVA/MXene composite aerogel by ice template method. (a_1) Schematic diagram of the preparation process. (a_2, a_4) Aerogel with microstructure mimicking penguin down. (a_3) Macroscopic morphology of aerogel. (Reproduced with permission from ref 87. Copyright 2022 Wiley-VCH GmbH & Co.) (b) Soft template method using surfactants to induce assembly at interfaces. (b_1) Schematic diagram of the process of assembling MXene aerogel. (b_2, b_3) Microscopic as well as macroscopic morphology of the prepared aerogel. (Reproduced with permission from ref 88. Copyright 2019 Wiley-VCH GmbH & Co.)

microspheres and inorganic nanoparticles are commonly used templates for building 3D porous structures. For example, PMMA microspheres are a commonly used polymeric template,[96−99] and MXene nanosheets are continuously and uniformly coated on the surface of PMMA microspheres driven by strong interactions between surface hydroxyl groups. The composite microspheres are separated from the liquid phase by means of extraction and centrifugation and then heat treated under an argon atmosphere to remove the PMMA template to obtain self-supported $Ti_3C_2T_x$ microspheres or $Ti_3C_2T_x$ films with macroporous structures. In addition, such $Ti_3C_2T_x$ microspheres can be compounded with other nanomaterials, which have promising applications in electromagnetic wave absorption, energy storage, and biomedicine (Figure 10a).

Unlike PMMA microspheres, PS microsphere templates are due to electrostatic interactions between the positive surface charge and the negative charge carried by the MXene.[100−103] Similar polymeric templates are also available for melamine−formaldehyde (MF) microspheres, where nitrogen-containing functional groups (−NH_2, −NH−) trap protons from solution, giving them a positive charge and thus an electrostatic interaction with the MXene.[104−106] However, it is worth noting that $Ti_3C_2T_x$ is doped by in situ nitrogen in the presence of gaseous ammonia produced by thermal annealing MF decomposition. These nitrogen-containing transition metal carbides and nitrides have been shown to be more active, and therefore, this porous framework structure developed for N-$Ti_3C_2T_x$ can effectively improve the electrochemical properties and enhance its performance in the energy storage direction.[107−110]

In addition, some inorganic particles are often used as templates, which can be removed in a gentler and easier way than polymeric microspheres.[89,111−115] For example, in an aqueous solution system, Zn^{2+} is generated in situ on the surface of zinc powder. Therefore, $Ti_3C_2T_x$ and GO are able to self-assemble on the surface of zinc powder driven by electrostatic interactions (Figure 10b_1–b_3).[89] Importantly, the material effectively inhibits the oxidation of MXene because of the antioxidant effect of zinc powder and the rational structural design, as shown in Figure 10b_4.

In general, the hard template method uses the interaction between MXene nanosheets and other building blocks and the surface of the template particles to spontaneously assemble

https://doi.org/10.1021/acs.iecr.3c00306
Ind. Eng. Chem. Res. 2023, 62, 7297−7335

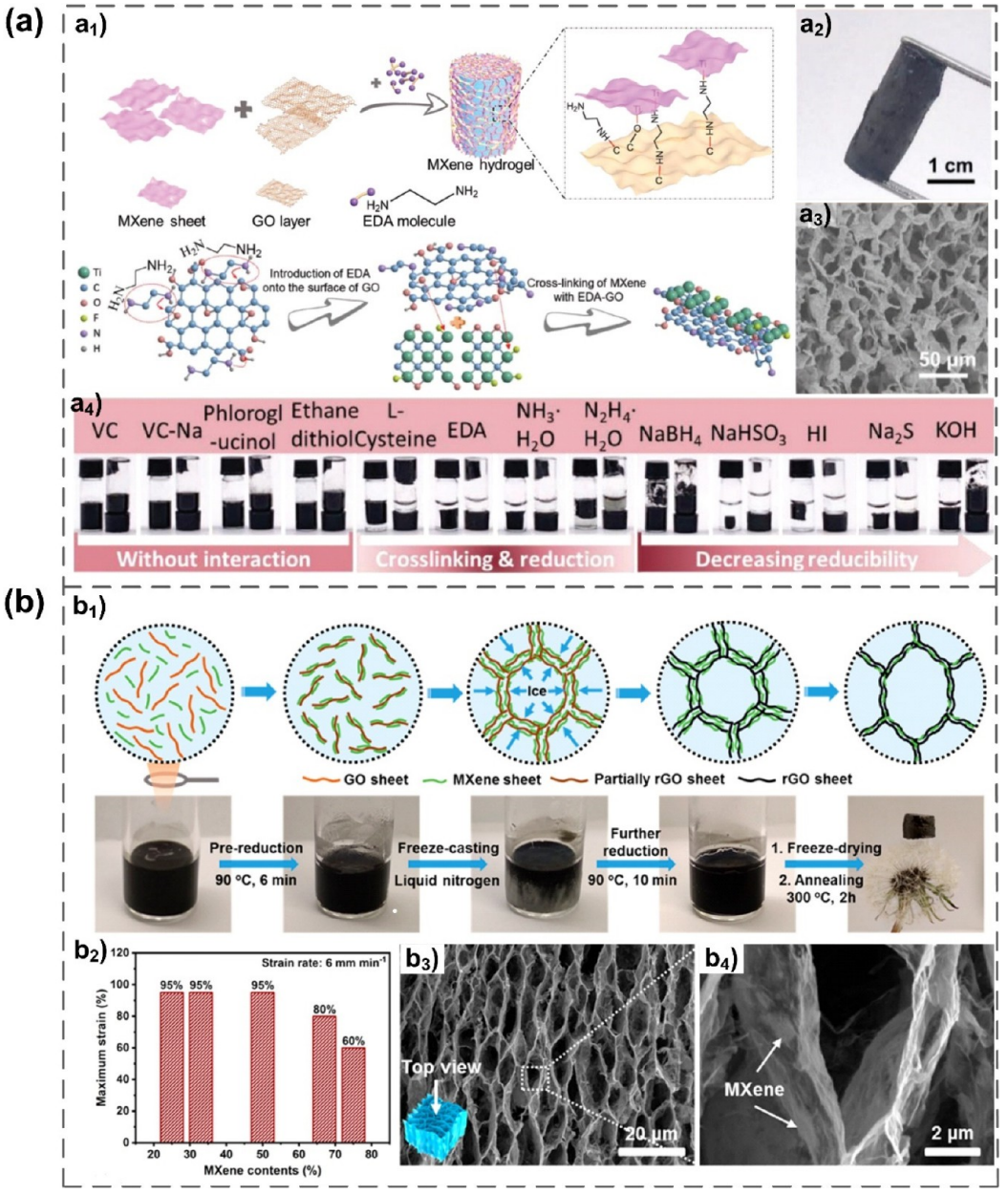

Figure 12. Addition of cross-linker induced MXene gelation. (a) Cross-linking MXene with rGO using EDA. (a_1) Schematic diagram of molding and possible mechanism. (a_2) Macroscopic morphology. (a_3) Microscopic morphology of porosity. (a_4) Photographs of whether different reducing agents can mold hydrogels. (Reproduced with permission from ref 90. Copyright 2019 Wiley-VCH GmbH & Co.) (b) Assisted assembly of MXene using GO. (b_1) Schematic diagram of molding. (b_2) Excellent mechanical properties of aerogel characterization. (b_3, b_4) Microstructure of aerogel. (Reproduced from ref 123. Copyright 2021 American Chemical Society.)

MXene nanosheets onto the template surface. After that, it is separated from the aqueous phase by means of centrifugation or extraction, and the template is removed by certain operations to obtain MXene-based 3D porous structures. Obviously, the shape and size of the template particles can be controlled to precisely regulate the pore structure of the three-dimensional material. Moreover, whether it is polymer microspheres or inorganic nanoparticles, the process is now more mature and particles of various sizes can be easily obtained for use as templates. However, it is worth noting that the removal of hard templates often requires tedious steps and relatively harsh conditions, which may not only leave impurities in the material but also easily cause oxidation of the MXene material, which is not conducive to the retention of the excellent properties of the material itself.

The ice template method is a frequently used method for building three-dimensional porous aerogels and is also known as the freeze casting technique.[87,116−119] Compared to the conventional templates mentioned above, ice templates are easy to construct and remove, and most importantly, the desired porous structure can be customized by simply changing the freezing conditions. For example, a temperature gradient can be constructed to control the ice crystal growth direction and thus modulate the pore structure. Han et al.[118] cleverly constructed bidirectional freezing by setting an inclination angle between the copper plate and the MXene dispersion, allowing the MXene nanosheets to be arranged into a laminar

https://doi.org/10.1021/acs.iecr.3c00306
Ind. Eng. Chem. Res. 2023, 62, 7297−7335

structure and assembled into a compressible anisotropic aerogel. The unique structural design results in a tunable electromagnetic shielding performance.

In addition to the above example of controlling the freezing direction, a study reported the ice structure freeze casting technique (ISFC) with the addition of poly(vinyl alcohol) (PVA) to the modified SM-$Ti_3C_2T_x$ precursor solution, where the presence of PVA alters the freezing rate of the precursor solution and thus modulates the pore structure of the final aerogel. Thus, the microscopic morphology of the aerogel is a unique graded porous structure with a morphology similar to that of a penguin feather (Figure 11a). This unique structure allows for good thermal management and is well-suited for solar desalination under low light conditions.[87] It is worth pointing out that the advantage of ice templates over the traditional hard template method is not only that the final pore structure can be easily regulated but also that no complex postprocessing is required to remove the template, which can retain the excellent properties of the MXene material to the greatest extent.

3.1.2. Soft Templates. Compared to hard templates, soft templates are usually liquid crystals, emulsions, micelles, etc. with low structural strength and stiffness and variable structure and shape.[88,120−122] More importantly, soft templates can often be removed by simple means, greatly simplifying the preparation steps, and are excellent template materials to help form MXene-based 3D structures with tunable pore sizes. Lu et al.[120] successfully reduced the hydrophilicity of $Ti_3C_2T_x$ by using electrostatic interactions between cetyltrimethylammonium bromide (CTAB) and MXene surface groups, so the modified $Ti_3C_2T_x$ could aggregate at the interface of oil and water phases. It is worth pointing out that, under alkaline and neutral conditions, high concentrations of Pickering emulsions and solid porous materials based on such emulsion templates can be prepared by this method, but stable emulsions cannot be formed if the hydrogen ion concentration in the aqueous phase is too high.

Analogously, Shi et al.[88] demonstrated that oil-soluble amine-functionalized polyhedral oligomeric sesquisiloxane (POSS-NH_2) can induce MXene assembly at the two-phase interface (Figure 11b). Specifically, when added to an oil−water mixture, it will cause the oil−water interface to exhibit a positive charge, thus causing the MXene to aggregate at the oil−water interface. Due to the electrostatic interaction, the MXene was rapidly adsorbed to the oil−water interface and assembled stably. When the $Ti_3C_2T_x$ dispersion was stirred vigorously with the oil dissolved with POSS-NH_2, it was able to form a homogeneous and stable Pickering emulsion. This oil-in-water Pickering emulsion was freeze-dried as a template to form a lightweight, hydrophobic, highly conductive, isotropic porous composite aerogel (Figure 11b_1) and applied to oil adsorption and electromagnetic interference shielding. Compared with the hard template method, soft templates such as emulsion droplets and micelles do not require complicated steps to remove the templates; the morphology of the porous structure can be tuned by adjusting the template concentration. However, it is difficult to precisely control the size and shape of the pores in porous materials, and the soft template method is less reproducible than the hard template method.

3.2. Sol−Gel Method. An MXene has an abundance of groups (−O, −OH, −F, etc.) on its surface and is therefore negatively charged overall,[123] and interlayer repulsion allows it to form stable dispersions in water. Based on this, the dispersion equilibrium between nanosheets can be broken by introducing a suitable driving force (cross-linker or weakening repulsion) to achieve phase separation, and a sol−gel transition can occur to build a three-dimensional structure.

First, the introduction of a cross-linking agent into the system is an effective strategy to induce the MXene to achieve the sol−gel transition. The cross-linker molecules can bind the adjacent MXene nanosheets, thus disrupting the electrostatic equilibrium between MXene nanosheets and inducing them to gel and eventually form a three-dimensional porous structure. For example, the addition of a suitable amount of ethylenediamine (EDA) molecules to the MXene colloidal solution can induce a sol−gel transition of the MXene to form three-dimensional MXene hydrogels.[17] The interconnected channels and pores can effectively inhibit the restacking of Ti_3C_2 flakes, and the prepared 3D gels are able to reach a specific surface area of 176.3 $m^2\ g^{-1}$.

Similarly, Jiang et al.[124] formed covalent bonds between MXene nanosheets and cellulose with a large number of hydroxyl groups via epichlorohydrin as a cross-linking agent, resulting in a sol−gel transition. Finally, a highly interconnected hierarchical network with excellent microwave absorption properties was obtained by freeze-drying.

GO is also a commonly used cross-linking agent because of its good gelation ability, and it is often used as a gelation agent to assist the 3D assembly of other low-dimensional nanomaterials.[19,123,125] It has been demonstrated that a MXene has a tight interfacial interaction with the rGO backbone, and driven by this interaction, the MXene can be incorporated into the formed rGO backbone, resulting in a 3D monolithic structure.[125] As shown in Figure 12b, Jiang et al.[123] used the joint action of rGO and ice template, MXene nanosheets were attracted and adhered to the rGO backbone to form a hybrid hydrogel of MXene and rGO, and the 3D MXene/rGO aerogel obtained after lyophilization had excellent mechanical properties. Further, Shang et al.[90] triggered the gelation of the MXene with GO by a relatively weak reducing agent, EDA (Figure 12a). The reaction mechanism is shown in Figure 12a_1. Through the reducing effect of EDA, it first reacts with the epoxy group on the surface of GO to open its ring and form an oxygen suspension bond and then replaces the −F group on the surface of the MXene so that MXene and GO are cross-linked together by chemical bonding, forming a 3D hydrogel with a good structure. The ability of different reducing agents to assist in the assembly of MXene/GO gels was also systematically investigated. It is difficult to form well-structured hydrogels if the reduction degree is too strong or too weak for reducing agents with similar reduction mechanisms.

Because of the ability to form covalent bonds between MXene nanosheets and other building blocks, 3D porous structures prepared by cross-linking agent induced sol−gel transition often have good structural strengths, especially when a suitable second building block (e.g., GO) is added, which enables the prepared 3D materials to have good mechanical stabilities, making them of great practical application.

Unlike the addition of cross-linking agents that react with MXene surface groups, another idea to induce MXene gelation is to break the electrostatic equilibrium between nanosheets. Therefore, some positively charged substances are often added to MXene dispersions to induce rapid gelation of the MXene.[91,126,127] Yang et al.[126] systematically investigated the effect of metal ions on MXene gelation. As shown in Figure 13a, Fe^{2+} in the system can rapidly disrupt the electrostatic

https://doi.org/10.1021/acs.iecr.3c00306
Ind. Eng. Chem. Res. 2023, 62, 7297−7335

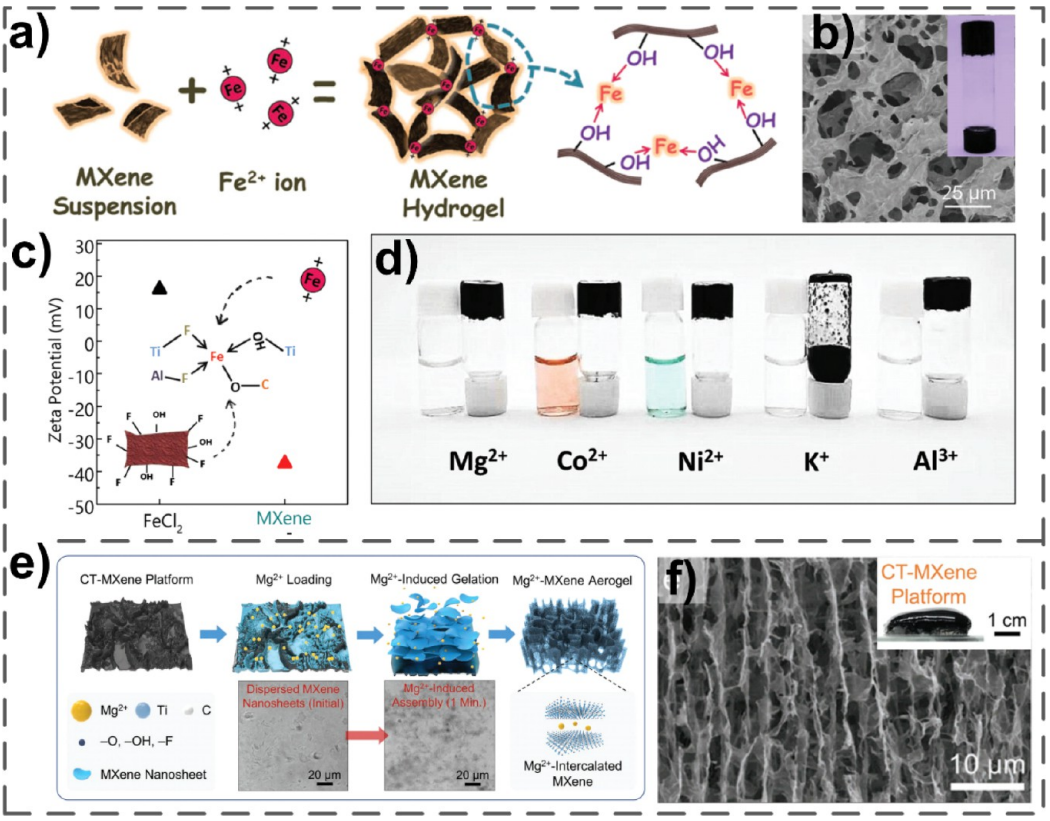

Figure 13. Induction of MXene gelation by breaking the electrostatic equilibrium. (a) Schematic diagram of Fe^{2+}-induced MXene gelation. (b) Morphology of the gel. (c) Zeta potential of MXene as well as Fe^{2+}. (d) Photographs of different metal ion induced gels. (Reproduced with permission from ref 126. Copyright 2019 Wiley-VCH GmbH & Co.) (e) Schematic diagram of Mg^{2+} loading by a bionic CT-MXene platform and scalable fabrication of Mg^{2+}-MXene aerogels. IRM images show the changes of dispersed MXene nanosheets before and after being loaded induced by Mg^{2+} into the films. (f) Structure of Mg^{2+}-induced gels. (Reproduced with permission from ref 91. Copyright 2021 Wiley-VCH GmbH & Co.)

exclusion between MXene nanosheets and act as cross-linking points to link MXene nanosheets together to form a 3D network (Figure 13b shows the structure of the hydrogel prepared by Fe^{2+} cross-linking). The formation of the three-dimensional network effectively reduces the restacking of nanosheets, thus greatly improving the surface utilization of the material.

In addition, it is reported that metal ions of different valences have different Gibbs free energies of hydration energy. In contrast, the 3-valent ions have higher hydration energy and can break the electrostatic equilibrium between MXene nanosheets faster and form gels with smaller pore size. In contrast, the hydration energy of 1-valent metal ions is much smaller than those of divalent and 3-valent ions and can lead to coagulation but not to the initiation of gel formation (Figure 13c,d).

On the basis of this principle, Ding et al.[91] innovatively designed a $Ti_3C_2T_x$-MXene platform with a pleated texture. This platform has a hierarchical structure similar to that of *Phrynosoma cornutum* and exhibits enhanced hydrophilicity and fast water transport rate, thus facilitating Mg^{2+}-induced assembly of the MXene (Figure 13e,f). Conformal formation of large-area Mg^{2+}-MXene aerogels in the absence of binder can be achieved by this technique. By avoiding the use of binders with poor electrical properties, the freestanding MXene electrodes prepared by this method have extraordinary potential for many applications in energy storage, CDI, and other fields.

The advantage of this method is that only a short interval is usually required for gelation, avoiding the MXene oxidation that may result from tedious and long processing times, thus maximizing the retention of the excellent properties of the material, but its structural strength is often inferior to that of 3D gels induced using cross-linking agents.

3.3. 3D Printing. Three-dimensional printing is an emerging strategy for the rapid production of 3D structures, allowing the use of suitable inks for the construction of a variety of complex structures, especially structures that are difficult to prepare with traditional construction techniques. In a typical 3D printing process, materials are first prepared as inks and then extruded through nozzles and deposited layer by layer on the substrate to form 3D structures. One study reported aqueous inks composed of 2D $Ti_3C_2T_x$ with atomic-level thickness (1−3 nm) as well as large lateral dimensions of 8 μm, with desirable viscoelastic properties without the addition of binders.[69] MXene aqueous inks with a concentration of more than 50 mg mL^{-1} pass through the narrow nozzle very smoothly and resume solid-like behavior immediately, making them very suitable for 3D printing. The printed 3D wet structures were freeze-dried, and individual printed filaments (326 μm in diameter) were seen to form interlaced structures without bending, indicating the formation of stable 3D structures. The internal MXene of the structure is assembled into a 3D porous network in which the interconnected mesh pore size is about 3−35 μm (as shown in Figure 14a). Crossed finger electrodes prepared by 3D printing and freeze-drying have excellent electrical properties.

https://doi.org/10.1021/acs.iecr.3c00306
Ind. Eng. Chem. Res. 2023, 62, 7297−7335

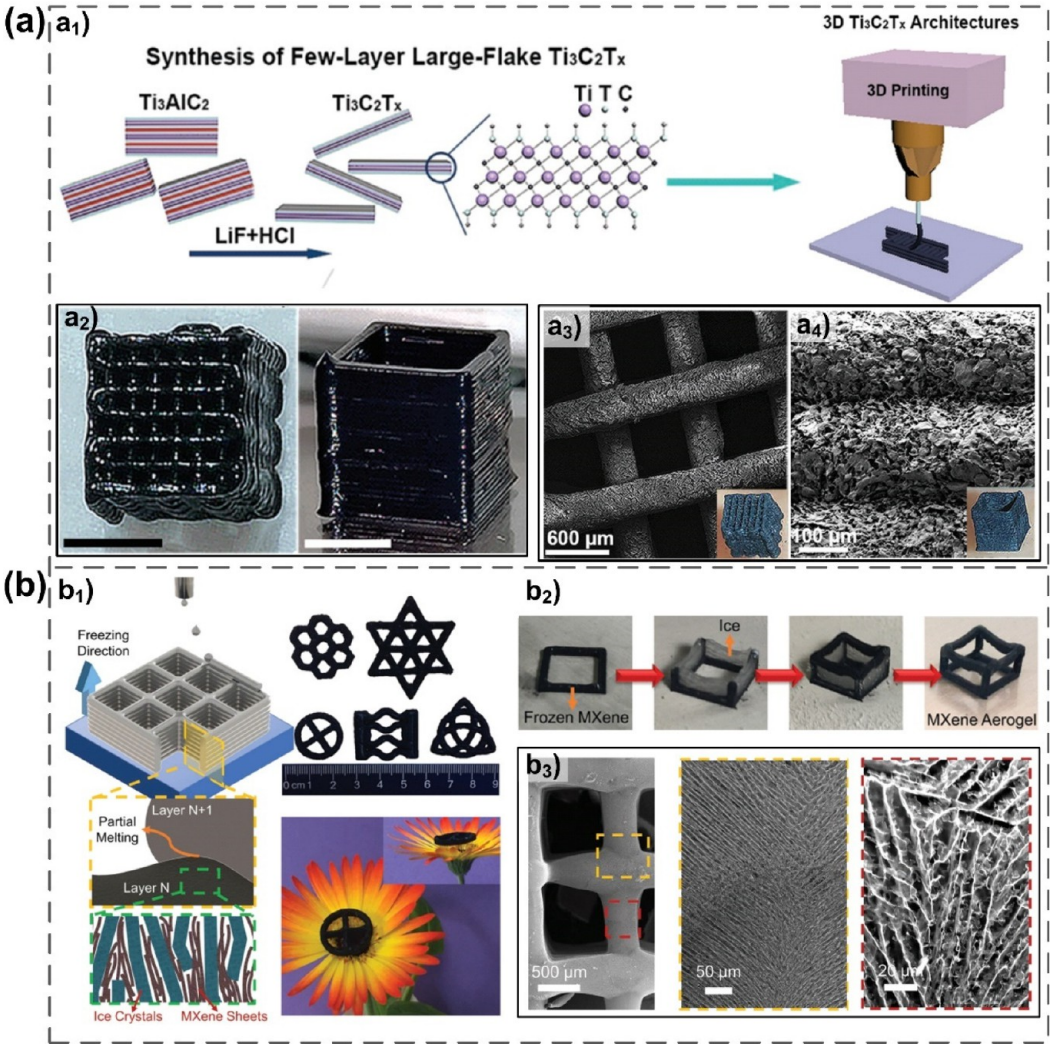

Figure 14. Three-dimensional printing preparation of MXene 3D structures. (a) Direct 3D printing with no-additive MXene inks. (a_1) Schematic of the printing process. (a_2) 3D printed wet gel. (a_3, a_4) SEM images of the microscopic morphology of individual printed filaments, illustrated with digital photographs of freestanding printed microlattices. (Reproduced with permission from ref 69. Copyright 2019 Wiley-VCH GmbH & Co.) (b) 3D freeze printing strategy. (b_1) Schematic diagram of 3D freeze printing. The inset shows the MXene ink deposited onto the frozen substrate in a layer-by-layer fashion, while the vertical upward temperature gradient causes the ice crystals to grow directionally, forming vertically aligned pores. (b_2) The photograph shows the steps to prepare 3D MXene aerogels with overhang truss structures by this strategy. (b_3) SEM images show the upper surface of the MXene aerogel produced by this strategy, showing the oriented arrangement of MXene nanosheets. (Reproduced with permission from ref 92. Copyright 2022 Wiley-VCH GmbH & Co.)

In recent years, research on MXene 3D printing has been in full swing, and MXene inks enable 3D printing based on having desirable rheological properties.[69,92,105,128−130]

However, the MXene inks currently used for 3D printing still have significant limitations. For example, applicable nonadditive MXene inks often require extremely high MXene concentrations to have the right rheological properties, which is not only extremely difficult to achieve but also greatly increases the cost. In addition, the difficulty of creating 3D structures with fine and complex shapes greatly limits the use of this technology.[131,132]

To address the above problem, Lin et al.[92] reported a 3D freeze printing (3DFP) technique to fabricate ultralight 3D MXene aerogel structures (as shown in Figure 14b). Specifically, on-demand MXene inks are deposited layer by layer on a frozen substrate, while ice can be used as a building block between layers to produce ultralight aerogels with complex structures (Figure 14b_2). Importantly, the MXene inks used in this strategy do not require ultrahigh MXene concentrations, which greatly reduces the cost. Due to the ordered arrangement of the microstructure, the aerogel fabricated by it has excellent mechanical and electrical properties (Figure 14b_3). In summary, this strategy combining 3D printing with directional freezing has extraordinary potential for the preparation of 3D electrical components with fine structures.

3.4. Other Assembly Methods. In addition to the above assembly methods, many other methods have been explored for assembling 3D porous structures of MXene, including the foaming method, skeleton coating method, electrostatic spinning method, etc. The study of various assembly methods has laid the groundwork for the application of MXene 3D structures in various fields.

3.4.1. Foaming Method. The foaming method is a technical method to prepare porous materials by foaming using chemical/physical/mechanical means. When some nitrogen-

https://doi.org/10.1021/acs.iecr.3c00306
Ind. Eng. Chem. Res. 2023, 62, 7297−7335

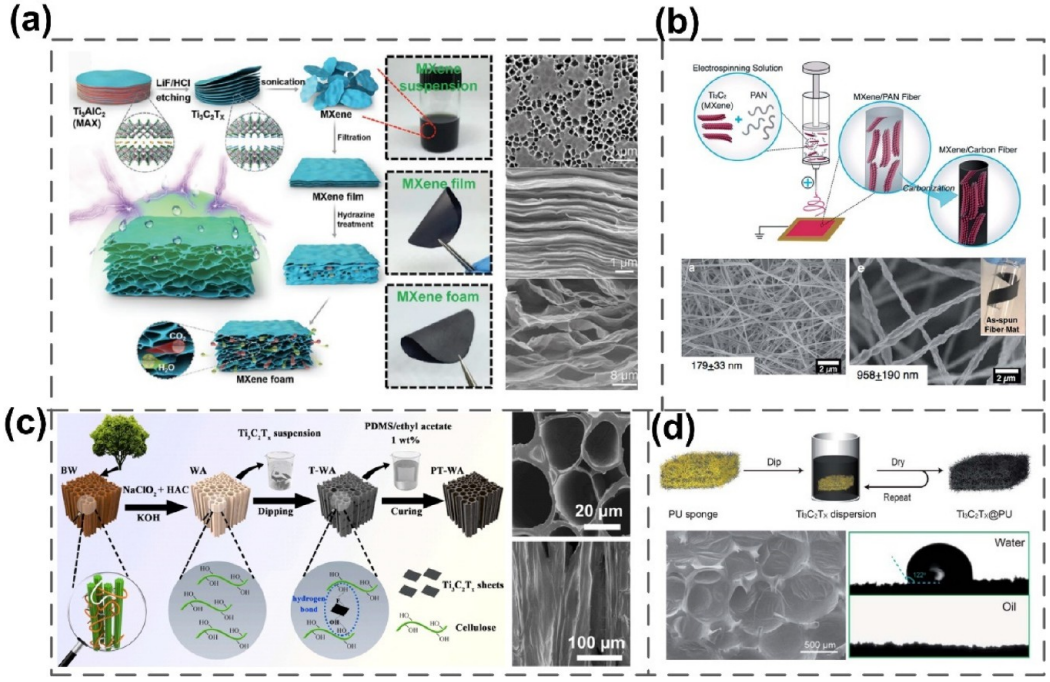

Figure 15. Other methods to prepare 3D MXene architecture. (a) Hydrazine foaming to prepare MXene 3D foam. The inset shows the photographs of MXene film as well as the foamed MXene foam and its microscopic morphology. (Reproduced with permission from ref 93. Copyright 2017 Wiley-VCH GmbH & Co.) (b) Electrostatic spinning method used to prepare PAN/MXene. The inset is an SEM image of PAN/MXene. (Reproduced with permission from ref 95. Copyright 2019 Royal Society of Chemistry.) (c) Schematic of MXene coated natural wood sponge and its SEM image. (Reproduced with permission from ref 94. Copyright 2022 Elsevier.) (d) Schematic of MXene coated commercial PU sponge, showing its micromorphology and wettability. (Reproduced with permission from ref 135. Copyright 2020 Royal Society of Chemistry.)

containing compounds, such as urea,[114] ammonia,[133] and hydrazine hydrate,[93] enter the MXene interlayer for heating, they are able to react with the MXene surface groups to produce a large amount of gas. For example, Yu et al.[93] reported the preparation of MXene foams with clear porous structures by applying hydrazine hydrate to the MXene film surface and then heating (as shown in Figure 15a). In particular, since the hydrazine hydrate consumed a significant number of functional groups on the MXene surface during the foaming process, the material showed overall hydrophobicity and enhanced the environmental sustainability of the material. This 3D MXene foam has a substantially improved electromagnetic shielding performance compared with MXene films of the same quality because of the porous structure construction.

Similarly, Zhu et al.[114] prepared 3D porous MXene foams by heating MXene−urea composite films at 550 °C for 2 h. It is worth mentioning that the experiments pointed out that the urea particles first acted as a template to prevent the nanosheets from restacking, and then when the template was removed by heating, a large amount of gaseous material was generated, in which the CO_2 produced etched the carbon on the MXene structure, thus drilling holes in the layers and eventually building 3D porous foams.

The foaming method allows for the convenient construction of porous structures and the doping of nitrogen in the MXene by changing the foaming agent, which can improve the electrical properties of the material as well as increase the active sites. However, there are still few foaming agents suitable for MXene materials, the foaming process is not easy to control, and it is difficult to prepare 3D porous structures with a certain thickness.

3.4.2. Skeleton Coating Method. Because of the weak gelation abilities of MXenes, the mechanical properties of MXene three-dimensional structures prepared by the above methods are often unsatisfactory. An effective strategy is to use existing three-dimensional porous skeletons, such as polymer foam,[106,121,134,135] wood sponge,[136] and foam metal, to load the MXene onto the three-dimensional skeleton by means of impregnation and spraying to form a uniform and continuous three-dimensional network. By adjusting the morphology of the skeleton, 3D structures with different structures can be easily constructed. More importantly, this approach combines the functionality of MXene nanosheets with the excellent mechanical properties of 3D skeletons, which has broad application prospects in the field of wastewater treatment, especially in offshore crude oil adsorption and seawater desalination. As shown in Figure 15c, Zheng et al.[94] used natural wood to produce a wood sponge with a vertical array pore structure by delignification and hemilignification, then loaded a MXene onto the surface of the wood sponge by impregnation to build a functional layer for photothermal conversion, and finally coated it with PDMS to achieve hydrophobization and enhance its mechanical stability. The loading of the MXene enables it to be self-heating, and the vertical array of pores enables it to clean superviscous crude oil from the sea surface driven by solar energy. The excellent compressive resilience makes it possible to work continuously for long periods of time.

In addition, PU sponge (Figure 15d),[135] MF sponge, carbon sponge, etc. can be used as a skeleton to prepare composite three-dimensional materials, compared to MXene material self-assembly. With the help of the skeleton, a MXene can easily form a continuous three-dimensional conductive network and

https://doi.org/10.1021/acs.iecr.3c00306
Ind. Eng. Chem. Res. 2023, 62, 7297−7335

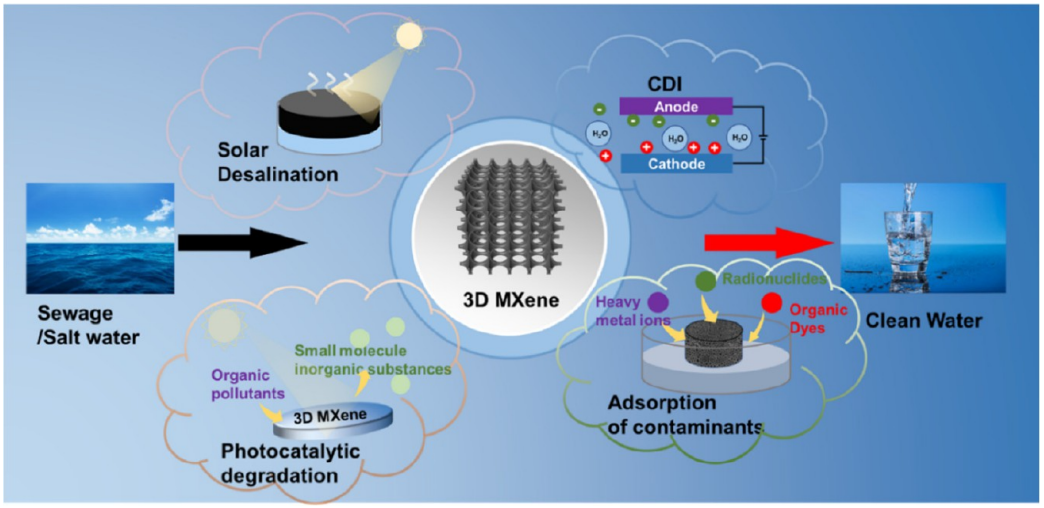

Figure 16. Schematic diagram of the progress of the application of 3D MXene structures in wastewater treatment (adsorption of water pollutants, photocatalytic degradation) and water reclamation (solar water desalination and CDI).

so in the field of wastewater treatment, electromagnetic shielding, energy storage, etc. have a wide range of potential applications.

3.4.3. Electrostatic Spinning Method. The electrostatic spinning technology is also a common method for preparing thin films with high porosities and three-dimensional structures. It is a process that uses the electric potential between the solution droplets and the collector to overcome the surface tension of the solution and thus generate ultrafine jets, which are stretched, thinned, and solidified when they reach the collector through an electric field, and these fibers are randomly stacked together to form a 3D network. As mentioned earlier, a MXene has good solvent processability and can form stable dispersions in water or some polar organic solvents, so the MXene can be easily blended with some polymers for electrostatic spinning. As shown in Figure 15b, $Ti_3C_2T_x$ was mixed with polyacrylonitrile (PAN) in water to produce a homogeneous mixture, and $Ti_3C_2T_x$/PAN composite networks with abundant mesopores were obtained after electrostatic spinning at an applied voltage of 18 kV; the literature reports an increasing diameter of electrostatic spun yarn with increasing MXene content.[95] Currently, poly(ethylene oxide) (PEO)[137] and PVA have also been reported to be coblended with MXene for electrostatic spinning.[138]

In Table S2 we briefly summarize the advantages and drawbacks of various current assembly methods of MXenes. However, for the time being, it is still difficult to realize the industrial preparation of conventionally manufactured 3D MXene functional materials, first because their assembly process requires strict control of conditions. Although various assembly schemes based on templates, cross-linking, and other mechanisms have been developed, a reasonable design and fine manufacturing of their structures are indispensable to achieving their high performance, which is still difficult to realize. Second, the currently reported 3D MXene functional materials often have defects such as poor mechanical properties and poor stabilities, which are very unfavorable both for the wastewater treatment field and the desalination field that needs to overcome harsh weather, so more high-performance composites with high mechanical stabilities need to be developed.

4. 3D MXene MATERIALS USED FOR WASTEWATER TREATMENT AND WATER RECLAMATION

MXenes, as emerging 2D nanomaterials, have high adsorption, reduction, excellent photothermal conversion, high electrical properties, etc., and their unique combination of hydrophilicity and electrical conductivity has led to an increasing interest in using MXenes and their derivatives in the fields of wastewater treatment and water reclamation. Compared with 2D materials, the assembly of MXenes into 3D structures not only maintains the excellent properties of the MXenes but also has unique advantages in wastewater treatment. Specifically, MXenes and their composites have been shown to be effective in the adsorption of pollutants in water and desalination through photothermal conversion and capacitive deionization, in addition to photocatalytic degradation of pollutants, as shown in Figure 16. This article reviews the applications of MXene three-dimensional porous structures in the above-mentioned fields in recent years, and gives an outlook on future developments.

4.1. Seawater Desalination. The shortage of water resources, especially fresh water, has been a severe challenge for the world. The development of environmentally friendly green water purification technology has become urgent. What is more, the distribution of water resources on the earth is extremely uneven, with the ocean occupying 97% of the global water reserves, while fresh water occupies only 3% and a large part of it is in glaciers and ice caps, which can hardly become drinking water. Therefore, the development of energy-efficient green desalination technology can fundamentally solve the problem of water scarcity. There are numerous desalination methods, among which distillation, reverse osmosis (RO), and membrane distillation (MD) have been widely used. However, these technologies often have huge energy and capital consumptions. In recent years, new low-energy, sustainable technologies such as solar-powered desalination and capacitive deionization have been receiving increasing attention.

4.1.1. Desalination Mechanism of MXenes and Their Composites. At present, MXenes have been widely used in seawater desalination and have achieved good results, which is important to solve the scarcity of fresh water resources. MXene materials are applied to seawater desalination mainly in the

https://doi.org/10.1021/acs.iecr.3c00306
Ind. Eng. Chem. Res. 2023, 62, 7297−7335

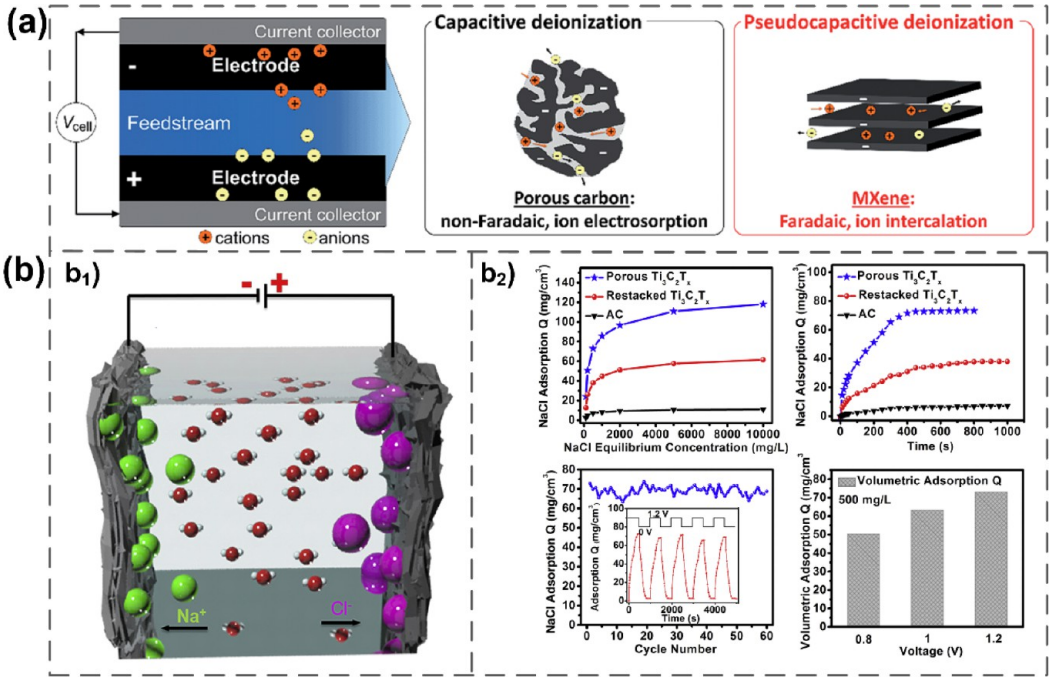

Figure 17. MXene electrodes for CDI technology. (a) Schematic diagram of electrochemical desalination. Schematic diagram of Faraday capacitance by ion insertion and non-Faraday capacitance by ion electrosorption. (From ref 141. CC BY 3.0.) (b) Porous MXene for capacitive deionization. (Reproduced with permission from ref 15. Copyright 2018 Elsevier.) (b_1) Concept diagram of porous MXene for CDI. (b_2) CDI performance of porous MXene electrodes. The salt adsorption capacity (SAC), salt adsorption rate (SAR), good cycling stability, and effects of different operating conditions on its SAC are demonstrated.

form of ion sieve membranes, capacitive deionization, and photothermal desalination.

First, MXenes' own two-dimensional nanomorphology and high hydrophilicity make them ideal materials for the construction of separation membranes with well-defined size nanochannels. On the one hand, this can be achieved by defining the size of the nanochannels of the MXene membrane material, thus allowing the passage of water molecules but trapping hydrated ions based on size sieving. On the other hand, the many negatively charged groups present on the MXene surface play an important role in the ion repulsion process. Many studies have shown that, for lamellar membranes constructed from MXene materials, strong electrostatic interactions between multivalent cations and the MXene lead to a narrowing of the nanochannels, resulting in a gradual decrease in the permeation rate, whereas monovalent cations such as Na^+ can be easily adsorbed between each layer of the lamellar membrane material to form a double electric layer, thus expanding the size of the nanochannels.

The excellent potential of MXene materials for capacitive deionization is another important discovery in the field of desalination in recent years. The unique two-dimensional layer structures of MXenes provide the largest possible specific surface areas, which, together with their excellent electrical conductivities, makes them very suitable for use as CDI electrodes. In addition, many studies have shown that MXenes have a different salt adsorption mechanism than conventional carbon electrodes; i.e., the rapid embedding and de-embedding of ions between MXene atomic layers provides a large salt storage capacity and a high adsorption/desorption rate, which are not available for conventional electrodes that form a double layer on the electrode surface by adsorbing ions. The synergistic effect of the two mechanisms makes MXene materials have a broad scope for use as CDI electrodes.

In addition, a MXene's photothermal conversion capability gives it extraordinary potential in the field of solar-powered desalination. Photothermal desalination is the oldest method of applying solar energy. There are two main points affecting solar-driven desalination: first, the ability to have the highest possible absorption of sunlight and convert it to heat; second, good thermal and water management to maximize energy utilization efficiency. Various studies have reported that MXenes have high light absorption capacities in the full wavelength band of sunlight and a theoretical 100% photothermal conversion efficiency, making them very good photothermal conversion materials. On the downside, the instability of MXene material in a water−oxygen environment and their own high thermal conductivities seriously limit their development in the field of photothermal seawater desalination. Fortunately, these problems have the potential to be solved by the structure and material design of the evaporator. The use of a MXene as a photothermal module, supplemented by various rational structural designs, is an important way to build a high-performance solar evaporator.

4.1.2. Capacitive Deionization (CDI). Capacitive deionization (CDI) is an emerging desalination technology in recent years, in which anions and cations in solution are deposited at the two poles according to their charges by applying a potential difference, thus achieving desalination of brine. In CDI technology, the electrode material is the key factor affecting its salt adsorption ability. At present, the most commonly used CDI electrodes are various carbon material electrodes, which are reported to be capable of achieving a salt adsorption capacity (SAC) of 15−20 mg g^{-1}, but in practice, the CDI performances of carbon electrodes are often less than ideal

https://doi.org/10.1021/acs.iecr.3c00306
Ind. Eng. Chem. Res. 2023, 62, 7297−7335

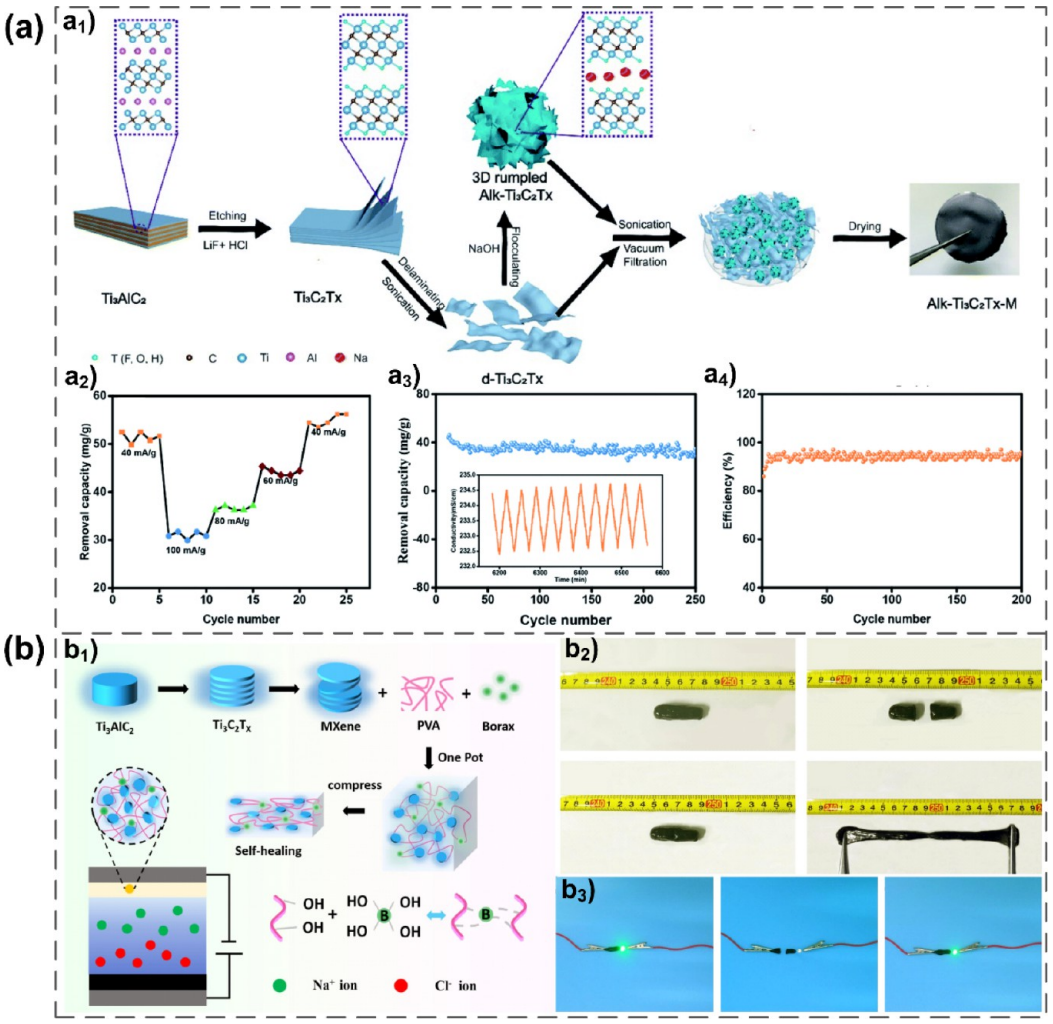

Figure 18. CDI electrodes with long runtime stability. (a) Alk-$Ti_3C_2T_x$-M film electrode. (a_1) Schematic diagram of preparation and synthesis. (a_2–a_4) Alk-$Ti_3C_2T_x$-M film electrode with excellent cycling stability. (Reproduced with permission from ref 150. Copyright 2020 Royal Society of Chemistry.) (b) PVA/MXene hydrogel electrode. (b_1) Synthesis principle and electrode preparation of MXene hydrogel. (b_2, b_3) Self-healing ability, demonstrating that the hydrogel has good electrical properties and self-healing ability. (Reproduced with permission from ref 151. Copyright 2021 Elsevier.)

because of limitations in their comparable surface areas and other factors.[139]

4.1.2.1. MXene-Based CDI Electrodes. In recent years, the performance of MXene materials in the field of CDI has attracted a lot of attention. The advantages of MXenes as CDI electrode materials are mainly as follows: First, the outstanding conductivity of a MXene itself provides the basis for its use as a CDI electrode. Second, its layered structure provides the largest possible specific surface area. Most importantly, the rapid insertion of ions between the atomic layers of a MXene leads to its high capacitance, resulting in a high salt adsorption capacity and fast adsorption/desorption response.[6] Thus, unlike conventional CDI electrode materials that adsorb stored ions by forming a double electric layer capacitance (EDLC) mechanism,[140] a MXene because of its rapid ion intercalation/delamination mechanism provides a new CDI electrode material—Faradaic CDI material—which allows it to overcome the limitations in the use of conventional electrodes. Srimuk et al.[141] coated a MXene on a porous polymer substrate and used MXene electrodes for the first time in the field of CDI. The electrodes were tested and showed an excellent salt adsorption performance with outstanding cycling stability. Importantly, it was also shown that MXene electrodes store charge by inserting ions between the lamellae of a two-dimensional nanosheet structure, exhibit capacitive electrical response upon insertion of anions and cations, have extremely high bulk capacitances and highly reversible ion insertion/layering in aqueous media, and behave as ideal pseudocapacitors. Thus, unlike the adsorption mechanism of conventional carbon electrodes that form a bilayer, MXene CDI electrodes achieve their adsorption performance by ion embedding (Figure 17a).

As mentioned earlier, CDI electrode materials should have high capacitances and large specific areas conducive to ion storage. A MXene can further improve its electrochemical performance by stripping it into nanosheets to increase the effective utilization of the two-dimensional surface.[142] However, two-dimensional nanomaterials have to be considered for their restacking during application, resulting in a low specific surface area with fewer active sites. In response to this problem, a study has successfully prepared MXene materials with aerogel-like porous structures by using a chloroform intercalation followed by freeze-drying strategy in the fabrication of $Ti_3C_2T_x$-MXene to increase the accessible

https://doi.org/10.1021/acs.iecr.3c00306
Ind. Eng. Chem. Res. 2023, 62, 7297−7335

specific surface area of the material and thus improve the salt adsorption capacity (as shown in Figure 17b).[15] The porous MXene material prepared by this method has a larger specific surface area as shown by the N_2 adsorption−desorption curve in Figure 17b_1. This, in turn, gives it an excellent CDI performance, and Figure 17b_2 demonstrates that the CDI electrode prepared from this material has a salt adsorption capacity of up to 45 mg g^{-1} at an initial concentration of 10 000 mg L^{-1} salt solution and an applied voltage of 1.2 V. It is worth pointing out that this electrode material also exhibits a faster electroadsorption rate and a cycling stability of up to 60 cycles, which may be due to the large specific surface area and the porous structure that not only increase the mass transfer rate of the electrode but also enhance the stability of the electrodes.

The above excellent electrosorption and salt storage capacity of porous $Ti_3C_2T_x$ can be attributed to the combined effect of the bilayer adsorption mechanism and the ion insertion mechanism. Specifically, while the porous $Ti_3C_2T_x$ prepared by freeze-drying prevents the nanosheets from restacking and improves the surface utilization efficiency, the three-dimensional network is constructed to provide multidimensional ion diffusion paths for Na^+ and Cl^-, which greatly improves the electron conduction and ion transport.

It is thus evident that assembling a MXene into a 3D structure, preventing its restacking and increasing the mass transfer rate of the material, is an excellent way to enhance its electrosorption capacitance and also its salt adsorption. On this basis, researchers prepared CLF@$Ti_3C_2T_x$ nanocomposites by using cellulose fibers (CLF) derived from tissue paper as a porous carbon substrate and assembling a shell composed of $Ti_3C_2T_x$ nanosheets on its surface by an improved dip-coating technique to further reduce costs and realize its potential for large-scale applications.[143] The rational assembly of the two materials combined with the ion embedding and bilayer adsorption mechanism resulted in an excellent CDI performance, and the salt adsorption capacity of the CDI electrode made from the materials was able to reach 35 mg g^{-1} at an initial salt solution concentration of 600 mg L^{-1} and an applied voltage of 1.2 V. More importantly, it is more cost-effective compared to CDI electrodes made of pure MXene materials.

4.1.2.2. Long-Term Operational Stability of MXene-Based Electrodes. In recent years, many efforts have been made to achieve the industrial feasibility of capacitive deionization (CDI).[144,145] In addition to the cost issues mentioned above, the cycling stability of CDI electrodes has been a major limiting factor. Several studies have reported that conventional CDI electrodes degrade more than 90% from their initial performance after just a few days of operation.[146,147] The decrease in desalination capacity is due to parasitic side reactions caused by carbon corrosion and the destruction of the pore structure, which allows the electrode to age and oxidize over long cycles.[148] Even with Faraday electrodes, the volume of the electrode will expand/contract with the repetition of the sodium ion embedding and de-embedding process thus generating mechanical stress, resulting in irreversible deformation and cracking of the crystal architecture of the electrode material.[149]

To solve the above problem, Shen et al.[150] formed 3D porous structures by an alkali-induced MXene, which could overcome the lattice changes caused by intercalation/delamination, which greatly improved the stability of the material itself. Meanwhile the open interconnected pore structure provides a high specific surface area and multiple adsorption sites ensuring fast ion diffusion and high Na^+ loading. As shown in Figure 18a, the pH change and the insertion of Na^+ between the MXene layers by adding NaOH led to the rapid flocculation of the monolayer MXene colloidal suspension to obtain the folded porous 3D structural network (Alk-$Ti_3C_2T_x$). The monolayer MXene (d-$Ti_3C_2T_x$) was then coextracted with Alk-$Ti_3C_2T_x$ to prepare CDI electrodes. Among them, d-$Ti_3C_2T_x$ nanosheets are used as conductive binders instead of conventional conductive binders, which can effectively adapt to volume changes and avoid the electrochemically inert components of conventional conductive binders, improving the capacitance and stability of the electrodes. Therefore, as shown in Figure 18a_2, the electrode can be directly used in the CDI technique and demonstrates a salt adsorption capacity of up to 50 ± 3 mg g^{-1} at an initial salt solution concentration of 1000 mg L^{-1} and an applied current density of 30 mA g^{-1} operating conditions. Moreover, when used as the anode for CDI, the performance did not decrease significantly for 250 cycles, which greatly improved the operational stability of the CDI electrode (as shown in Figure 18a_4).

An alternative solution was provided by Ai et al.,[151] who loaded MXene into a self-healing PVA hydrogel with a three-dimensional porous microstructure and nanostructure resulting in shorter diffusion paths and better three-dimensional connectivity (Figure 18b), which facilitates the transport of electrons and ions. The preparation of CDI electrodes from this hydrogel avoids the addition of adhesives, and the intact 3D porous structure can effectively reduce stress (Figure 18b_2). Most importantly, as shown in Figure 18b_3,b_4, the hydrogel exhibited excellent self-healing properties with up to 95.8% electrochemical healing performance making it extremely valuable in practical applications. The CDI electrode prepared from this hydrogel exhibited a salt adsorption capacity of up to 51 mg g^{-1} at a current density of 10 mA g^{-1} and a window voltage of 1 V with good cycling stability.

To date, many efforts have been put into exploring MXene-based CDI electrodes. To further enhance the efficiency of desalination, electrode materials with larger salt adsorption capacities, faster adsorption and desorption cycles, and higher cycle stabilities are needed. The above excellent research results provide ideas for the preparation of more efficient CDI electrode materials. By constructing a more complete three-dimensional porous network, the following advantages can be provided: (1) prevention of nanosheet stacking and provision of the largest possible available specific surface area provide large ion storage space; (2) more importantly, a complete three-dimensional porous network can provide a multidimensional ion transport pathway, which ensures fast electron conduction and ion transport, thus increasing the adsorption rate; (3) in addition, a complete three-dimensional porous structure can improve the overall stability of the material and help prolong the service life of the CDI electrode. Table S3 compiles the research on 3D MXene porous materials in the field of CDI in recent years.

4.1.3. Solar-Powered Desalination. Another way to use MXenes for desalination is photothermal conversion. Conversion of solar energy into thermal energy to produce steam is a green and low energy way to purify water. As mentioned earlier, MXenes have a wide absorption bandwidth of the solar spectrum,[75,152] high near-infrared absorption, and a theoretical 100% internal photothermal conversion efficiency.[74] Due to

https://doi.org/10.1021/acs.iecr.3c00306
Ind. Eng. Chem. Res. 2023, 62, 7297−7335

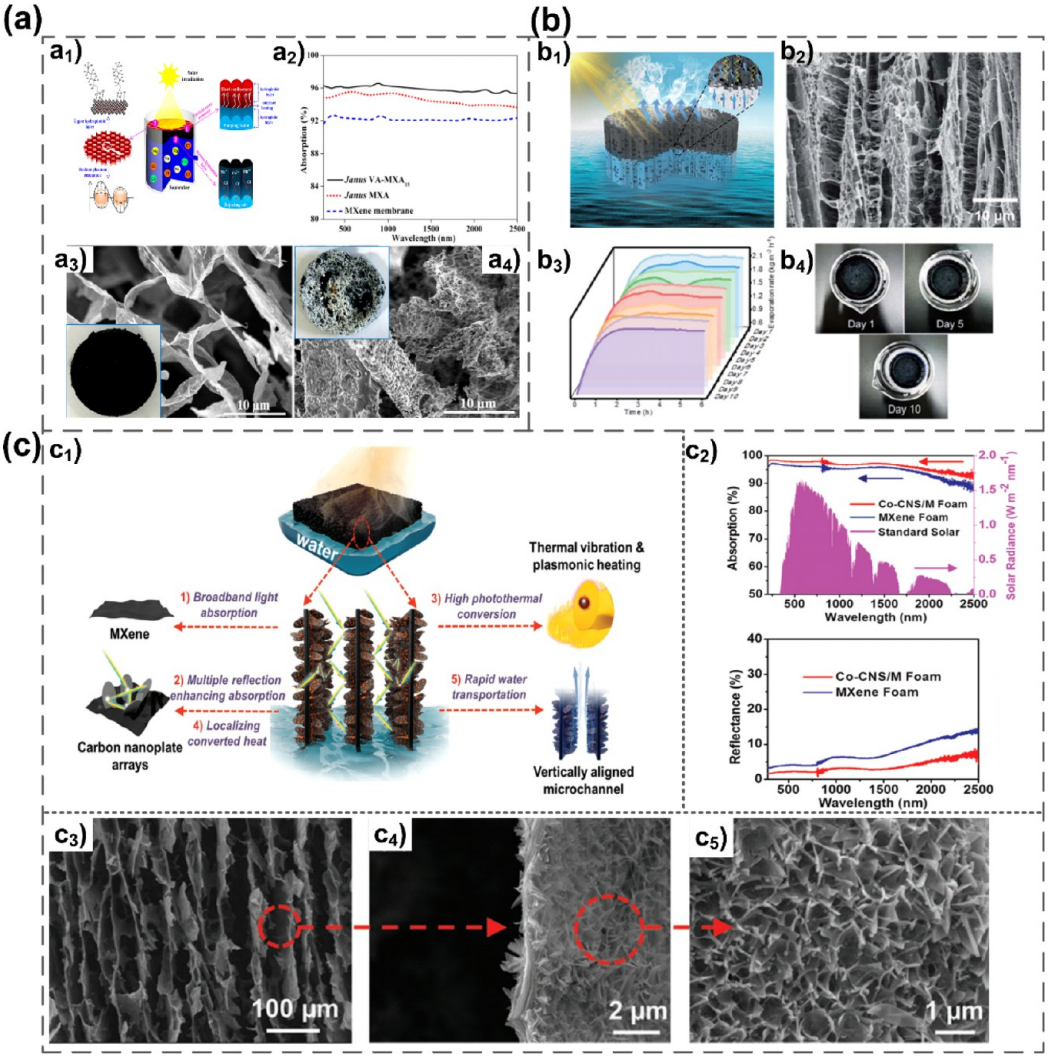

Figure 19. Solar evaporator based on aerogel structure. (a) Janus-MXene aerogel with vertical array pore structure. (a_1) Schematic of this aerogel for solar water desalination. (a_2) Enhanced light absorption properties due to vertical apertures. (a_3, a_4) SEM as well as digital photographs of both aerogels with Janus structure as well as non-Janus structure after long time operation (inset). (Reproduced from ref 8. Copyright 2019 American Chemical Society.) (b) MXene/CNF composite aerogel. (b_1) Schematic diagram of solar-driven evaporation. (b_2) SEM image of the vertically aligned pore structure. (b_3) Stability of the long run. (b_4) Digital photograph of the evaporator surface after a long run; no obvious salt crystals were observed. (Reproduced with permission from ref 117. Copyright 2021 Royal Society of Chemistry.) (c) Co−CNS/M foam. (c_1) Schematic diagram of Co−CNS/M foam for solar vapor generated efficiently by solar energy absorption. (c_2) Synergistic enhancement of light absorption by three photothermal conversion materials. (c_3−c_5) SEM images of the evaporator aperture wall. (Reproduced with permission from ref 159. Copyright 2020 Wiley-VCH GmbH & Co.)

the multiple advantages mentioned above, MXenes are highly competitive photothermal conversion materials in the field of solar-driven desalination.

Currently, the two main forms of solar-driven desalination using photothermal conversion materials are volumetric evaporation and interfacial evaporation. In the volumetric evaporation system,[153−155] the photothermal nanoparticles, which are energy conversion materials, are dispersed directly in the water, and the photothermal nanomaterials produce heat and conduct it to the body of the water. However, since the volumetric evaporation system heats the entire body of water, it generates considerable heat loss and is only capable of achieving an acceptable amount of evaporation under high intensity sunlight. The interfacial evaporation developed for this situation concentrates the photothermal conversion material at the interface between water and air and is responsible for absorbing sunlight and converting it into heat energy. Most importantly, the heat generated by the interface evaporator only heats a small amount of water at the interface, greatly reducing heat loss and making it possible to produce a significant amount of water even under ordinary light conditions.[156,157]

For an interfacial evaporation system, the core component is the interfacial evaporator. The ideal interfacial evaporator needs to meet the following conditions: (i) efficient solar light capture and the highest possible photothermal conversion capacity; (ii) good thermal management; (iii) stable self-floating; (iv) reasonable water transfer and steam escape channel.

In this section, we review these fascinating research works mainly in terms of the effect of different 3D structures of MXene-based interfacial evaporators on the evaporation efficiency.

https://doi.org/10.1021/acs.iecr.3c00306
Ind. Eng. Chem. Res. 2023, 62, 7297−7335

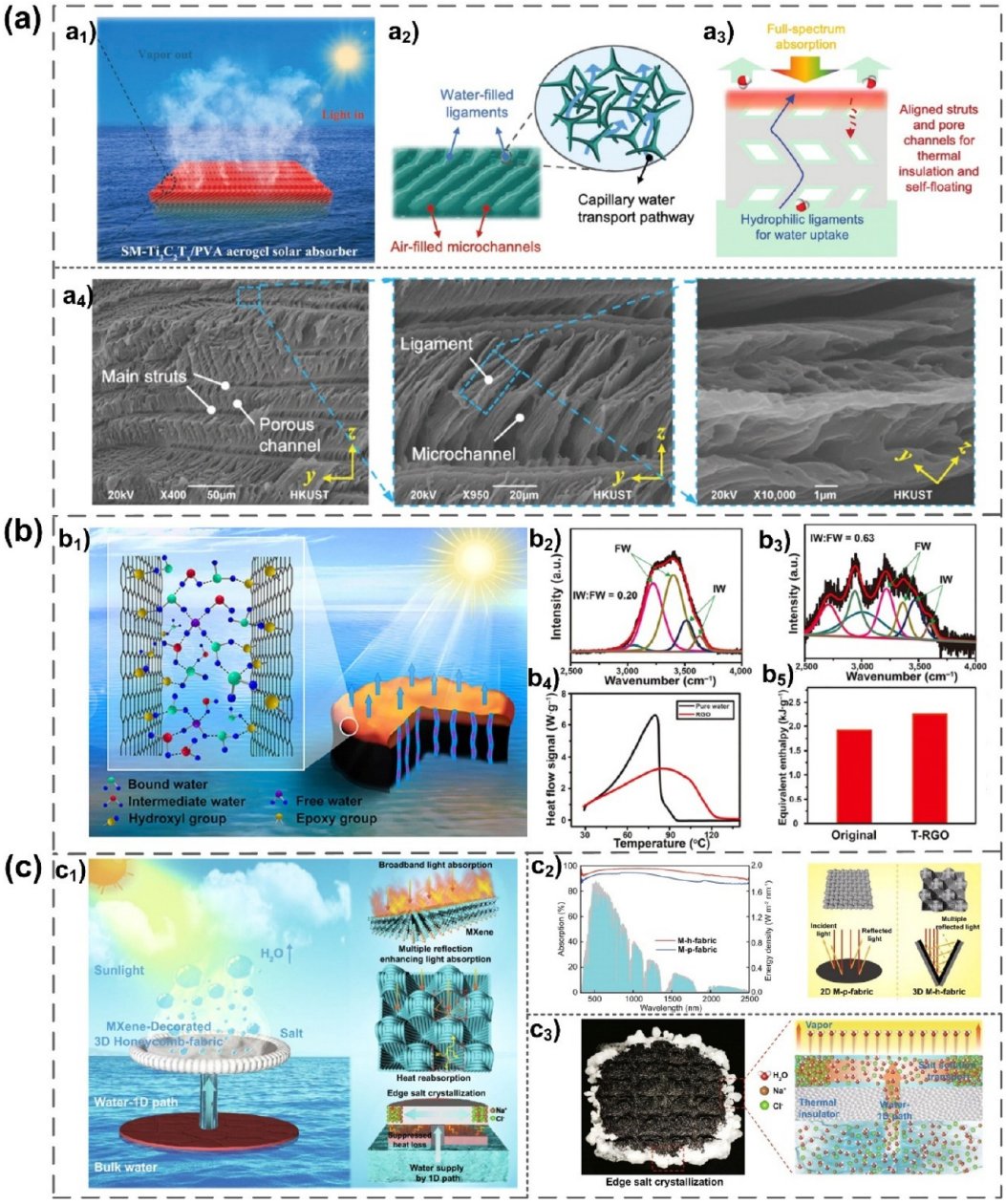

Figure 20. Solar water evaporator with different structures. (a) PVA/MXene aerogel with bionic structure. (a_1) Schematic of solar driven evaporation. (a_2) Schematic of evaporator water management. (a_3) Schematic of good thermal management of evaporator. (a_4) SEM image of hierarchical structure of aerogel.[87] (b) MXene/rGO hydrogel evaporator. (b_1) Schematic diagram of the MXene/rGO composite hydrogel and the three different states of water in the hydrogel network. (b_2, b_3) Raman spectra of pure water as well as water in MXene/rGO composite hydrogels, where IW and FW represent intermediate water and free water, separately. (b_4) The evaporation enthalpy of water in pure water as well as MXene/rGO composite hydrogel was tested separately by DSC. It can be seen that the heat absorbed by water in the hydrogel is significantly less than that of pure water. (b_5) Changes in the evaporation enthalpy of the composite hydrogel before and after heat treatment at 200 °C to demonstrate the effect from the incomplete reduction with rGO. (Reproduced with permission from ref 165. Copyright 2020 Springer Nature.) (c) Fabric with 3D microstructure. (c_1) Schematic diagram of evaporation system consisting of MXene coated fabric. (c_2) Schematic diagram of 3D microstructure with enhanced light trapping ability with absorption spectra. (c_3) Photograph of a one-dimensional water transport pathway to crystallize its salt at the edge of the fabric and a schematic diagram of the mechanism. (From ref 80. CC BY 4.0.)

4.1.3.1. Solar Evaporator Based on Aerogel Structure. In a pioneering study of MXene materials for solar-powered desalination applications, a MXene was prepared as a two-dimensional membrane material. In this study, MXene films were hydrophobically modified using fluorinated silanes, and a hydrophobic film was assembled as a photothermal conversion layer with a commercial PS foam to form an interfacial evaporation system.[158] The system had an evaporation rate of 1.31 kg m^{-2} h^{-1} under 1 sun and was able to achieve an energy utilization efficiency of 71%.

Compared with two-dimensional thin film materials, three-dimensional aerogel structures can effectively reduce the reflection of light on the evaporator surface due to their well-developed pores and rich porous networks, and they can enhance the ability of the material to capture sunlight through the scattered light within its pores at the same time, and by

https://doi.org/10.1021/acs.iecr.3c00306
Ind. Eng. Chem. Res. 2023, 62, 7297−7335

adjusting its porous structure to construct suitable water transmission channels to facilitate evaporation. In addition, the aerogel structure has the advantages of light weight and low thermal conductivity, making it a more ideal choice for solar-driven interfacial evaporators.

On this basis, Zhang et al.[8] prepared three-dimensional MXene-based aerogels with vertically aligned pore structures by the directed freezing technique. As shown in Figure 19a, the Janus structure was constructed by subsequent unilateral surface fluorinated silane modification, which effectively prevented the salt from crystallizing and precipitating on its photothermal surface. Thanks to its rational structural design, the evaporator was able to achieve an evaporation rate of 1.46 kg m^{-2} h^{-1} and an energy utilization efficiency of 87%. The Janus structure has been tested to ensure stable operation for 15 consecutive days.

Compared with the uneven pore size distribution and irregular network structure, the evaporator with a vertical array pore structure (Figure 19b), which has stronger capillary force, has a competitive advantage in rapid water supply. In addition, during the actual use of the evaporator, due to the quick vaporization of water, the salt crystallizes on its surface and further affects the absorption of sunlight and vapor escape of the material, which seriously affects its evaporation efficiency. The introduction of the Janus structure can help avoid salt crystallization on the surface effectively and improve the operational stability of the material. However, due to some inherent properties of MXene materials, such as high thermal conductivity,[160,161] moderate broadband light reflection,[162] and easy oxidation, these properties limit the advancement of MXene materials in the fabrication of high-performance solar evaporators. At present, the efficiency of solar evaporators is generally improved from the following two directions: (1) enhancing the sunlight capture of the absorber by modifying MXene nanosheets or compounding other photothermal conversion materials; (2) making the evaporator with good thermal management and improve energy utilization efficiency by appropriate strategies, including compounding low thermal conductivity polymer materials, introducing pleated structures, microporous structures, Janus structure, etc.

Based on this, Fan et al.[159] designed and fabricated a hierarchical solar-absorbing architecture: cobalt nanoparticles (CoNP)−carbon nanosheets/MXene foam (Co−CNS/M foam) (Figure 19c). The structure has a 3D microporous backbone assembled by vertically aligned MXene nanosheets, while the backbone is later modified by 2D carbon nanoplates embedded with cobalt nanoparticles derived from cobalt metal−organic frameworks (Co-MOFs). As shown in Figure 19c_1, the foam has the following unique advantages: first, vertically aligned MXene nanosheets and two-dimensional carbon nanosheets grown on the surface of the nanosheets are able to enhance light absorption through multiple reflections of incident light (Figure 19c_2); second, the combination of three photothermal conversion materials allows it to combine the photothermal mechanisms of molecular thermal vibration and plasma local heating, ensuring high photothermal conversion efficiency of the material itself; the vertically aligned porous structure and its inherent hydrophilicity ensure fast water delivery. It is worth pointing out that, due to the modification of amorphous carbon nanosheets, the composite not only has a very low thermal conductivity but also effectively prevents the oxidation of the MXene, which greatly enhances the long-term stability of the material (Figure 19c_3).

Because of the above excellent structural design, the structure can achieve a solar steam conversion efficiency of 93.4% under 1 sun and can be maintained at more than 91% for 100 h (10 h per day, 10 days of continuous operation).

Unlike composite other photothermal conversion materials, Zhang et al.[87] prepared spectrally modified SM-$Ti_3C_2T_x$ nanosheets by continuous oxidation of $Ti_3C_2T_x$ and simple calcination with the introduction of Ti^{3+}−TiO_2 as well as amorphous carbon nanoparticles on the nanosheet surface. This SM-$Ti_3C_2T_x$ nanosheet was then used as a photothermal module to prepare structure-specific 3D aerogels by the ice structure freeze casting (ISFC) technique with the addition of PVA (Figure 20a). The aerogel has each anisotropic graded structure with a microscopic morphology highly similar to that of penguin down. As shown in Figure 20a_4, the size of its main pores is 10−20 μm, but the large pore walls still have directionally arranged submicrometer pores that are capable of generating stronger capillary forces. Therefore, water tends to be transported through submicrometer pores within the macropore walls, leaving low density air to fill the micro-channels. The unique graded structure gives the material a suitable water supply rate as well as thermal insulation properties, and Figure 20a_2,a_3 shows a schematic of this aerogel for water management as well as thermal management.

In addition, the study noted that, in practical applications, the solar irradiation intensity is often less than 1 kW/m^2 due to weather and seasonal variations, and this aerogel maximizes the use of solar energy due to both enhanced light captures and good thermal management. Therefore, even under the weak irradiation intensity of 0.5 sun, the aerogel is able to achieve a high energy rate of 88.52% and an evaporation efficiency of 0.92 kg m^{-2} h^{-1}.

From the above excellent research results, we can get the inspiration that the design of three-dimensional aerogel structure should start from the following elements: (1) enhance the capture and absorption of incident light on the surface by designing reasonable surface microstructures and compounding other photothermal materials; (2) reduce the overall thermal conductivity of the material to achieve good thermal management; (3) design reasonable water supply paths to reduce convective heat loss.

4.1.3.2. Solar Evaporator Based on 3D Hydrogel Structure. Another popular structure for solar water desalination is the three-dimensional hydrogel. It has been reported that, due to the interaction between polymer and water, some of the water in the molecular lattice of a polymer hydrogel can be activated, which can effectively decrease the enthalpy of evaporation of water, thus significantly enhancing the efficiency of energy utilization.[163]

Based on this, Yu et al.[164] prepared a photothermal hydrogel with horizontally aligned channels by the directed freezing technique using PVA and a MXene as raw materials. Due to its structural design and hydrogel activation, the hydrogel was able to achieve a high performance of 90.7% energy efficiency and evaporation from 1 sun of 2.71 kg m^{-2} h^{-1}.

In contrast, Li et al.[165] prepared rGO hydrogels with vertical structures by light reduction and liquid nitrogen directed freeze casting and then assembled a MXene on the 3D hydrogel backbone to obtain rGO/MXene composite hydrogels with vertical arrays. The structure achieves fast water pumping and also enhances the light trapping through multiple scattering of light. More importantly, it has been pointed out that a significant amount of oxygen-containing functional groups on

https://doi.org/10.1021/acs.iecr.3c00306
Ind. Eng. Chem. Res. 2023, 62, 7297−7335

the surface of intentionally controlled and slightly reduced graphene oxide can effectively decrease the enthalpy of vaporization of water (Figure 20b).

As shown in the Raman spectra in Figure 20b_2,b_3, the water in this MXene/rGO composite hydrogel is not in the same state as pure water, and the composite hydrogel contains a higher amount of intermediate water, so the water in the hydrogel is more likely to evaporate.[163] This is mainly due to the effect of the large number of oxygen-containing functional groups still contained on the surface of the initially reduced rGO. To prove this conclusion, the composite hydrogel was subjected to heat treatment to further reduce rGO in Figure 20b_4, and the results showed that the further reduced composite hydrogel lost the ability to reduce the enthalpy of water evaporation.

In summary, the reasonable structural design enables fast water supply and enhanced solar light capture; the composite with lightly reduced rGO can effectively reduce the enthalpy of water vaporization. As a result, the composite hydrogel is able to achieve an evaporation rate of 2.09 kg m^{-2} h^{-1} and an energy conversion efficiency of up to 93.5% under 1 sun. In addition, this report is also the first to investigate the effect of inorganic hydrogels on the evaporation enthalpy, which avoids the addition of polymeric materials that affect solar absorption and provides a new idea for the development of high-performance solar evaporators.

4.1.3.3. Fabrics/Film with 3D Microstructure. In addition to the three-dimensional gel structure, thin films/fabrics with 3D microstructures are also one of the options for preparing solar evaporators. Peng et al.[84] prepared an asymmetric photothermal evaporation system by asymmetric deposition of MXene nanosheets on cotton fabric. This unique design was able to create a concentration difference on its surface, thus effectively preventing salt deposition. It is worth pointing out that the material is able to maintain a high evaporation rate of 1.38 kg m^{-2} h^{-1} in 1 sun with a conversion efficiency of 83.1% while generating 363 mV by forming an asymmetric double electrode layer within the $Ti_3C_2T_x$-MXene nanochannel in the immersed state, thereby generating continuous electrical energy.

Recently, a study reported a fabric with a 3D honeycomb microstructure for use as a photothermal conversion layer in solar evaporation systems (Figure 20c).[80] As shown in Figure 20c_2, the periodic concave array structure on the fabric surface enables multiple scattering and omnidirectional light absorption of sunlight, which works synergistically with the surface-loaded MXene to achieve maximum light capture. The entire evaporation system consists of a loaded MXene honeycomb fabric, an insulating foam, and a cotton fiber rod in the center of the foam (Figure 20c_1). In particular, the low thermal conductivity hydrophobic foam and the cotton fiber rods in its center form a one-dimensional water transfer channel that minimizes convective heat loss due to water supply. As a result, the evaporation system was able to achieve a high energy utilization efficiency of 93.5% and an evaporation rate of 1.62 kg m^{-2} h^{-1} under 1 sun. Notably, the system was designed with the 1D water supply channel in the center of the MXene fabric, so the salt solution can form a concentration gradient from the center to the edge of the evaporation surface during evaporation, thus allowing the salt to crystallize and precipitate at the edge (e.g., Figure 20c_3).The ingenious design allows for effective collection of salt from the water while preventing salt from crystallizing on the evaporation surface and impeding subsequent evaporation.

From the above excellent work, we can obtain some important information. First, the synergistic use of multicomponent photothermal materials is not simply one plus one, but can combine different photothermal mechanisms to synergistically enhance the photothermal conversion performance of the materials. In addition, the reasonable structural design can further improve the evaporation rate as well as the energy utilization efficiency of the evaporator. Specifically, the combination of multicomponent photothermal materials and reasonable surface structure design can effectively reduce the reflection of light on the surface and improve the efficiency of sunlight capture. A reasonable structure design can ensure rapid pumping and vapor escape while achieving good thermal management and improving the efficiency of energy utilization, promote evaporation by designing hydration in the material, and introduce a Janus structure or build salt solution on the surface concentration gradient. Other structural designs can effectively prevent salt from crystallizing on the evaporator surface and achieve long-term stable operation. These works provide us with more guidance for the preparation of high-performance solar evaporators in the future. Table S4 summarizes the recent progress on 3D MXene materials for solar evaporation/desalination and their efficiency and innovation.

4.2. Adsorption of Contaminants in Water. With the booming development of modern industry, various pollutants are discharged into inadequately treated water, causing serious environmental pollution and human health hazards. To date, a variety of technologies have been used for the removal of contaminants from water, for instance, coagulation, ion exchange, adsorption, membrane filtration, chemical precipitation, biodegradation, and photocatalytic oxidation. Among these technologies, adsorption is one of the most attractive wastewater treatment technologies because of its simplicity of operation, quick results, and cost-effectiveness. Due to their large aspect ratios, abundant surface groups and large numbers of active sites, MXenes and their composites are very practical adsorption materials.

However, similar to other nanomaterials, MXene materials have problems in wastewater treatment such as easy agglomeration, difficult recovery, and secondary pollution. By assembling a MXene into a three-dimensional porous structure, it can effectively prevent the reaccumulation of nanosheets with a large number of accessible surfaces as well as active sites, which is important for expanding the application of MXene materials in the field of pollutant adsorption in water.

4.2.1. Adsorption Mechanism of MXene-Based Materials. In recent years, MXenes and their composites have been used as efficient adsorbents for the removal of contaminants such as water-soluble dyes, heavy metal ions, and radionuclides. Many studies have been done on the adsorption mechanisms of MXene materials, which involve various mechanisms, including electrostatic interactions, ion exchange, coordination, chemisorption, physical adsorption, reductive adsorption, surface complexation, and van der Waals interactions. Among them, electrostatic interactions are generally the main influencing factor because of the large number of negatively charged functional groups on the MXene surface. For electrostatic interactions, the point of zero charge (PZC) of the adsorbent is a crucial parameter, and when the ambient pH is lower than

https://doi.org/10.1021/acs.iecr.3c00306
Ind. Eng. Chem. Res. 2023, 62, 7297−7335

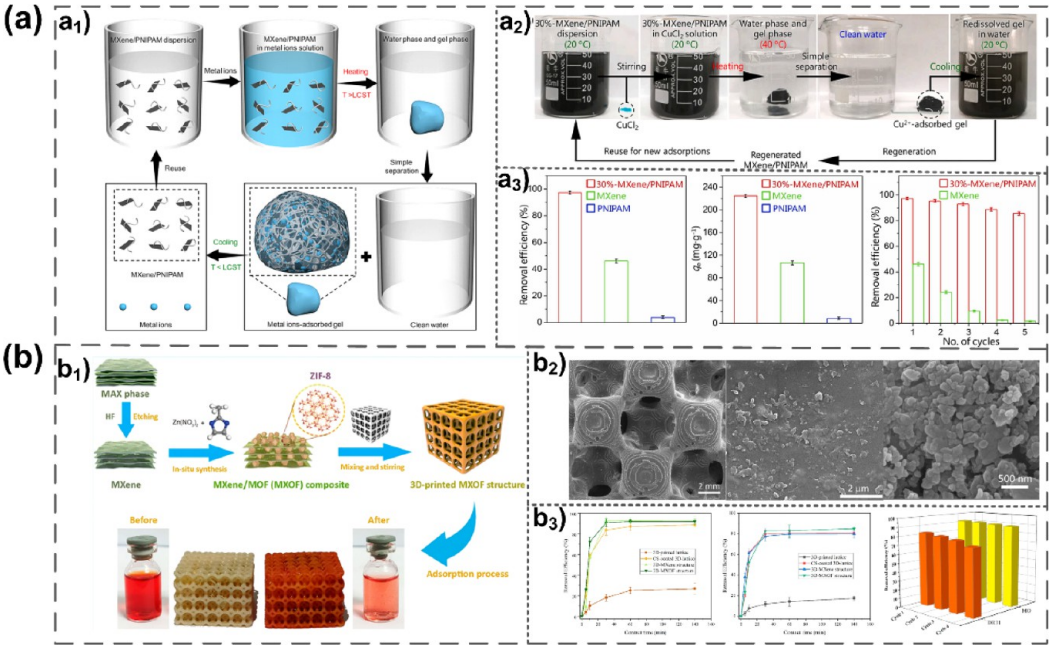

Figure 21. MXene 3D structure for adsorption of contaminants in water. (a) MXene/PNIPAM thermally responsive system. (Reproduced with permission from ref 172. Copyright 2022 Elsevier.) (a_1) Schematic diagram of the temperature controlled adsorption process. (a_2) Digital photograph of the process of 30%-MXene/PNIPAM gelation and adsorption of Cu^{2+} from water, followed by separation from water. (a_3) Adsorption performance of the system on Cu^{2+}. (b) MXene/metal−organic framework decorated with three-dimensional (3D) printed lattice structure (3D-MXOF). (Reproduced from ref 173. Copyright 2022 American Chemical Society.) (b_1) Schematic diagram of the preparation process of 3D-MXOF and the adsorption of organic dyes. The inset shows the changes of 3D-MXOF and the color of the solution before and after adsorption. (b_2) SEM images of the graded structure. (b_3) Adsorption performance of 3D-MXOF on the two dyes as well as the cycling stability.

the PZC, the protonation of the group causes a charge shift from significant adsorption of anionic contaminants.[166,167]

However, in some cases, ionic contaminants are still significantly removed in the presence of electrostatic repulsion. This implies that there are still other mechanisms, such as ion exchange and complexation, that dominate the adsorption process.[168,169] For instance, Peng et al. investigated the adsorption behavior of Alk-MXene obtained by alkaline intercalation treatment on Pb(II). The material showed an ultrahigh adsorption capacity as well as a high adsorption rate. Importantly, it was demonstrated that the adsorption behavior of Alk-MXene on Pb(II) was mainly carried out by ion exchange as well as complexation.[168]

It follows that the ion-exchange behavior also facilitates the adsorption of ionic contaminants, especially metal ions, usually by the exchange of ions attached to the functional groups on the MXene surface with contaminant ions in water. It has been reported that these ion-exchange behaviors are most likely achieved through the formation of hydroxyl potential traps in water by MXene surface groups with other ions (e.g., H^+, Na^+) attached.[170] In summary, the adsorption of MXenes on heavy metal ions, organic dyes, and other ionic pollutants is controlled by a combination of adsorption mechanisms.[171]

4.2.2. Adsorption of Inorganic Pollutants. With the development of modern industry, many inorganic pollutants, such as heavy metal ions and radionuclides, which are extremely harmful to human health as well as the natural environment, have been discharged into the water environment freely. More importantly, some pollutants are able to accumulate in living organisms, so they are more damaging than others and must therefore be removed in a more effective manner whenever possible. Yang et al.[90] developed a molding technique using ethylenediamine-assisted assembly of MXene/rGO hybrid hydrogels and prepared MXene/rGO porous foams by freeze-drying. The foam exhibited an excellent adsorption performance for heavy metal ions such as Pb(II) and Cu(II), with a capacity of 177 mg g^{-1} for Pb(II), and the robust three-dimensional structure provided excellent cycling stability.

Separation after adsorption is also a serious challenge for the use of nanomaterials as adsorbents. Peng et al.[172] designed and fabricated a temperature-controlled system using a MXene coblended with poly(*N*-isopropylacrylamide) (PNIPAM) (Figure 21a). The material has an excellent temperature response, and the composite system shrinks and separates into a gel phase and an aqueous phase when the ambient temperature is higher than its lower critical solution temperature (LCST). At this time, the composite gel phase will rapidly adsorb heavy metal ions from the aqueous phase and can easily separate the adsorbed contaminant gel from the aqueous phase. As shown in Figure 21a_3, the system can reach a high adsorption capacity of 224 mg g^{-1} for Cu^{2+}. The gel can be completely dissolved in the aqueous phase when the ambient temperature is lower than the LCST, so the cyclic regeneration of the composite system can be achieved by simply changing the ambient temperature (as shown in Figure 21a_2).

4.2.3. Adsorption of Organic Pollutants. In addition to the inorganic pollutants mentioned above, MXene composites also have excellent adsorption properties for some organic dyes and insoluble oil phases. Typically, Wu et al.[16] used chitosan-based porous carbon microspheres (CPCM) to avoid the restacking of $Ti_3C_2T_x$-MXene nanosheets to prepare CPCM@MXene composites with a very large specific surface area of more than 1800 m^2 g^{-1}. As a result, the material exhibited an adsorption capacity of up to 2750 mg g^{-1} for crystal violet.

https://doi.org/10.1021/acs.iecr.3c00306
Ind. Eng. Chem. Res. 2023, 62, 7297−7335

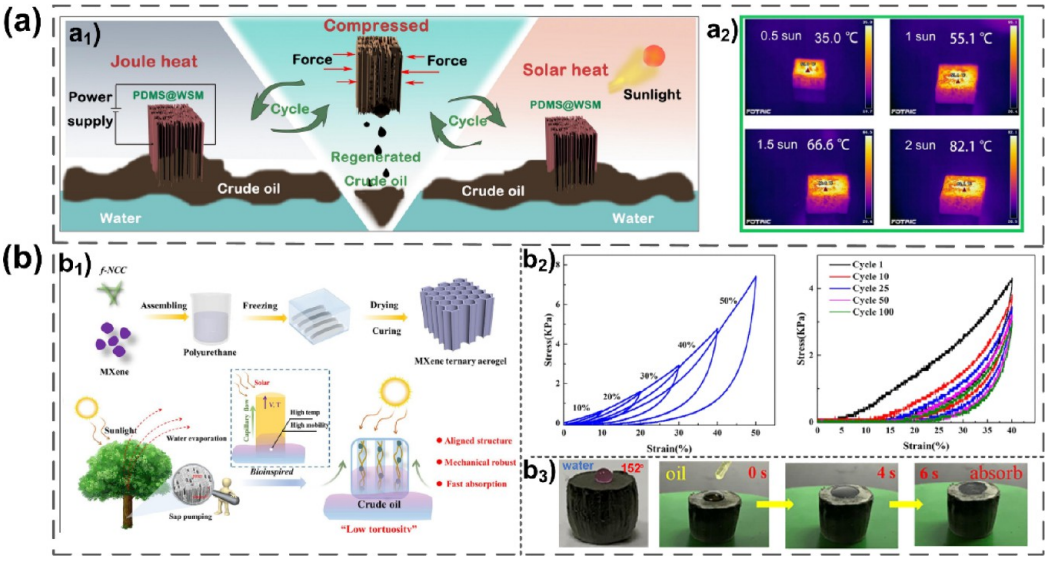

Figure 22. Three-dimensional MXene architecture for offshore crude oil cleanup. (a) MXene coated wood sponge for crude oil adsorption. (Reproduced with permission from ref 136. Copyright 2022 Elsevier.) (a_1) Schematic diagram of the material's all-weather crude oil adsorption by photothermal and Joule heat. (a_2) Temperature variation of this material under different intensities of sunlight. (b) Biomimetic MXene aerogel for crude oil cleanup. (Reproduced with permission from ref 175. Copyright 2021 Elsevier.) (b_1) Schematic diagram of the preparation process and crude oil adsorption mechanism. (b_2) Characterization of the mechanical properties of MXene aerogel. Stress−strain curve for cyclic compression. (b_3) Wettability characterization of MXene aerogels.

How to maximize the available specific surface areas of materials has been the focus of research in the field of pollutant adsorption. Recently, a study was conducted by growing metal−organic frameworks (MOFs) in situ on MXene nanosheets and modifying them on printed lattice structures with hierarchical structures prepared by 3D printing technology, the preparation process of which is shown in Figure 21b_1.[173] The SEM image in Figure 21b_2 shows the hierarchical structure of the composite, which provides an approximate very large specific surface area of 1232.5 m^2 g^{-1}. In the composite structure, the $Ti_3C_2T_x$-MXene layer is able to provide enough Lewis acid sites to interact with the electron-rich π-bonds in the dye molecule.[174] Due to the above advantages, the composite showed a high adsorption performance for anionic dyes, especially for methyl orange with 91.98% adsorption retention. It is worth mentioning that, due to its 3D monolithic structure, the adsorption process does not require centrifugation or filtration to recover the adsorbent, which greatly simplifies the operation process of adsorption and recovery with a sustainable adsorption performance−desorption cycle after four consecutive adsorptions (Figure 21b_3).

All of the above studies showed that, by assembling a MXene into a three-dimensional porous structure, it can provide the largest possible specific surface area as well as more adsorption sites to enhance the adsorption capacity of the material. Furthermore, a reasonable 3D porous network can provide multidimensional water transport pathways and increase the mass transfer efficiency, thus improving the adsorption rate of the material. Finally, the construction of the 3D structure makes MXene nanosheets easy to recover and also improves the overall stability of the material, which makes large-scale applications possible.

In addition to the above-mentioned small molecule pollutants, crude oil spills at sea have occurred in recent years, not only causing waste of resources but also seriously polluting the marine environment. Importantly, these ultra-viscous crude oils, which basically cannot flow at room temperature, are difficult to clean up with traditional adsorption sponges. The outstanding photothermal conversion properties of MXenes provide a new idea for cleaning up crude oil spills at sea. That is, by introducing MXenes in the three-dimensional porous network, a 3D porous material with a photothermal effect is prepared, so it can reduce the viscosity of contact crude oil by self-generation of heat under sunlight irradiation and then adsorb it by its own capillary force (as shown in Figure 22a). This is undoubtedly the most competitive green cleaning method as far as it is concerned.

For example, Wang et al.[136] used natural wood as a raw material to produce wood sponges by delignification and hemilignification. Then, a MXene was successfully loaded onto the surface of the wood sponge by impregnation to build a functional layer for photothermal conversion. Finally, PDMS was coated to achieve hydrophobization and enhance its mechanical stability. Compared with commercial sponges, this wood sponge has a vertical array of pore structure, which can enhance the capture of sunlight on the one hand and has a stronger capillary force on the other hand to realize the rapid cleaning of crude oil (Figure 22a). As shown in Figure 22a_2, the material can rapidly warm up to 66 °C at an irradiation intensity of 1.5 suns. In addition, an applied voltage can be applied to generate Joule heat, and experiments have shown that it can be rapidly warmed up to 80 °C at an applied voltage of only 4 V. Therefore, the material can be used for all-weather cleanup of crude oil spills at sea.

In addition to the natural wood sponges mentioned above, various commercial sponges have been used to composite MXenes to build three-dimensional structures for crude oil cleanup. This solution combines the photothermal conversion ability of the MXene material and the excellent mechanical properties of the 3D skeleton, giving it good cyclic stability and greater practical value in cleaning up crude oil spills at sea. Table S5 summarizes the various 3D MXene materials currently used for crude oil adsorption, including their

https://doi.org/10.1021/acs.iecr.3c00306
Ind. Eng. Chem. Res. 2023, 62, 7297−7335

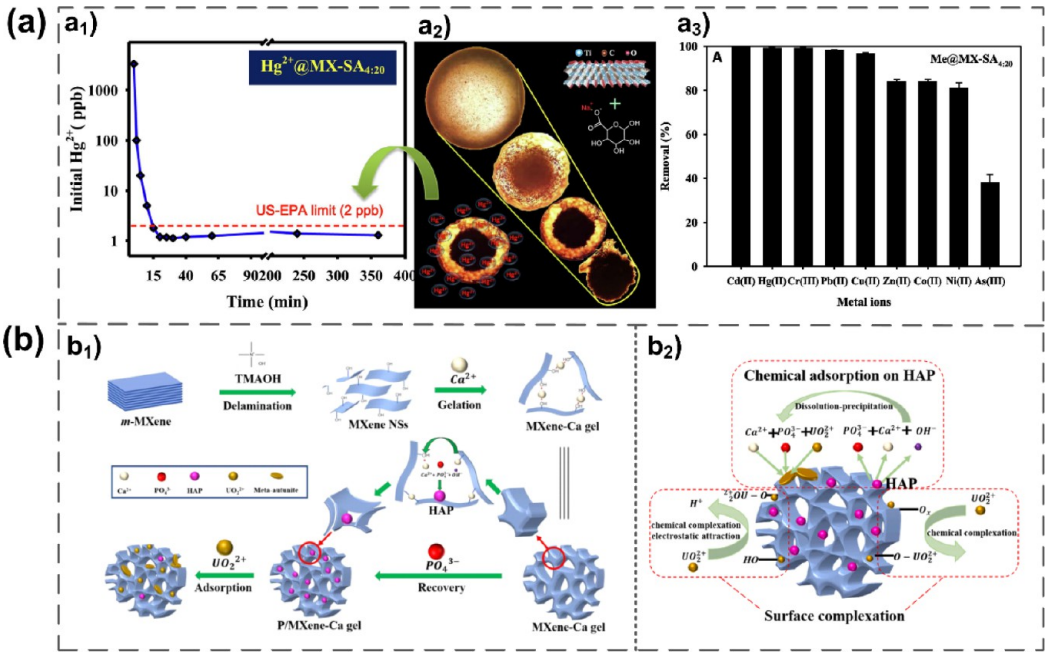

Figure 23. MXene 3D structure for the treatment of complex contaminants in water. (a) Adsorption of heavy metal ions by MXene/SA hybrid gel spheres. (Reproduced with permission from ref 176. Copyright 2019 Elsevier.) (a_1) Highly efficient adsorption capacity of MX-SA aerogel spheres for Hg^{2+}. (a_2) Structure diagram of MX-SA aerogel sphere. (a_3) Adsorption capacity of MX-SA4:20 in mixed ionic solutions. (b) MXene-Ca^{2+} gel for adsorption of phosphate and U(VI) in water. (Reproduced with permission from ref 177. Copyright 2021 Elsevier.) (b_1) Schematic diagram of the preparation of the composite gel and the adsorption of contaminants. (b_2) Schematic diagram of the mechanism of U(VI) adsorption by composite gel.

photothermal capabilities as well as their crude oil adsorption capacity.

4.2.4. MXene-Based Adsorbents for Complex Pollutants. The rapid development of industrial levels makes the water environment more and more complex and the variety of pollutants in water more and more; the single means of wastewater treatment seems to be stretched to the limit. The rich functionality of MXenes provides new inspiration for designing multifunctional all-weather wastewater treatment systems. Shahzad et al.[176] prepared core−shell structured aerogel spheres with outstanding adsorption capacity for Hg^{2+} using $Ti_3C_2T_x$ and sodium alginate (SA) as the main materials, as shown in Figure 23a. The gel spheres have a cage-like microstructure, as shown in Figure 23a_1, and provide high porosity and the largest possible specific surface area to effectively capture heavy metal ions in water, especially for Hg^{2+} with an adsorption capacity of 932.84 mg g^{-1}. Considering the complex water conditions in practical applications, for the mixed solution of eight metal ions in Figure 23a_3, the gel spheres still showed high adsorption capacity, especially for the five ions of Cd(II), Hg(II), Cr(III), Pb(II), and Cu(II), where the removal efficiency was greater than 90%. In addition, the material exhibits excellent adsorption efficiency in extreme situations (pH <0), as well as cycling stability. Notably, the unique three-dimensional structure of the material (small size spheres) makes it possible for large-scale applications (column packing devices) with continuous operation. This suggests that the available specific surface area can be effectively increased by constructing a three-dimensional porous structure to promote the adsorption efficiency.

In addition to heavy metal ions, the three-dimensional structure of a MXene can also be used to adsorb pollutants such as radionuclides from water due to its inherent excellent resistance to radiation. In addition, phosphate tends to cause eutrophication of water bodies and break the ecological environment, and it also needs to be cleaned up as much as possible. As shown in Figure 23b, He et al.[177] used Ca^{2+} to break the electrostatic equilibrium between MXene nanosheets, thus assembling a 3D MXene gel. This MXene gel cross-linked by Ca^{2+} ions has an excellent adsorption performance for phosphate in water.

It is noteworthy that phosphate and Ca^{2+} in the system react in the presence of OH^- to form hydroxyapatite (HAP) precipitates, which resulted in the formation of a complex gel with an extremely high affinity for U(VI) after adsorption of phosphate and showed an adsorption capacity of up to 823.6 mg g^{-1} (Figure 23b_2). This strategy provides an effective method for the removal of phosphate and U(VI) from water.

In summary, the rich functionality of a MXene itself gives it the potential to handle complex contaminants. In addition, by constructing a three-dimensional porous structure, it can not only be compounded with other functional materials for special applications but also be used to adsorb insoluble oils and the like, which greatly expands the application scope of MXene-based functional materials.

4.2.5. Cycling Stability of MXene-Based Adsorbents. The recycling performance of the adsorbent is also a key concern. Conventional adsorbents in powder form are not only difficult to recycle but also prone to secondary contamination. The assembled three-dimensional structure of the adsorbent can avoid this problem, which is not only safe and environmentally friendly but also highly cost-effective. For example, Yang et al.[90] cross-linked MXene nanosheets with GO nanosheets by EDA, thus preparing a three-dimensional porous foam that exhibited an excellent adsorption capacity for insoluble oil

https://doi.org/10.1021/acs.iecr.3c00306
Ind. Eng. Chem. Res. 2023, 62, 7297−7335

phases and heavy metal ions at room temperature and also showed an excellent recycling performance. Experiments showed that only a simple ethanol wash was required to complete the desorption, and the mass of residual pollutants after each cycle was less than 0.5% in 10 adsorption cycles of the material for phenoxin; the adsorption amount was stable at 165 mg g^{-1} in 10 adsorption cycles for Pb^{2+}.

The three-dimensional material with excellent mechanical stability is even more crucial for the adsorption of insoluble oil and other contaminants. For example, Cai et al.[175] fabricated hydrophobic MXene porous aerogels by combining aqueous polyurethane (WPU) with a MXene and functionalized cellulose crystals using a unidirectional freeze casting technique (Figure 22b).

As shown in Figure 22b_2,b_3, the aerogel exhibited stable hydrophobicity and excellent mechanical properties. Thus, the material exhibits high adsorption of light oil contaminants in water and it shows an efficient uptake of 24.5 g g^{-1} for ultraviscous crude oil under a single solar irradiation due to its efficient photothermal conversion capability. More importantly, due to its excellent cycling stability, continuous adsorption of sea surface crude oil can be achieved by a squeeze cycle or peristaltic pumping. All these examples show that, by assembling MXene into a 3D porous foam, it is beneficial to enhance its adsorption performance and, more importantly, it can effectively recover and recycle the adsorbent, which provides a basis for its industrial application.

4.3. Photocatalytic Degradation. With booming industry, more and more pollutants are being discharged into groundwater, rivers, oceans, and other water sources. In particular, pharmaceuticals such as organic dyes and antibiotics are released into the natural environment at will, posing a serious threat to human health and the ecological environment.

To date, many wastewater treatment methods, such as adsorption, sedimentation, membrane technology, biological treatment, and photocatalytic degradation, have been developed to treat various pollutants from wastewater.[178,179] However, these methods have problems such as low efficiency and easy secondary pollution. In recent years, photocatalytic degradation of organic materials by semiconductors under light illumination is undoubtedly the most attractive strategy for wastewater treatment because it can decompose organic substances into environmentally benign substances such as water, CO_2, and inorganic materials. It is an efficient and convenient method that does not require cumbersome post-treatment and can completely clean up pollutants.

4.3.1. Photocatalytic Degradation Mechanism. The commonly used photocatalysts are various semiconductor materials, which generally have a narrow band gap (E_g). In a typical procedure, when the incident light energy absorbed by the catalyst is greater than or equal to its own band gap, electrons can be excited from the valence band (VB) to the conduction band (CB), thus producing photogenerated electrons with high activity in the conduction band, leaving positively charged holes in the valence band. Subsequently, these photogenerated electrons react with the holes and the water and oxygen bound on the catalyst surface to generate hydroxyl radicals ($OH^•$), anionic superoxide ions (O^{2-}), and other active substances. These active substances are capable of redox reactions with pollutants adsorbed on the surface of semiconductors, thus degrading them to inorganic substances.[180−182]

Currently, conventional semiconductor photocatalysts suffer from various defects and tend to utilize only short wavelengths of UV light, which leads to their low photocatalytic degradation capacity in visible light. More importantly, although conventional semiconductor materials (e.g., TiO_2, silver-based semiconductors) have high catalytic degradation abilities, their inevitable rapid compounding of photogenerated electrons and holes and insufficient active sites lead to low degradation efficiency.[183−185]

The introduction of a cocatalyst is a strategy to effectively improve photocatalytic efficiency, and its role is mainly reflected in the following two aspects: (i) the cocatalyst has abundant photogenerated carrier trap positions and exhibits good electrical conductivity, which can effectively extract electrons from the photocatalyst to achieve the separation of electrons and holes;[186,187] (ii) the cocatalyst facilitates the reduction of the reaction activation energy and thus accelerates the degradation reaction.[188]

However, the widely used cocatalysts are generally precious metals (Au, Pt, Pd, Ru, etc.) and metal oxides (MnO_x, CoO_x, RuO_2, etc.).[189,190] These materials are costly and also do not fully meet the requirements of the cocatalyst.

As mentioned earlier, the unique electronic properties of a MXene as well as its hydrophilicity make it an ideal cocatalyst for the photocatalytic degradation of pollutants in water (Figure 24).[191,192] The salient features of a MXene as a

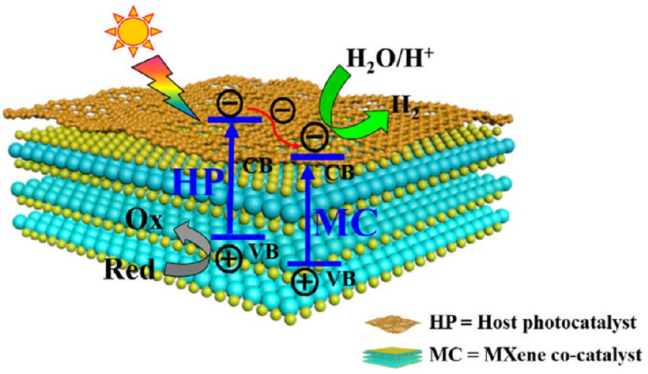

Figure 24. Schematic diagram of the photocatalytic mechanism of MXene-based photocatalyst. (Reproduced from ref 192. Copyright 2019 American Chemical Society.)

cocatalyst are highlighted as follows: (1) The two-dimensional morphology of the MXene itself and its ultrahigh conductivity facilitate the quick detachment and migration of photogenerated electrons and holes. (2) Exposed titanium metal on the surface of the MXene may provide a stronger redox site for photocatalysis, giving it greater oxidative reactivity than conventional carbon materials.[193] (3) The abundant surface functional groups contained on MXene nanosheets benefit its complexation with semiconductor photocatalysts, thus building heterogeneous structures to enhance interfacial charge transfer. In addition, it can also make it have good hydrophilicity and make it more suitable for degrading pollutants in water.[72,194−197]

Therefore, combining MXenes with conventional semiconductor catalysts and constructing three-dimensional network structures to synergistically promote their photocatalytic degradation abilities is an effective strategy to build high-performance photocatalysts. The advantages of 3D networks in the field of photocatalysis are mainly reflected in the following

https://doi.org/10.1021/acs.iecr.3c00306
Ind. Eng. Chem. Res. 2023, 62, 7297−7335

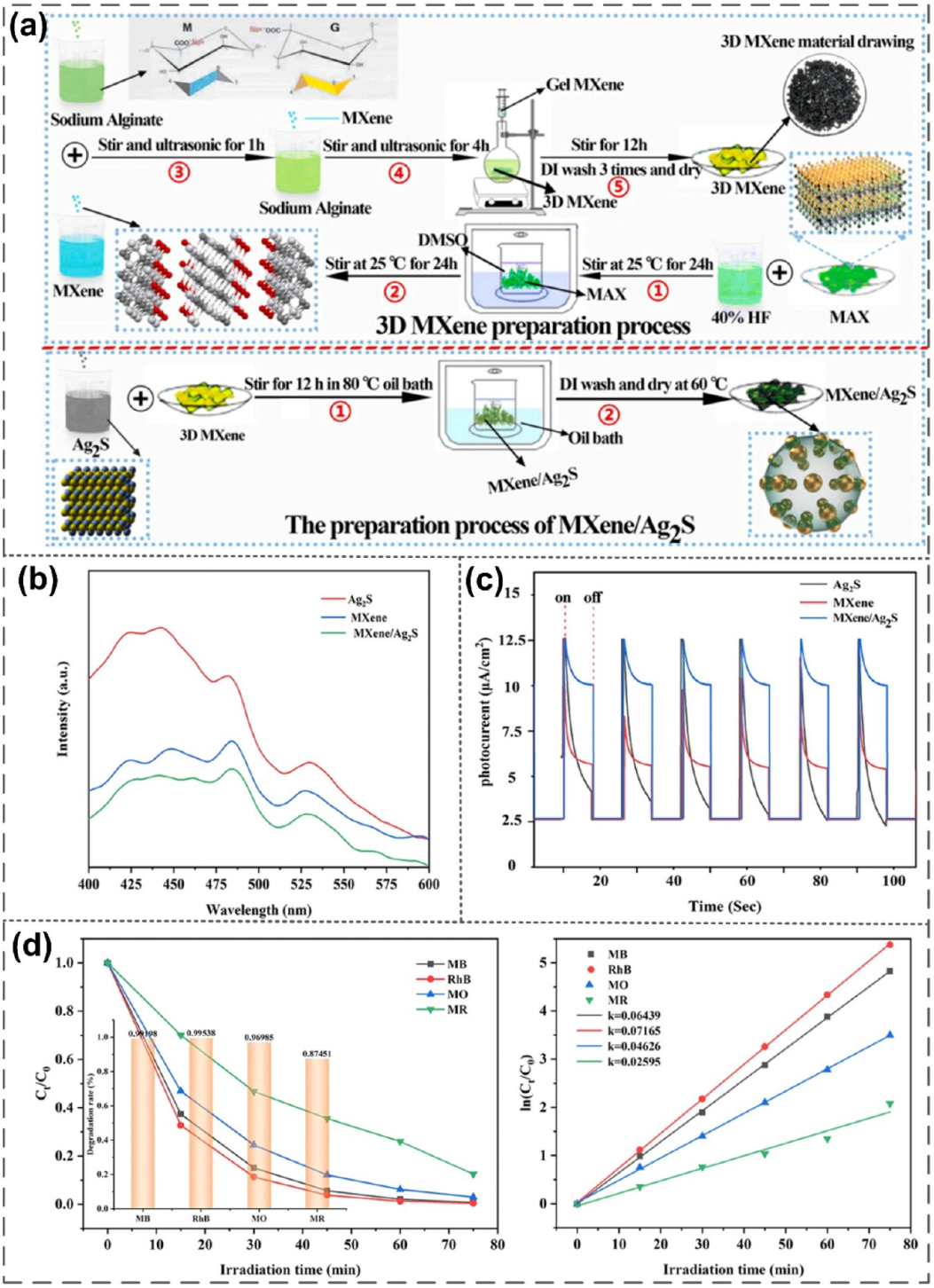

Figure 25. Schottky junction MXene/Ag_2S catalyst for photocatalytic degradation of pollutants. (Reproduced with permission from ref 183. Copyright 2021 Elsevier.) (a) Schematic diagram of the synthesis of 3D MXene as well as Ag_2S/MXene. (b) Comparison of the photoluminescence (PL) spectra of the composite catalyst with Ag_2S and MXene at 320 nm excitation wavelength shows that the structural design of the catalyst effectively reduces the complexation of photogenerated carriers. (c) Transient photocurrent response of different catalyst materials under visible light irradiation (>420 nm). (d) Ability of the MXene/Ag_2S catalyst to degrade the four mixed dyes in visible light, with the corresponding degradation curves and rate constants on the right.

aspects: (1) The networks have a larger specific surface area, which can promote the adsorption of contaminants. As mentioned earlier, in multiphase photocatalytic systems, the redox reactions for degrading pollutants occur mainly on the catalyst surface.[198] The adsorption ability of pollutants on the surface of the photocatalyst is improved, which helps to promote the photocatalytic degradation reaction. (2) The interconnected porous structure in the three-dimensional network provides a complete conductive network as well as a multidimensional electron transport path, which shortens the carrier migration distance from the generation center to the surface effectively, thus improving the charge carrier transport

https://doi.org/10.1021/acs.iecr.3c00306
Ind. Eng. Chem. Res. 2023, 62, 7297−7335

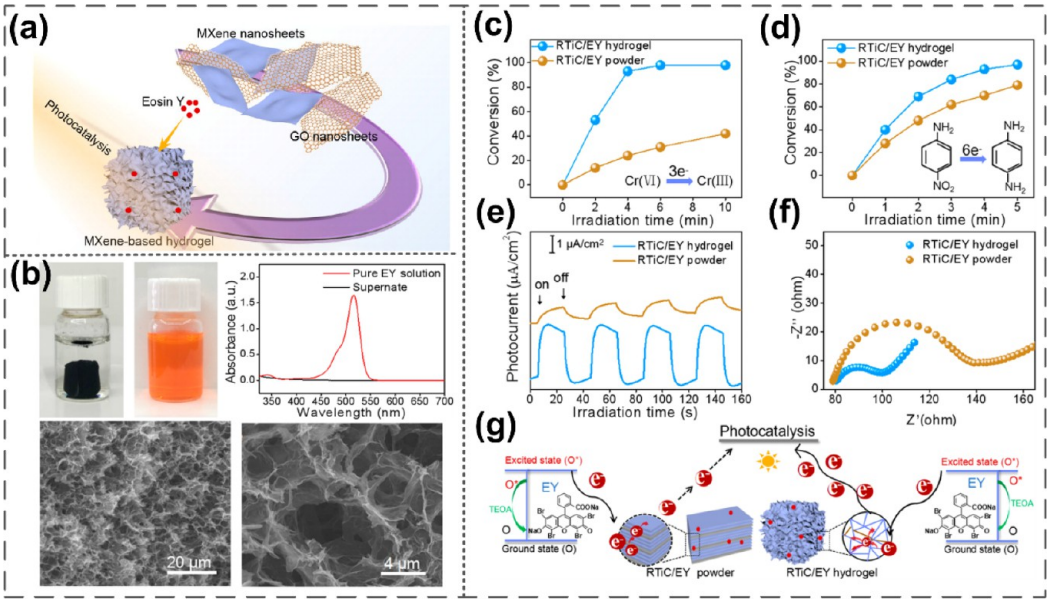

Figure 26. $Ti_3C_2T_x$-based three-dimensional hydrogel (RTiC) for enhanced photocatalytic redox process. (Reproduced from ref 19. Copyright 2019 American Chemical Society.) (a) Schematic diagram of RTiC complexed with Eosin Y for enhanced photocatalysis. (b) Characterization of functional RTiC/EY hydrogels. The digital photograph shows the supernatant after EY was immobilized compared with the pure EY solution (orange). The UV absorption curves of the supernatant and the pure EY solution are shown on the upper right, indicating that EY was completely immobilized on the hydrogel backbone. The SEM images (lower) show that the loading of EY did not affect the three-dimensional porous structure of the hydrogel. (c, d) Photocatalytic activity of RTiC/EY hydrogel. (e) Instantaneous photocurrent response test and (f) electrochemical impedance spectroscopy Nyquist plots of functional composite hydrogel and RTiC/EY composite powder. (g) Schematic diagram of RTiC/EY hydrogel and RTiC/EY powder photocatalytic mechanism.

efficiency and effectively suppressing the rapid compounding of photogenerated electrons and holes.

4.3.2. Photocatalytic Degradation for Pollutants. Based on the above principles, a study has prepared $Ti_3C_2T_x$-MXene (001-T/MX) modified with heterostructured derivatives of TiO_2 crystalline surface using a simple hydrothermal treatment.[20] In this system, 2D $Ti_3C_2T_x$ nanosheets were used as a substrate for loading photocatalyst TiO_2, and the Ti atoms on Ti_3C_2 acted as nucleation sites. Thus, the interfacial heterojunction formed at the atomic scale between the in situ generated TiO_2 and Ti_3C_2 nanosheets helps to decrease the defect-induced complexation of photoexcited charge carriers. This material is capable of decomposing the organic dyes methyl orange (MO)[199] and rhodamine B (RhB),[200] under light conditions, the drug carbamazepine (CBZ),[136,201] and other contaminants.

However, the restacking of 2D nanomaterials in water is still a nonnegligible problem. It leads to the loss of active sites and also limits the effective separation of photogenerated electrons from holes, which greatly reduces the photocatalytic degradation efficiency. The construction of three-dimensional structural networks used as a substrate platform for photocatalytic reactions is a feasible solution to the above problem. For example, Feng et al.[183] first prepared 3D MXene gel spheres by using sodium alginate (SA) to assist MXene assembly. With this as a substrate, a homogeneous 3D MXene/Ag_2S Schottky junction catalyst was constructed by depositing Ag_2S catalyst onto its surface through chemical sedimentary and electrostatic self-assembly strategies, as shown in Figure 25a. Due to the effective scattering of incident light by the uniform microstructure of the surface, the visible light absorption ability of this material is significantly better than that of the pristine Ag_2S catalyst. The nonhomogeneous catalysts prepared by this strategy not only exhibit a decreased apparent band gap but also are able to promote the effective separation of photogenerated carriers. The lower photoluminescence (PL) spectroscopy signal in Figure 25b indicates that the structure effectively reduces the charge carrier complexation, mainly attributed to the charge transfer mechanism of the Schottky structure and the synergistic effect of the silver ion plasmon resonance effect. The excellent photocurrent sensitivity of the MXene/Ag_2S material in Figure 25c also illustrates this issue. It is noteworthy that, after six cycles, the photocurrent of the material does not change significantly, indicating its stable photoelectrochemical properties. This special structural design effectively solves the problem of the extremely high charge carrier complexation rate brought about by the silver-based semiconductor due to its own very low potential in the conduction band.

Therefore, MXene/Ag_2S catalysts have better photocatalytic degradation efficiency for organic dyes and antibiotics (as shown in Figure 25d). It is worth pointing out that the three-dimensional structure design makes it different from other powder photocatalysts, with better recyclability and recycling performance.

In addition, Chen et al.[19] constructed a three-dimensional MXene/rGO hydrogel as well as a powder of this composite, added the photosensitive catalyst Eosin Y (EY) to both (Figure 26a–c), and found that the hydrogel photocatalytic performance improved with increasing MXene content. As shown in Figure 26d, under 10 min visible light irradiation, RTiC/EY hydrogels were effective in reducing 99.3% of Cr(VI) as well as enabling 97% photocatalytic hydrogenation of 4-nitroaniline (4-NA). In contrast, the photocatalytic degradation function of the 3D skeleton was better than that of the composite powder in both cases. To explain the above phenomenon, the transient

https://doi.org/10.1021/acs.iecr.3c00306
Ind. Eng. Chem. Res. 2023, 62, 7297−7335

photocurrent response of MXene/rGO composite hydrogel with added EY and MXene/rGO composite powder was tested, as shown in Figure 26e. The transient photocurrent response of the photocatalyst with the composite hydrogel as the matrix was significantly increased, which indicates that the photogenerated carriers generated by the catalyst achieve rapid migration and separation in the conductive three-dimensional network. The Nyquist curve shown in Figure 26f similarly confirms that the 3D hydrogel suppresses the complexation of photogenerated carriers more effectively.

In summary, the RTiC/EY hydrogel catalyst prepared by this strategy can provide a multidimensional electron transfer pathway, thus facilitating the effective separation of photogenerated electrons from holes. In addition, the large specific surface area provided by the three-dimensional porous structure effectively promotes the adsorption of pollutants, thus facilitating the photocatalytic degradation reaction. Therefore, the functional hydrogel has a more outstanding photocatalytic efficiency compared to EY.

At present, there are relatively few studies to achieve efficient photocatalytic degradation by constructing 3D MXene/semiconductor structures. It is clear from the above studies that this preparation strategy/route has great research value as well as application potential. Table S6 summarizes the current studies to improve the photocatalytic degradation performance of the 3D MXene-based materials.

5. MXene-BASED MEMBRANES FOR WASTEWATER TREATMENT AND DESALINATION

Membrane technology is a water purification technology that has been developing rapidly in recent years. Compared with traditional adsorption, sedimentation, and biological treatments, it has advantages such as good water purification effect and green energy saving. However, traditional separation membranes often have defects such as easy contamination, swelling, and instability, while MXenes are ideal materials for building advanced separation membranes due to their activated metal hydroxide sites, surface functionalities, high hydrophilicities, high specific surface areas, and high adsorption reduction capacities. These makes them have potential for application in wastewater treatment and seawater desalination.

Aiming for wastewater treatment, MXenes can be used to prepare separation membrane materials with defined size nanochannels for the treatment of an insoluble oil phase, heavy metal ions, dyes, and other contaminants in water. For example, Zeng et al.[202] constructed a Hal@MXene-PDA composite membrane for oil−water separation using halloysite nanotubes as well as poly(dopamine) to synergistically modify the MXene. In this work, PDA can be used for cross-linking between the MXene and Hal nanomaterials, which results in stronger adhesion on the support layer and improves the swelling resistance of the membrane in solution. In addition, the reducing property of PDA prevents the MXene from being oxidized, and the large number of oxygen-containing functional groups on the Hal and PDA structures help improve the hydrophilicity of the composite membrane. As a result, the composite membrane exhibits a pure water flux of up to 5036.2 L m^{-2} h^{-1} bar^{-1} and shows a retention efficiency of up to 99.8% for oil-in-water emulsions. In addition, it exhibits good resistance to oil contamination due to its good hydrophilic/strong surface.

The removal of water-soluble dyes and other small molecule contaminants is more problematic than oil−water emulsions. The trade-off between permeate flux and retention efficiency has been the focus of membrane separation technology. To address this, Ma et al.[203] constructed a layered membrane material for the removal of various dyes from water by assembling small-sized graphene oxide nanosheets layer by layer on a substrate material and inserting MXene nanosheets between the layers. The small size of these nanosheets allows for shorter and more direct transport channels, while the MXene intercalation layer allows for wider layer spacing. As a result, high permeate flux and high retention efficiency can be achieved simultaneously when removing dyes from water. The material is reported to be capable of achieving a pure water flux of 136.68 L m^{-2} h^{-1} bar^{-1} and retaining over 99.99% of various dyes. It also has excellent antiswelling stability and is suitable for wastewater treatment tasks in harsh environments.

As for the desalination field, the stacking of two-dimensional (2D) nanomaterials into laminar membranes is a promising technology to achieve high selectivity and permeability in seawater desalination. MXenes have ultrahigh water permeabilities due to their excellent hydrophilicities coupled with atomic lamellar structures. In addition, the layered structures of MXenes allow the design of nanochannels with ideal dimensions, and the surfaces of MXenes also contain a large number of negatively charged groups. In summary, the laminar membranes constructed by MXene materials are very suitable for separating hydrated ions for seawater desalination.

However, the poor rejection performance of MXene-based 2D membrane materials for monovalent metal ions still poses a considerable challenge for membrane materials applied in seawater desalination. The reasons for this are analyzed: first, membrane materials tend to swell in water, leading to an increase in the layer spacing; second, monovalent ions can be more easily inserted between the layers of the laminar membrane and adsorbed on its surface to form a bilayer, further expanding the layer spacing; in addition, the electrostatic interaction between monovalent ions and MXene membranes is relatively weak.

To solve the above problems, researchers have made many attempts. First, it was Ding et al. who innovatively fabricated a swelling-resistant Al^{3+} intercalated MXene membrane with a high retention efficiency of up to 96.5% for NaCl solution and a permeate flux of 2.8 m^{-2} h^{-1}, which is of superb application in seawater desalination.[204] Lu et al.[205] prepared a self-cross-linked MXene film, which, through a simple heat treatment, formed Ti−O−Ti bonds by using the hydroxyl groups on adjacent nanosheets to self-cross-link. It has excellent rejection of monovalent metal ions and an excellent antiswelling property, and it can operate continuously and stably for 70 h. In addition, MXene-based 2D films are also commonly used for solar-powered desalination due to their own excellent photothermal conversion properties.[206] However, compared to three-dimensional materials, two-dimensional planar structures result in low solar light capture due to stronger light reflection.

In summary, due to the 2D nanomorphology and many excellent properties of MXene, MXene-based 2D films can realize the separation of pollutants (including insoluble oil phase, organic dyes, and metal ions) in water based on size sieving and electrostatic interactions and have great potential for application in wastewater treatment and seawater desalination. However, there are many problems in applying MXene-based 2D films for wastewater treatment and desalination. For example, the low flux leads to low treatment efficiency, the short pore channel is easily fouled, and the

https://doi.org/10.1021/acs.iecr.3c00306
Ind. Eng. Chem. Res. 2023, 62, 7297−7335

environmental instability of MXenes is also an important factor affecting their large-scale application.

6. CONCLUSION AND OUTLOOK

The development of wastewater treatment and water reclamation means is an effective way to solve today's water scarcity problems. Here, we present an objective review of MXene materials and their innovative work in the fields of wastewater treatment and water reclamation. First, we introduce the synthesis pathways and excellent properties of MXenes and explain the feasibility of MXene materials for wastewater treatment and water reclamation, including large aspect ratios, abundant surface groups, customizable surfaces, and outstanding photothermal conversion properties. Second, we focus on the assembly strategy based on the 3D structure of MXene materials and summarize its recent progress in the fields of wastewater treatment and water reclamation (mainly pollutant adsorption, photocatalytic degradation, and desalination). By assembling MXenes into 3D porous structures, it is possible to build multiscale pore channels and effectively suppress the tendency of nanosheet restacking. Undoubtedly, after rapid development in recent years, MXene-based 3D porous materials have shown remarkable results in terms of their application properties and mechanisms in various applications including water treatment.

However, compared with other nanomaterials, the research on MXenes and their 3D structures is still at the initial stage; especially there is a big gap between the initial design of 3D MXene-based materials for wastewater treatment and their subsequent practical applications. Therefore, there are still many problems and challenges to be solved for 3D MXene materials applied in wastewater treatment and water reclamation.

6.1. Mass Production of High Quality MXene. The fluorine-free preparation of MXenes and the industrial production of MXenes are still two of the main focuses of research. The currently used fluorinated nanosheets still have the possibility of secondary contamination in wastewater treatment; therefore, fluorine-free high-quality MXene nanosheets for wastewater treatment applications are worth being expected. Although many emerging strategies for fluorine-free syntheses of MXenes have been developed, such as electrochemical etching and acoustic wave assisted etching, it is how to solve the problem of their high cost that is the key to promoting their further industrialization. Also, how to develop a green and safe production route and transfer them from the laboratory to the factory for mass production while ensuring the quality of MXenes is also a main challenge of concern.

6.2. Poor Stability of the 3D MXene-Based Structures. The mechanical stability of a MXene is often unsatisfactory due to the weak gelation ability of the MXene itself, which leads to weak interaction between the lamellae in the MXene 3D structure and the limited contact area of the connection. Currently, the addition of other components during the assembly process to enhance the mechanical stability is a common solution strategy. However, the addition of other components may cause the loss of some of the excellent properties of MXenes, such as electrical conductivity and photothermal conversion properties. Therefore, how to grasp the relationship between material properties and structure and achieve the joint optimization of material stability and application performance is the key to improving their mechanical properties. In addition, MXenes are very fragile and their high surface energies make them highly susceptible to oxidation in water/oxygen-rich environments, which affects the application of MXene-based functional materials in the field of wastewater treatment. How to enhance the oxidation resistance of MXenes in long-term use is a key issue.

6.3. Large-Scale Preparation of 3D MXene Functional Materials Is Difficult. In practical applications, it is still challenging to obtain highly tunable 3D MXene porous materials in an efficient and scalable manner. A variety of assembly strategies have been developed that require precise and complex experimental conditions. For example, the ice template method requires precise control of the freezing direction and rate; 3D printing requires ultrahigh MXene dispersion concentration. These factors pose problems for the large-scale preparation of 3D MXene functional materials. In addition, the excellent application performance of 3D MXene functional materials is often closely related to their structures; however, how to ensure the structural stability of the materials in the large-scale preparation is of great significance for their industrial applications.

6.4. The Mechanism of Application in the Direction of Water Treatment Is Not Fully Understood. MXene-based 3D porous materials have made considerable progress in the field of wastewater treatment. However, at present, the specific mechanism is still not completely clear. For example, the photothermal conversion mechanism of a MXene is usually considered to be the LSPR effect. However, due to the diversity of surface group types and arrangements, there also exist semimetallic MXenes, and the photothermal conversion mechanism of such MXenes cannot be explained by the LSPR effect. In addition, the current 3D MXene functional materials applied in the field of wastewater treatment are basically based on $Ti_3C_2T_x$, while the research and development of other members of the MXene family are still relatively few. Researchers should further focus on the mechanistic study of MXenes in the field of wastewater treatment, so as to select or tailor suitable MXene materials from the demand perspective instead of the single selection of $Ti_3C_2T_x$.

In this regard, many efforts have been made, for example, (1) the preparation of bare MXenes and MXenes with special surface functional groups through specific synthetic strategies, (2) the dispersion of MXenes in suitable polymer networks to improve the overall mechanical and chemical stabilities of the materials, and (3) the ease of compounding with other functional materials to expand the functionalities of the materials for applications.

Besides, the future development trends in this field will be focused on the exploitation of the 3D MXene functional materials featuring excellent application versatility and stability in the water treatment field. MXene functional materials that can simultaneously treat wastewater and regenerate seawater resources have very great design potential, and this versatility expands the access to drinking water from the environment. The full exploitation of MXene functionalities for the preparation of all-weather multifunctional water purification materials is the focus of future research.

In addition, the outstanding electrical conductivities of MXenes makes their performance in photovoltaic devices very bright, and some byproducts in the process of wastewater treatment and water resource regeneration, such as waste heat power generation and steam power generation, also have important research value. These multidisciplinary integrations and collaborations enable researchers to fully and effectively

https://doi.org/10.1021/acs.iecr.3c00306
Ind. Eng. Chem. Res. 2023, 62, 7297−7335

utilize MXenes and provide novel ideas for future development in several fields.

■ ASSOCIATED CONTENT

Supporting Information

The Supporting Information is available free of charge at https://pubs.acs.org/doi/10.1021/acs.iecr.3c00306.

Advantages and disadvantages of various MXene preparation methods and MXene assembly strategies; summaries of desalination performances of MXene electrodes in CDI, solar evaporation performances of 3D MXene evaporators, photothermal performances of 3D MXene composites and their crude oil adsorption capacities, and photocatalytic degradation performances of 3D MXene structures (PDF)

■ AUTHOR INFORMATION

Corresponding Authors

Guangfa Zhang − *Key Laboratory of Rubber-Plastics, Ministry of Education/Shandong Provincial Key Laboratory of Rubber-Plastics, School of Polymer Science and Engineering, Qingdao University of Science & Technology, Qingdao 266042, People's Republic of China;* orcid.org/0000-0002-8632-1264; Email: gfzhang@qust.edu.cn

Yehai Yan − *Key Laboratory of Rubber-Plastics, Ministry of Education/Shandong Provincial Key Laboratory of Rubber-Plastics, School of Polymer Science and Engineering, Qingdao University of Science & Technology, Qingdao 266042, People's Republic of China;* orcid.org/0000-0002-3235-4247; Email: yhyan@qust.edu.cn

Authors

Yuekang Zhang − *Key Laboratory of Rubber-Plastics, Ministry of Education/Shandong Provincial Key Laboratory of Rubber-Plastics, School of Polymer Science and Engineering, Qingdao University of Science & Technology, Qingdao 266042, People's Republic of China*

Shuai Zhao − *Key Laboratory of Rubber-Plastics, Ministry of Education/Shandong Provincial Key Laboratory of Rubber-Plastics, School of Polymer Science and Engineering, Qingdao University of Science & Technology, Qingdao 266042, People's Republic of China*

Ailin Gao − *Key Laboratory of Rubber-Plastics, Ministry of Education/Shandong Provincial Key Laboratory of Rubber-Plastics, School of Polymer Science and Engineering, Qingdao University of Science & Technology, Qingdao 266042, People's Republic of China*

Jian Cui − *Key Laboratory of Rubber-Plastics, Ministry of Education/Shandong Provincial Key Laboratory of Rubber-Plastics, School of Polymer Science and Engineering, Qingdao University of Science & Technology, Qingdao 266042, People's Republic of China*

Complete contact information is available at: https://pubs.acs.org/10.1021/acs.iecr.3c00306

Notes

The authors declare no competing financial interest.

■ ACKNOWLEDGMENTS

The authors thank the National Natural Science Foundation of China (No. 51703113) and the Open Project of Key Laboratory of Rubber-Plastic Materials and Engineering of Ministry of Education (Qingdao University of Science and Technology, No. KF2020004) for financial support of this work.

■ ABBREVIATIONS

CDI = capacitive deionization
DFT = density functional theory
MILD = minimum intensity layer delamination
TMA-OH = tetramethylammonium hydroxide
CVD = chemical vapor deposition
SEM = scanning electron microscope
RP = red phosphorus
LSPR = localized surface plasmon resonance
PTT = photothermal therapy
PMMA = poly(methyl methacrylate)
PS = polystyrene
MF = melamine foam
GO = graphene oxide
rGO = reduced graphene oxide
PAN = polyacrylonitrile
PEO = poly(ethylene oxide)
RO = reverse osmosis
EDLC = electrochemical double-layer capacitance
SAR = salt adsorption rate
Co-MOF = cobalt metal−organic framework
PZC = point of zero charge
PNIPAM = poly(*N*-isopropylacrylamide)
Cu(II) = copper ion
Hg(II) = mercury ion
Cd(II) = cadmium ion
CPCM = chitosan-based porous carbon microspheres
WPU = waterborne polyurethane
CB = conduction band
RhB = rhodamine B
SA = sodium alginate
Hal = halloysite nanotubes
SAW = surface acoustic waves
ACN = acetonitrile
DMF = *N*,*N*-dimethylformamide
DMSO = dimethyl sulfoxide
PC = propylene carbonate
NMP = *N*-methyl-2-pyrrolidone
ISFC = ice structure freeze casting
PVA = poly(vinyl alcohol)
POSS-NH_2 = amine-functionalized polyhedral oligomeric sesquisiloxane
CTAB = cetyltrimethylammonium bromide
EDA = ethylenediamine
3DFP = 3D freeze printing
IRM = interference reflection microscopy
PDMS = polydimethylsiloxane
PU = polyurethane
MD = membrane distillation
SAC = salt adsorption capacity
EY = Eosin Y
CLF = cellulose fibers
Co−CNS/M foam = cobalt nanoparticles (CoNPs)−carbon nanosheets/MXene foam
LCST = lower critical solution temperature
Pb(II) = lead ion
U(VI) = uranium ion
Cr(III) = chromium ion

https://doi.org/10.1021/acs.iecr.3c00306
Ind. Eng. Chem. Res. 2023, 62, 7297−7335

3D-MXOF = MXene/metal−organic framework decorated with three-dimensional (3D) printed lattice structure
MOF = metal−organic framework
VB = valence band
MO = methyl orange
CBZ = carbamazepine
PL = photoluminescence
4-NA = 4-nitroaniline

REFERENCES

(1) Alam, I.; Guiney, L. M.; Hersam, M. C.; Chowdhury, I. Pressure-driven water transport behavior and antifouling performance of two-dimensional nanomaterial laminated membranes. *J. Membr. Sci.* **2020**, *599*, 117812.

(2) Ihsanullah, I. MXenes (two-dimensional metal carbides) as emerging nanomaterials for water purification: Progress, challenges and prospects. *Chem. Eng. J.* **2020**, *388*, 124340.

(3) Dixit, F.; Zimmermann, K.; Dutta, R.; Prakash, N. J.; Barbeau, B.; Mohseni, M.; Kandasubramanian, B. Application of MXenes for water treatment and energy-efficient desalination: A review. *J. Hazard. Mater.* **2022**, *423*, 127050.

(4) Naguib, M.; Kurtoglu, M.; Presser, V.; Lu, J.; Niu, J.; Heon, M.; Hultman, L.; Gogotsi, Y.; Barsoum, M. W. Two-dimensional nanocrystals produced by exfoliation of Ti_3AlC_2. *Adv. Mater.* **2011**, *23* (37), 4248−4253.

(5) Karahan, H. E.; Goh, K.; Zhang, C. J.; Yang, E.; Yildirim, C.; Chuah, C. Y.; Ahunbay, M. G.; Lee, J.; Tantekin-Ersolmaz, S. B.; Chen, Y.; Bae, T. H. MXene Materials for Designing Advanced Separation Membranes. *Adv. Mater.* **2020**, *32* (29), 1906697.

(6) Levi, M. D.; Lukatskaya, M. R.; Sigalov, S.; Beidaghi, M.; Shpigel, N.; Daikhin, L.; Aurbach, D.; Barsoum, M. W.; Gogotsi, Y. Solving the Capacitive Paradox of 2D MXene using Electrochemical Quartz-Crystal Admittance and In Situ Electronic Conductance Measurements. *Adv. Energy Mater.* **2015**, *5* (1), 1400815.

(7) Zhang, J.; Kong, N.; Uzun, S.; Levitt, A.; Seyedin, S.; Lynch, P. A.; Qin, S.; Han, M.; Yang, W.; Liu, J.; Wang, X.; Gogotsi, Y.; Razal, J. M. Scalable Manufacturing of Free-Standing, Strong $Ti_3C_2T_x$ MXene Films with Outstanding Conductivity. *Adv. Mater.* **2020**, *32* (23), 2001093.

(8) Zhang, Q.; Yi, G.; Fu, Z.; Yu, H.; Chen, S.; Quan, X. Vertically Aligned Janus MXene-Based Aerogels for Solar Desalination with High Efficiency and Salt Resistance. *ACS Nano* **2019**, *13* (11), 13196−13207.

(9) Othman, Z.; Mackey, H. R.; Mahmoud, K. A. A critical overview of MXenes adsorption behavior toward heavy metals. *Chemosphere* **2022**, *295*, 133849.

(10) Sun, X.; Jia, X.; Yang, J.; Wang, S.; Li, Y.; Shao, D.; Song, H. MXenes—An Emerging Class of 2D Materials for Solar Water Desalination: Feasibility and Recent Advances. *Sol. RRL* **2022**, *6* (2), 2100888.

(11) Murali, G.; Reddy Modigunta, J. K.; Park, Y. H.; Lee, J. H.; Rawal, J.; Lee, S. Y.; In, I.; Park, S. J. A Review on MXene Synthesis, Stability, and Photocatalytic Applications. *ACS Nano* **2022**, *16* (9), 13370−13429.

(12) Li, K.; Liang, M.; Wang, H.; Wang, X.; Huang, Y.; Coelho, J.; Pinilla, S.; Zhang, Y.; Qi, F.; Nicolosi, V.; Xu, Y. 3D MXene Architectures for Efficient Energy Storage and Conversion. *Adv. Funct. Mater.* **2020**, *30* (47), 2000842.

(13) Wu, Z.; Shang, T.; Deng, Y.; Tao, Y.; Yang, Q. H. The Assembly of MXenes from 2D to 3D. *Adv. Sci.* **2020**, *7* (7), 1903077.

(14) Li, K.; Li, J.; Zhu, Q.; Xu, B. Three-Dimensional MXenes for Supercapacitors: A Review. *Small Methods.* **2022**, *6* (4), 2101537.

(15) Bao, W.; Tang, X.; Guo, X.; Choi, S.; Wang, C.; Gogotsi, Y.; Wang, G. Porous Cryo-Dried MXene for Efficient Capacitive Deionization. *Joule* **2018**, *2* (4), 778−787.

(16) Wu, Z.; Deng, W.; Tang, S.; Ruiz-Hitzky, E.; Luo, J.; Wang, X. Pod-inspired MXene/porous carbon microspheres with ultrahigh adsorption capacity towards crystal violet. *Chem. Eng. J.* **2021**, *426*, 130776.

(17) Li, L.; Zhang, M.; Zhang, X.; Zhang, Z. New Ti_3C_2 aerogel as promising negative electrode materials for asymmetric supercapacitors. *J. Power Sources* **2017**, *364*, 234−241.

(18) Chen, Z.; Ding, Z.; Chen, Y.; Xu, X.; Liu, Y.; Lu, T.; Pan, L. Three-dimensional charge transfer pathway in close-packed nickel hexacyanoferrate−on−MXene nano-stacking for high-performance capacitive deionization. *Chem. Eng. J.* **2023**, *452*, 139451.

(19) Chen, Y.; Xie, X.; Xin, X.; Tang, Z. R.; Xu, Y. J. $Ti_3C_2T_x$-Based Three-Dimensional Hydrogel by a Graphene Oxide-Assisted Self-Convergence Process for Enhanced Photoredox Catalysis. *ACS Nano* **2019**, *13* (1), 295−304.

(20) Zhang, X.; Zhang, Z.; Zhou, Z. MXene-based materials for electrochemical energy storage. *J. Energy Chem.* **2018**, *27* (1), 73−85.

(21) Gogotsi, Y.; Huang, Q. MXenes: Two-Dimensional Building Blocks for Future Materials and Devices. *ACS Nano* **2021**, *15* (4), 5775−5780.

(22) Ming, F.; Liang, H.; Huang, G.; Bayhan, Z.; Alshareef, H. N. MXenes for Rechargeable Batteries Beyond the Lithium-Ion. *Adv. Mater.* **2021**, *33* (1), 2004039.

(23) Wyatt, B. C.; Rosenkranz, A.; Anasori, B. 2D MXenes: Tunable Mechanical and Tribological Properties. *Adv. Mater.* **2021**, *33* (17), 2007973.

(24) Naguib, M.; Barsoum, M. W.; Gogotsi, Y. Ten Years of Progress in the Synthesis and Development of MXenes. *Adv. Mater.* **2021**, *33* (39), 2103393.

(25) Gogotsi, Y.; Anasori, B. The Rise of MXenes. *ACS Nano* **2019**, *13* (8), 8491−8494.

(26) Khazaei, M.; Ranjbar, A.; Esfarjani, K.; Bogdanovski, D.; Dronskowski, R.; Yunoki, S. Insights into exfoliation possibility of MAX phases to MXenes. *Phys. Chem. Chem. Phys.* **2018**, *20* (13), 8579−8592.

(27) Sun, Z.; Music, D.; Ahuja, R.; Li, S.; Schneider, J. M. Bonding and classification of nanolayered ternary carbides. *Phys. Rev. B* **2004**, *70* (9), 092102.

(28) Naguib, M.; Mochalin, V. N.; Barsoum, M. W.; Gogotsi, Y. 25th anniversary article: MXenes: a new family of two-dimensional materials. *Adv. Mater.* **2014**, *26* (7), 992−1005.

(29) Alhabeb, M.; Maleski, K.; Anasori, B.; Lelyukh, P.; Clark, L.; Sin, S.; Gogotsi, Y. Guidelines for Synthesis and Processing of Two-Dimensional Titanium Carbide ($Ti_3C_2T_x$ MXene). *Chem. Mater.* **2017**, *29* (18), 7633−7644.

(30) Urbankowski, P.; Anasori, B.; Makaryan, T.; Er, D.; Kota, S.; Walsh, P. L.; Zhao, M.; Shenoy, V. B.; Barsoum, M. W.; Gogotsi, Y. Synthesis of two-dimensional titanium nitride Ti_4N_3 (MXene). *Nanoscale* **2016**, *8* (22), 11385−11391.

(31) Limbu, T. B.; Chitara, B.; Orlando, J. D.; Garcia Cervantes, M. Y.; Kumari, S.; Li, Q.; Tang, Y.; Yan, F. Green synthesis of reduced $Ti_3C_2T_x$ MXene nanosheets with enhanced conductivity, oxidation stability, and SERS activity. *J. Mater. Chem. C* **2020**, *8* (14), 4722−4731.

(32) Gao, L.; Li, C.; Huang, W.; Mei, S.; Lin, H.; Ou, Q.; Zhang, Y.; Guo, J.; Zhang, F.; Xu, S.; Zhang, H. MXene/Polymer Membranes: Synthesis, Properties, and Emerging Applications. *Chem. Mater.* **2020**, *32* (5), 1703−1747.

(33) Huang, X.; Wu, P. A Facile, High-Yield, and Freeze-and-Thaw-Assisted Approach to Fabricate MXene with Plentiful Wrinkles and Its Application in On-Chip Micro-Supercapacitors. *Adv. Funct. Mater.* **2020**, *30* (12), 1910048.

(34) Akuzum, B.; Maleski, K.; Anasori, B.; Lelyukh, P.; Alvarez, N. J.; Kumbur, E. C.; Gogotsi, Y. Rheological Characteristics of 2D Titanium Carbide (MXene) Dispersions: A Guide for Processing MXenes. *ACS Nano* **2018**, *12* (3), 2685−2694.

(35) Naguib, M.; Unocic, R. R.; Armstrong, B. L.; Nanda, J. Large-scale delamination of multi-layers transition metal carbides and carbonitrides "MXenes". *Dalton Trans.* **2015**, *44* (20), 9353−9358.

https://doi.org/10.1021/acs.iecr.3c00306
Ind. Eng. Chem. Res. 2023, 62, 7297−7335

(36) Anasori, B.; Lukatskaya, M. R.; Gogotsi, Y. 2D metal carbides and nitrides (MXenes) for energy storage. *Nat. Rev. Mater.* **2017**, *2* (2), 16098.
(37) Ghidiu, M.; Lukatskaya, M. R.; Zhao, M. Q.; Gogotsi, Y.; Barsoum, M. W. Conductive two-dimensional titanium carbide 'clay' with high volumetric capacitance. *Nature* **2014**, *516* (7529), 78−81.
(38) Feng, A.; Yu, Y.; Jiang, F.; Wang, Y.; Mi, L.; Yu, Y.; Song, L. Fabrication and thermal stability of NH_4HF_2 -etched Ti_3C_2 MXene. *Ceram. Int.* **2017**, *43* (8), 6322−6328.
(39) Wang, L.; Zhang, H.; Wang, B.; Shen, C.; Zhang, C.; Hu, Q.; Zhou, A.; Liu, B. Synthesis and electrochemical performance of $Ti_3C_2T_x$ with hydrothermal process. *Electron. Mater. Lett.* **2016**, *12* (5), 702−710.
(40) Srivastava, P.; Mishra, A.; Mizuseki, H.; Lee, K. R.; Singh, A. K. Mechanistic Insight into the Chemical Exfoliation and Functionalization of Ti_3C_2 MXene. *ACS Appl. Mater. Interfaces* **2016**, *8* (36), 24256−24264.
(41) Zhang, T.; Pan, L.; Tang, H.; Du, F.; Guo, Y.; Qiu, T.; Yang, J. Synthesis of two-dimensional $Ti_3C_2T_x$ MXene using HCl+LiF etchant: Enhanced exfoliation and delamination. *J. Alloys Compd.* **2017**, *695*, 818−826.
(42) Kim, Y.-J.; Kim, S. J.; Seo, D.; Chae, Y.; Anayee, M.; Lee, Y.; Gogotsi, Y.; Ahn, C. W.; Jung, H.-T. Etching Mechanism of Monoatomic Aluminum Layers during MXene Synthesis. *Chem. Mater.* **2021**, *33* (16), 6346−6355.
(43) Yang, S.; Zhang, P.; Wang, F.; Ricciardulli, A. G.; Lohe, M. R.; Blom, P. W. M.; Feng, X. Fluoride-Free Synthesis of Two-Dimensional Titanium Carbide (MXene) Using A Binary Aqueous System. *Angew. Chem., Int. Ed.* **2018**, *57* (47), 15491−15495.
(44) Li, G.; Tan, L.; Zhang, Y.; Wu, B.; Li, L. Highly Efficiently Delaminated Single-Layered MXene Nanosheets with Large Lateral Size. *Langmuir* **2017**, *33* (36), 9000−9006.
(45) Li, T.; Yao, L.; Liu, Q.; Gu, J.; Luo, R.; Li, J.; Yan, X.; Wang, W.; Liu, P.; Chen, B.; Zhang, W.; Abbas, W.; Naz, R.; Zhang, D. Fluorine-Free Synthesis of High-Purity $Ti_3C_2T_x$ (T═OH, O) via Alkali Treatment. *Angew. Chem., Int. Ed.* **2018**, *57* (21), 6115−6119.
(46) Li, M.; Lu, J.; Luo, K.; Li, Y.; Chang, K.; Chen, K.; Zhou, J.; Rosen, J.; Hultman, L.; Eklund, P.; Persson, P. O. A.; Du, S.; Chai, Z.; Huang, Z.; Huang, Q. Element Replacement Approach by Reaction with Lewis Acidic Molten Salts to Synthesize Nanolaminated MAX Phases and MXenes. *J. Am. Chem. Soc.* **2019**, *141* (11), 4730−4737.
(47) Li, Y.; Shao, H.; Lin, Z.; Lu, J.; Liu, L.; Duployer, B.; Persson, P. O. A.; Eklund, P.; Hultman, L.; Li, M.; Chen, K.; Zha, X. H.; Du, S.; Rozier, P.; Chai, Z.; Raymundo-Pinero, E.; Taberna, P. L.; Simon, P.; Huang, Q. A general Lewis acidic etching route for preparing MXenes with enhanced electrochemical performance in non-aqueous electrolyte. *Nat. Mater.* **2020**, *19* (8), 894−899.
(48) Geng, D.; Zhao, X.; Chen, Z.; Sun, W.; Fu, W.; Chen, J.; Liu, W.; Zhou, W.; Loh, K. P. Direct Synthesis of Large-Area 2D Mo_2C on In Situ Grown Graphene. *Adv. Mater.* **2017**, *29* (35), 1700072.
(49) Liu, Z.; Xu, C.; Kang, N.; Wang, L.; Jiang, Y.; Du, J.; Liu, Y.; Ma, X. L.; Cheng, H. M.; Ren, W. Unique Domain Structure of Two-Dimensional alpha-Mo_2C Superconducting Crystals. *Nano Lett.* **2016**, *16* (7), 4243−4250.
(50) Xu, C.; Wang, L.; Liu, Z.; Chen, L.; Guo, J.; Kang, N.; Ma, X. L.; Cheng, H. M.; Ren, W. Large-area high-quality 2D ultrathin Mo_2C superconducting crystals. *Nat. Mater.* **2015**, *14* (11), 1135−1141.
(51) Feng, W.; Luo, H.; Wang, Y.; Zeng, S.; Tan, Y.; Zhang, H.; Peng, S. Ultrasonic assisted etching and delaminating of Ti_3C_2 MXene. *Ceram. Int.* **2018**, *44* (6), 7084−7087.
(52) Zou, J.; Wu, J.; Wang, Y.; Deng, F.; Jiang, J.; Zhang, Y.; Liu, S.; Li, N.; Zhang, H.; Yu, J.; Zhai, T.; Alshareef, H. N. Additive-mediated intercalation and surface modification of MXenes. *Chem. Soc. Rev.* **2022**, *51* (8), 2972−2990.
(53) Mashtalir, O.; Naguib, M.; Mochalin, V. N.; Dall'Agnese, Y.; Heon, M.; Barsoum, M. W.; Gogotsi, Y. Intercalation and delamination of layered carbides and carbonitrides. *Nat. Commun.* **2013**, *4*, 1716.
(54) Mashtalir, O.; Lukatskaya, M. R.; Zhao, M. Q.; Barsoum, M. W.; Gogotsi, Y. Amine-Assisted Delamination of Nb2C MXene for Li-Ion Energy Storage Devices. *Adv. Mater.* **2015**, *27* (23), 3501−3506.
(55) Hantanasirisakul, K.; Alhabeb, M.; Lipatov, A.; Maleski, K.; Anasori, B.; Salles, P.; Ieosakulrat, C.; Pakawatpanurut, P.; Sinitskii, A.; May, S. J.; Gogotsi, Y. Effects of Synthesis and Processing on Optoelectronic Properties of Titanium Carbonitride MXene. *Chem. Mater.* **2019**, *31* (8), 2941−2951.
(56) Lukatskaya, M. R.; Mashtalir, O.; Ren, C. E.; Dall'Agnese, Y.; Rozier, P.; Taberna, P. L.; Naguib, M.; Simon, P.; Barsoum, M. W.; Gogotsi, Y. Cation intercalation and high volumetric capacitance of two-dimensional titanium carbide. *Science* **2013**, *341* (6153), 1502−1505.
(57) Han, M.; Shuck, C. E.; Rakhmanov, R.; Parchment, D.; Anasori, B.; Koo, C. M.; Friedman, G.; Gogotsi, Y. Beyond $Ti_3C_2T_x$: MXenes for Electromagnetic Interference Shielding. *ACS Nano* **2020**, *14* (4), 5008−5016.
(58) Hu, A.; Yu, J.; Zhao, H.; Zhang, H.; Li, W. One-step synthesis for cations intercalation of two-dimensional carbide crystal Ti_3C_2 MXene. *Appl. Surf. Sci.* **2020**, *505*, 144538.
(59) Qian, A.; Hyeon, S. E.; Seo, J. Y.; Chung, C.-H. Capacitance changes associated with cation-transport in free-standing flexible $Ti_3C_2T_x$ (T═O, F, OH) MXene film electrodes. *Electrochim. Acta* **2018**, *266*, 86−93.
(60) Yuan, Y.; Pan, Y. T.; Zhang, W.; Feng, M.; Wang, N.; Wang, D. Y.; Yang, R. Delamination and Engineered Interlayers of Ti_3C_2 MXenes using Phosphorous Vapor toward Flame-Retardant Epoxy Nanocomposites. *ACS Appl. Mater. Interfaces* **2021**, *13* (40), 48196−48207.
(61) Shi, H.; Zhang, P.; Liu, Z.; Park, S.; Lohe, M. R.; Wu, Y.; Shaygan Nia, A.; Yang, S.; Feng, X. Ambient-Stable Two-Dimensional Titanium Carbide (MXene) Enabled by Iodine Etching. *Angew. Chem., Int. Ed.* **2021**, *60* (16), 8689−8693.
(62) Ghazaly, A. E.; Ahmed, H.; Rezk, A. R.; Halim, J.; Persson, P. O. Å.; Yeo, L. Y.; Rosen, J. Ultrafast, One-Step, Salt-Solution-Based Acoustic Synthesis of Ti_3C_2 MXene. *ACS Nano* **2021**, *15* (3), 4287−4293.
(63) Xue, N.; Li, X.; Zhang, M.; Han, L.; Liu, Y.; Tao, X. Chemical-Combined Ball-Milling Synthesis of Fluorine-Free Porous MXene for High-Performance Lithium Ion Batteries. *ACS Appl. Energy Mater.* **2020**, *3* (10), 10234−10241.
(64) Halim, J.; Lukatskaya, M. R.; Cook, K. M.; Lu, J.; Smith, C. R.; Naslund, L. A.; May, S. J.; Hultman, L.; Gogotsi, Y.; Eklund, P.; Barsoum, M. W. Transparent Conductive Two-Dimensional Titanium Carbide Epitaxial Thin Films. *Chem. Mater.* **2014**, *26* (7), 2374−2381.
(65) Natu, V.; Pai, R.; Sokol, M.; Carey, M.; Kalra, V.; Barsoum, M. W. 2D $Ti_3C_2T_z$ MXene Synthesized by Water-free Etching of Ti_3AlC_2 in Polar Organic Solvents. *Chem.* **2020**, *6* (3), 616−630.
(66) Zhao, X.; Radovic, M.; Green, M. J. Synthesizing MXene Nanosheets by Water-free Etching. *Chem.* **2020**, *6* (3), 544−546.
(67) Dash, A.; Vaßen, R.; Guillon, O.; Gonzalez-Julian, J. Molten salt shielded synthesis of oxidation prone materials in air. *Nat. Mater.* **2019**, *18* (5), 465−470.
(68) Shuck, C. E.; Sarycheva, A.; Anayee, M.; Levitt, A.; Zhu, Y.; Uzun, S.; Balitskiy, V.; Zahorodna, V.; Gogotsi, O.; Gogotsi, Y. Scalable Synthesis of $Ti_3C_2T_x$ MXene. *Adv. Eng. Mater.* **2020**, *22* (3), 1901241.
(69) Yang, W.; Yang, J.; Byun, J. J.; Moissinac, F. P.; Xu, J.; Haigh, S. J.; Domingos, M.; Bissett, M. A.; Dryfe, R. A. W.; Barg, S. 3D Printing of Freestanding MXene Architectures for Current-Collector-Free Supercapacitors. *Adv. Mater.* **2019**, *31* (37), 1902725.
(70) Hope, M. A.; Forse, A. C.; Griffith, K. J.; Lukatskaya, M. R.; Ghidiu, M.; Gogotsi, Y.; Grey, C. P. NMR reveals the surface functionalisation of Ti_3C_2 MXene. *Phys. Chem. Chem. Phys.* **2016**, *18* (7), 5099−5102.
(71) Maleski, K.; Mochalin, V. N.; Gogotsi, Y. Dispersions of Two-Dimensional Titanium Carbide MXene in Organic Solvents. *Chem. Mater.* **2017**, *29* (4), 1632−1640.

https://doi.org/10.1021/acs.iecr.3c00306
Ind. Eng. Chem. Res. 2023, 62, 7297−7335

(72) Hong, L.-f.; Guo, R.-t.; Yuan, Y.; Ji, X.-y.; Li, Z.-s.; Lin, Z.-d.; Pan, W.-g. Recent progress of two-dimensional MXenes in photocatalytic applications: a review. *Mater. Today Energy* **2020**, *18*, 100521.
(73) Come, J.; Black, J. M.; Lukatskaya, M. R.; Naguib, M.; Beidaghi, M.; Rondinone, A. J.; Kalinin, S. V.; Wesolowski, D. J.; Gogotsi, Y.; Balke, N. Controlling the actuation properties of MXene paper electrodes upon cation intercalation. *Nano Energy* **2015**, *17*, 27−35.
(74) Li, R.; Zhang, L.; Shi, L.; Wang, P. MXene Ti_3C_2: An Effective 2D Light-to-Heat Conversion Material. *ACS Nano* **2017**, *11* (4), 3752−3759.
(75) Lin, H.; Wang, X.; Yu, L.; Chen, Y.; Shi, J. Two-Dimensional Ultrathin MXene Ceramic Nanosheets for Photothermal Conversion. *Nano Lett.* **2017**, *17* (1), 384−391.
(76) Fan, X.; Ding, Y.; Liu, Y.; Liang, J.; Chen, Y. Plasmonic $Ti_3C_2T_x$ MXene Enables Highly Efficient Photothermal Conversion for Healable and Transparent Wearable Device. *ACS Nano* **2019**, *13* (7), 8124−8134.
(77) Wang, L.; Zhang, M.; Yang, B.; Tan, J.; Ding, X. Highly Compressible, Thermally Stable, Light-Weight, and Robust Aramid Nanofibers/Ti_3AlC_2 MXene Composite Aerogel for Sensitive Pressure Sensor. *ACS Nano* **2020**, *14* (8), 10633−10647.
(78) Wang, H.; Zhou, R.; Li, D.; Zhang, L.; Ren, G.; Wang, L.; Liu, J.; Wang, D.; Tang, Z.; Lu, G.; Sun, G.; Yu, H. D.; Huang, W. High-Performance Foam-Shaped Strain Sensor Based on Carbon Nanotubes and $Ti_3C_2T_x$ MXene for the Monitoring of Human Activities. *ACS Nano* **2021**, *15* (6), 9690−9700.
(79) Shi, M.; Shen, M.; Guo, X.; Jin, X.; Cao, Y.; Yang, Y.; Wang, W.; Wang, J. $Ti_3C_2T_x$ MXene-Decorated Nanoporous Polyethylene Textile for Passive and Active Personal Precision Heating. *ACS Nano* **2021**, *15* (7), 11396−11405.
(80) Lei, Z.; Sun, X.; Zhu, S.; Dong, K.; Liu, X.; Wang, L.; Zhang, X.; Qu, L.; Zhang, X. Nature Inspired MXene-Decorated 3D Honeycomb-Fabric Architectures Toward Efficient Water Desalination and Salt Harvesting. *Nano-Micro Lett.* **2022**, *14* (1), 10.
(81) Wang, Y.; Qi, Q.; Fan, J.; Wang, W.; Yu, D. Simple and robust MXene/carbon nanotubes/cotton fabrics for textile wastewater purification via solar-driven interfacial water evaporation. *Sep. Purif. Technol.* **2021**, *254*, 117615.
(82) Zhang, Q.; Chen, S.; Fu, Z.; Yu, H.; Quan, X. Temperature-difference-induced electricity during solar desalination with bilayer MXene-based monoliths. *Nano Energy* **2020**, *76*, 105060.
(83) Xu, D.; Li, Z.; Li, L.; Wang, J. Insights into the Photothermal Conversion of 2D MXene Nanomaterials: Synthesis, Mechanism, and Applications. *Adv. Funct. Mater.* **2020**, *30* (47), 2000712.
(84) Peng, H.; Wang, D.; Fu, S. Unidirectionally Driving Nanofluidic Transportation via an Asymmetric Textile Pump for Simultaneous Salt-Resistant Solar Desalination and Drenching-Induced Power Generation. *ACS Appl. Mater. Interfaces* **2021**, *13* (32), 38405−38415.
(85) Chen, M.; Li, L.; Deng, Z.; Min, P.; Yu, Z. Z.; Zhang, C. J.; Zhang, H. B. Two-Dimensional Janus MXene Inks for Versatile Functional Coatings on Arbitrary Substrates. *ACS Appl. Mater. Interfaces.* **2023**, *15* (3), 4591−4600.
(86) Pazniak, H.; Benchakar, M.; Bilyk, T.; Liedl, A.; Busby, Y.; Noel, C.; Chartier, P.; Hurand, S.; Marteau, M.; Houssiau, L.; Larciprete, R.; Lacovig, P.; Lizzit, D.; Tosi, E.; Lizzit, S.; Pacaud, J.; Celerier, S.; Mauchamp, V.; David, M. L. Ion Implantation as an Approach for Structural Modifications and Functionalization of $Ti_3C_2T_x$ MXenes. *ACS Nano* **2021**, *15* (3), 4245−4255.
(87) Zhang, H.; Shen, X.; Kim, E.; Wang, M.; Lee, J. H.; Chen, H.; Zhang, G.; Kim, J. K. Integrated Water and Thermal Managements in Bioinspired Hierarchical MXene Aerogels for Highly Efficient Solar-Powered Water Evaporation. *Adv. Funct. Mater.* **2022**, *32* (19), 2111794.
(88) Shi, S.; Qian, B.; Wu, X.; Sun, H.; Wang, H.; Zhang, H. B.; Yu, Z. Z.; Russell, T. P. Self-Assembly of MXene-Surfactants at Liquid-Liquid Interfaces: From Structured Liquids to 3D Aerogels. *Angew. Chem., Int. Ed.* **2019**, *58* (50), 18171−18176.
(89) Yang, X.; Wang, Q.; Zhu, K.; Ye, K.; Wang, G.; Cao, D.; Yan, J. 3D Porous Oxidation-Resistant MXene/Graphene Architectures Induced by In Situ Zinc Template toward High-Performance Supercapacitors. *Adv. Funct. Mater.* **2021**, *31* (20), 2101087.
(90) Shang, T.; Lin, Z.; Qi, C.; Liu, X.; Li, P.; Tao, Y.; Wu, Z.; Li, D.; Simon, P.; Yang, Q. H. 3D Macroscopic Architectures from Self-Assembled MXene Hydrogels. *Adv. Funct. Mater.* **2019**, *29* (33), 1903960.
(91) Ding, M.; Li, S.; Guo, L.; Jing, L.; Gao, S. P.; Yang, H.; Little, J. M.; Dissanayake, T. U.; Li, K.; Yang, J.; Guo, Y. X.; Yang, H. Y.; Woehl, T. J.; Chen, P. Y. Metal Ion-Induced Assembly of MXene Aerogels via Biomimetic Microtextures for Electromagnetic Interference Shielding, Capacitive Deionization, and Microsupercapacitors. *Adv. Energy Mater.* **2021**, *11* (35), 2101494.
(92) Tetik, H.; Orangi, J.; Yang, G.; Zhao, K.; Mujib, S. B.; Singh, G.; Beidaghi, M.; Lin, D. 3D Printed MXene Aerogels with Truly 3D Macrostructure and Highly Engineered Microstructure for Enhanced Electrical and Electrochemical Performance. *Adv. Mater.* **2022**, *34* (2), 2104980.
(93) Liu, J.; Zhang, H. B.; Sun, R.; Liu, Y.; Liu, Z.; Zhou, A.; Yu, Z. Z. Hydrophobic, Flexible, and Lightweight MXene Foams for High-Performance Electromagnetic-Interference Shielding. *Adv. Mater.* **2017**, *29* (38), 1702367.
(94) Zheng, D.; Yao, W.; Sun, C.; Chen, X.; Wang, Z.; Wang, B.; Tan, H.; Zhang, Y. Solar-assisted self-heating $Ti_3C_2T_x$-decorated wood aerogel for adsorption and recovery of highly viscous crude oil. *J. Hazard. Mater.* **2022**, *435*, 129068.
(95) Levitt, A. S.; Alhabeb, M.; Hatter, C. B.; Sarycheva, A.; Dion, G.; Gogotsi, Y. Electrospun MXene/carbon nanofibers as supercapacitor electrodes. *J. Mater. Chem. A* **2019**, *7* (1), 269−277.
(96) Li, X.; Yin, X.; Song, C.; Han, M.; Xu, H.; Duan, W.; Cheng, L.; Zhang, L. Self-Assembly Core-Shell Graphene-Bridged Hollow MXenes Spheres 3D Foam with Ultrahigh Specific EM Absorption Performance. *Adv. Funct. Mater.* **2018**, *28* (41), 1803938.
(97) Gao, W.; Zhang, W.; Yu, H.; Xing, W.; Yang, X.; Zhang, Y.; Liang, C. 3D CNT/MXene microspheres for combined photothermal/photodynamic/chemo for cancer treatment. *Front. Bioeng. Biotechnol.* **2022**, *10*, 996177.
(98) Zhao, M. Q.; Xie, X.; Ren, C. E.; Makaryan, T.; Anasori, B.; Wang, G.; Gogotsi, Y. Hollow MXene Spheres and 3D Macroporous MXene Frameworks for Na-Ion Storage. *Adv. Mater.* **2017**, *29* (37), 1702410.
(99) Lukatskaya, M. R.; Kota, S.; Lin, Z.; Zhao, M.-Q.; Shpigel, N.; Levi, M. D.; Halim, J.; Taberna, P.-L.; Barsoum, M. W.; Simon, P.; Gogotsi, Y. Ultra-high-rate pseudocapacitive energy storage in two-dimensional transition metal carbides. *Nat. Energy* **2017**, *2* (8), 17105.
(100) Li, K.; Wang, X.; Wang, X.; Liang, M.; Nicolosi, V.; Xu, Y.; Gogotsi, Y. All-pseudocapacitive asymmetric MXene-carbon-conducting polymer supercapacitors. *Nano Energy* **2020**, *75*, 104971.
(101) Sun, R.; Zhang, H.-B.; Liu, J.; Xie, X.; Yang, R.; Li, Y.; Hong, S.; Yu, Z.-Z. Highly Conductive Transition Metal Carbide/Carbonitride (MXene)@polystyrene Nanocomposites Fabricated by Electrostatic Assembly for Highly Efficient Electromagnetic Interference Shielding. *Adv. Funct. Mater.* **2017**, *27* (45), 1702807.
(102) Yao, M.; Chen, Y.; Wang, Z.; Shao, C.; Dong, J.; Zhang, Q.; Zhang, L.; Zhao, X. Boosting gravimetric and volumetric energy density via engineering macroporous MXene films for supercapacitors. *Chem. Eng. J.* **2020**, *395*, 124057.
(103) Guo, M.; Zhong, S.; Xu, T.; Huang, Y.; Xia, G.; Zhang, T.; Yu, X. 3D hollow MXene (Ti_3C_2)/reduced graphene oxide hybrid nanospheres for high-performance Li-ion storage. *J. Mater. Chem. A* **2021**, *9* (42), 23841−23849.
(104) Yu, L.; Fan, Z.; Shao, Y.; Tian, Z.; Sun, J.; Liu, Z. Versatile N-Doped MXene Ink for Printed Electrochemical Energy Storage Application. *Adv. Energy Mater.* **2019**, *9* (34), 1901839.
(105) Fan, Z.; Wei, C.; Yu, L.; Xia, Z.; Cai, J.; Tian, Z.; Zou, G.; Dou, S. X.; Sun, J. 3D Printing of Porous Nitrogen-Doped Ti_3C_2 MXene Scaffolds for High-Performance Sodium-Ion Hybrid Capacitors. *ACS Nano* **2020**, *14* (1), 867−876.

https://doi.org/10.1021/acs.iecr.3c00306
Ind. Eng. Chem. Res. 2023, 62, 7297−7335

(106) Zhang, J.; Jiang, D.; Liao, L.; Cui, L.; Zheng, R.; Liu, J. $Ti_3C_2T_x$ MXene based hybrid electrodes for wearable supercapacitors with varied deformation capabilities. *Chem. Eng. J.* **2022**, *429*, 132232.
(107) Yu, H.; Yang, X.; Xiao, X.; Chen, M.; Zhang, Q.; Huang, L.; Wu, J.; Li, T.; Chen, S.; Song, L.; Gu, L.; Xia, B. Y.; Feng, G.; Li, J.; Zhou, J. Atmospheric-Pressure Synthesis of 2D Nitrogen-Rich Tungsten Nitride. *Adv. Mater.* **2018**, *30* (51), 1805655.
(108) Tian, Y.; Ju, M.; Luo, Y.; Bin, X.; Lou, X.; Que, W. In situ oxygen doped $Ti_3C_2T_x$ MXene flexible film as supercapacitor electrode. *Chem. Eng. J.* **2022**, *446*, 137451.
(109) Jiang, D.; Wei, M.; Du, X.; Qin, M.; Shan, X.; Chen, Z. One-pot synthesis of ZnO quantum dots/N-doped Ti_3C_2 MXene: Tunable nitrogen-doping properties and efficient electrochemiluminescence sensing. *Chem. Eng. J.* **2022**, *430*, 132771.
(110) Li, J.; Yan, D.; Hou, S.; Li, Y.; Lu, T.; Yao, Y.; Pan, L. Improved sodium-ion storage performance of $Ti_3C_2T_x$ MXenes by sulfur doping. *J. Mater. Chem. A* **2018**, *6* (3), 1234−1243.
(111) Lieu, W. Y.; Fang, D.; Li, Y.; Li, X. L.; Lin, C.; Thakur, A.; Wyatt, B. C.; Sun, S.; Ghosh, T.; Anasori, B.; Ng, M. F.; Yang, H. Y.; Seh, Z. W. Spherical Templating of $CoSe_2$ Nanoparticle-Decorated MXenes for Lithium-Sulfur Batteries. *Nano Lett.* **2022**, *22* (21), 8679−8687.
(112) Sun, B.; Qin, F.; Jiang, L.; Gao, J.; Liu, Z.; Wang, J.; Zhang, Y.; Fan, J.; Kan, K.; Shi, K. Room-temperature gas sensors based on three-dimensional $Co_3O_4/Al_2O_3@Ti_3C_2T_x$ MXene nanocomposite for highly sensitive NO_x detection. *Sens. Actuators B Chem.* **2022**, *368*, 132206.
(113) Kang, J.; Byun, S.; Kim, S.; Lee, J.; Jung, M.; Hwang, H.; Kim, T. W.; Song, S. H.; Lee, D. Design of Three-Dimensional Hollow-Sphere Architecture of $Ti_3C_2T_x$ MXene with Graphitic Carbon Nitride Nanoshells for Efficient Photocatalytic Hydrogen Evolution. *ACS Appl. Energy Mater.* **2020**, *3* (9), 9226−9233.
(114) Zhu, Y.; Rajouâ, K.; Le Vot, S.; Fontaine, O.; Simon, P.; Favier, F. Modifications of MXene layers for supercapacitors. *Nano Energy* **2020**, *73*, 104734.
(115) Fan, Z.; Wang, Y.; Xie, Z.; Xu, X.; Yuan, Y.; Cheng, Z.; Liu, Y. A nanoporous MXene film enables flexible supercapacitors with high energy storage. *Nanoscale* **2018**, *10* (20), 9642−9652.
(116) Xu, H.; Yin, X.; Li, X.; Li, M.; Liang, S.; Zhang, L.; Cheng, L. Lightweight Ti_2CT_x MXene/Poly(vinyl alcohol) Composite Foams for Electromagnetic Wave Shielding with Absorption-Dominated Feature. *ACS Appl. Mater. Interfaces* **2019**, *11* (10), 10198−10207.
(117) Han, X.; Ding, S.; Fan, L.; Zhou, Y.; Wang, S. Janus biocomposite aerogels constituted of cellulose nanofibrils and MXenes for application as single-module solar-driven interfacial evaporators. *J. Mater. Chem. A* **2021**, *9* (34), 18614−18622.
(118) Han, M.; Yin, X.; Hantanasirisakul, K.; Li, X.; Iqbal, A.; Hatter, C. B.; Anasori, B.; Koo, C. M.; Torita, T.; Soda, Y.; Zhang, L.; Cheng, L.; Gogotsi, Y. Anisotropic MXene Aerogels with a Mechanically Tunable Ratio of Electromagnetic Wave Reflection to Absorption. *Adv. Optical Mater.* **2019**, *7* (10), 1900267.
(119) Jin, L.; Wang, P.; Cao, W.; Song, N.; Ding, P. Isolated Solid Wall-Assisted Thermal Conductive Performance of Three-Dimensional Anisotropic MXene/Graphene Polymeric Composites. *ACS Appl. Mater. Interfaces* **2022**, *14* (1), 1747−1756.
(120) Bian, R.; Lin, R.; Wang, G.; Lu, G.; Zhi, W.; Xiang, S.; Wang, T.; Clegg, P. S.; Cai, D.; Huang, W. 3D assembly of Ti_3C_2-MXene directed by water/oil interfaces. *Nanoscale* **2018**, *10* (8), 3621−3625.
(121) Jin, L.; Cao, W.; Wang, P.; Song, N.; Ding, P. Interconnected MXene/Graphene Network Constructed by Soft Template for Multi-Performance Improvement of Polymer Composites. *Nano-Micro Lett.* **2022**, *14* (1), 133.
(122) Zhang, J.; Ma, Y.; Han, Y.; Xu, K.; Yao, S.; Shi, L.; Zhu, M. 3D porous structure assembled from MXene via breath figure method for electrochemical detection of dopamine. *Chem. Eng. J.* **2023**, *452*, 139414.
(123) Jiang, D.; Zhang, J.; Qin, S.; Wang, Z.; Usman, K. A. S.; Hegh, D.; Liu, J.; Lei, W.; Razal, J. M. Superelastic $Ti_3C_2T_x$ MXene-Based Hybrid Aerogels for Compression-Resilient Devices. *ACS Nano* **2021**, *15* (3), 5000−5010.
(124) Jiang, Y.; Xie, X.; Chen, Y.; Liu, Y.; Yang, R.; Sui, G. Hierarchically structured cellulose aerogels with interconnected MXene networks and their enhanced microwave absorption properties. *J. Mater. Chem. C* **2018**, *6* (32), 8679−8687.
(125) Zhao, S.; Zhang, H. B.; Luo, J. Q.; Wang, Q. W.; Xu, B.; Hong, S.; Yu, Z. Z. Highly Electrically Conductive Three-Dimensional $Ti_3C_2T_x$ MXene/Reduced Graphene Oxide Hybrid Aerogels with Excellent Electromagnetic Interference Shielding Performances. *ACS Nano* **2018**, *12* (11), 11193−11202.
(126) Deng, Y.; Shang, T.; Wu, Z.; Tao, Y.; Luo, C.; Liang, J.; Han, D.; Lyu, R.; Qi, C.; Lv, W.; Kang, F.; Yang, Q. H. Fast Gelation of $Ti_3C_2T_x$ MXene Initiated by Metal Ions. *Adv. Mater.* **2019**, *31* (43), 1902432.
(127) Gholamirad, F.; Taheri-Qazvini, N. Three-Dimensional Porous $Ti_3C_2T_x$ MXene-Based Hybrids Formed by Charge-Driven Assembly. *Chem. Mater.* **2021**, *33* (24), 9560−9570.
(128) Orangi, J.; Hamade, F.; Davis, V. A.; Beidaghi, M. 3D Printing of Additive-Free 2D $Ti_3C_2T_x$ (MXene) Ink for Fabrication of Micro-Supercapacitors with Ultra-High Energy Densities. *ACS Nano* **2020**, *14* (1), 640−650.
(129) Shi, G.; Zhu, Y.; Batmunkh, M.; Ingram, M.; Huang, Y.; Chen, Z.; Wei, Y.; Zhong, L.; Peng, X.; Zhong, Y. L. Cytomembrane-Inspired MXene Ink with Amphiphilic Surfactant for 3D Printed Microsupercapacitors. *ACS Nano* **2022**, *16* (9), 14723−14736.
(130) Rastin, H.; Zhang, B.; Mazinani, A.; Hassan, K.; Bi, J.; Tung, T. T.; Losic, D. 3D bioprinting of cell-laden electroconductive MXene nanocomposite bioinks. *Nanoscale* **2020**, *12* (30), 16069−16080.
(131) Li, X.; Li, H.; Fan, X.; Shi, X.; Liang, J. 3D-Printed Stretchable Micro-Supercapacitor with Remarkable Areal Performance. *Adv. Energy Mater.* **2020**, *10* (14), 1903794.
(132) Yu, L.; Li, W.; Wei, C.; Yang, Q.; Shao, Y.; Sun, J. 3D Printing of $NiCoP/Ti_3C_2$ MXene Architectures for Energy Storage Devices with High Areal and Volumetric Energy Density. *Nano-Micro Lett.* **2020**, *12* (1), 143.
(133) Wang, X.; Fu, Q.; Wen, J.; Ma, X.; Zhu, C.; Zhang, X.; Qi, D. 3D $Ti_3C_2T_x$ aerogels with enhanced surface area for high performance supercapacitors. *Nanoscale* **2018**, *10* (44), 20828−20835.
(134) Wang, M.; Zhu, J.; Zi, Y.; Huang, W. 3D MXene Sponge: Facile Synthesis, Excellent Hydrophobicity, and High Photothermal Efficiency for Waste Oil Collection and Purification. *ACS Appl. Mater. Interfaces* **2021**, *13* (39), 47302−47312.
(135) Gong, C.; Lao, J.; Wang, B.; Li, X.; Li, G.; Gao, J.; Wan, Y.; Sun, X.; Guo, R.; Luo, J. Fast and all-weather cleanup of viscous crude-oil spills with $Ti_3C_2T_x$ MXene wrapped sponge. *J. Mater. Chem. A* **2020**, *8* (38), 20162−20167.
(136) Wang, P. L.; Ma, C.; Yuan, Q.; Mai, T.; Ma, M. G. Novel $Ti_3C_2T_x$ MXene wrapped wood sponges for fast cleanup of crude oil spills by outstanding Joule heating and photothermal effect. *J. Colloid Interface Sci.* **2022**, *606*, 971−982.
(137) Mayerberger, E. A.; Street, R. M.; McDaniel, R. M.; Barsoum, M. W.; Schauer, C. L. Antibacterial properties of electrospun $Ti_3C_2T_z$ (MXene)/chitosan nanofibers. *RSC Adv.* **2018**, *8* (62), 35386−35394.
(138) Jiang, C.; Wu, C.; Li, X.; Yao, Y.; Lan, L.; Zhao, F.; Ye, Z.; Ying, Y.; Ping, J. All-electrospun flexible triboelectric nanogenerator based on metallic MXene nanosheets. *Nano Energy* **2019**, *59*, 268−276.
(139) Xing, W.; Liang, J.; Tang, W.; He, D.; Yan, M.; Wang, X.; Luo, Y.; Tang, N.; Huang, M. Versatile applications of capacitive deionization (CDI)-based technologies. *Desalination* **2020**, *482*, 114390.
(140) Tang, W.; He, D.; Zhang, C.; Kovalsky, P.; Waite, T. D. Comparison of Faradaic reactions in capacitive deionization (CDI) and membrane capacitive deionization (MCDI) water treatment processes. *Water Res.* **2017**, *120*, 229−237.
(141) Srimuk, P.; Kaasik, F.; Krüner, B.; Tolosa, A.; Fleischmann, S.; Jäckel, N.; Tekeli, M. C.; Aslan, M.; Suss, M. E.; Presser, V. MXene as a novel intercalation-type pseudocapacitive cathode and anode for

https://doi.org/10.1021/acs.iecr.3c00306
Ind. Eng. Chem. Res. 2023, 62, 7297−7335

capacitive deionization. *J. Mater. Chem. A* **2016**, *4* (47), 18265−18271.
(142) Xie, X.; Zhao, M.-Q.; Anasori, B.; Maleski, K.; Ren, C. E.; Li, J.; Byles, B. W.; Pomerantseva, E.; Wang, G.; Gogotsi, Y. Porous heterostructured MXene/carbon nanotube composite paper with high volumetric capacity for sodium-based energy storage devices. *Nano Energy* **2016**, *26*, 513−523.
(143) Anwer, S.; Anjum, D. H.; Luo, S.; Abbas, Y.; Li, B.; Iqbal, S.; Liao, K. 2D $Ti_3C_2T_x$ MXene nanosheets coated cellulose fibers based 3D nanostructures for efficient water desalination. *Chem. Eng. J.* **2021**, *406*, 126827.
(144) Yuan, J.; Ma, Y.; Yu, F.; Sun, Y.; Dai, X.; Ma, J. Simultaneous in situ nutrient recovery and sustainable wastewater purification based on metal anion- and cation-targeted selective adsorbents. *J. Hazard. Mater.* **2020**, *382*, 121039.
(145) Chen, F.; Huang, Y.; Guo, L.; Sun, L.; Wang, Y.; Yang, H. Y. Dual-ions electrochemical deionization: a desalination generator. *Energy Environ. Sci.* **2017**, *10* (10), 2081−2089.
(146) Cohen, I.; Avraham, E.; Bouhadana, Y.; Soffer, A.; Aurbach, D. Long term stability of capacitive de-ionization processes for water desalination: The challenge of positive electrodes corrosion. *Electrochim. Acta* **2013**, *106*, 91−100.
(147) Yu, J.; Jo, K.; Kim, T.; Lee, J.; Yoon, J. Temporal and spatial distribution of pH in flow-mode capacitive deionization and membrane capacitive deionization. *Desalination* **2018**, *439*, 188−195.
(148) Jia, B.; Zhang, W. Preparation and Application of Electrodes in Capacitive Deionization (CDI): a State-of-Art Review. *Nanoscale Res. Lett.* **2016**, *11* (1), 64.
(149) Yoon, H.; Lee, J.; Kim, S.; Yoon, J. Review of concepts and applications of electrochemical ion separation (EIONS) process. *Sep. Purif. Technol.* **2019**, *215*, 190−207.
(150) Shen, X.; Hai, R.; Wang, X.; Li, Y.; Wang, Y.; Yu, F.; Ma, J. Free-standing 3D alkalized $Ti_3C_2T_x$/$Ti_3C_2T_x$ nanosheet membrane electrode for highly efficient and stable desalination in hybrid capacitive deionization. *J. Mater. Chem. A* **2020**, *8* (37), 19309−19318.
(151) Ai, J.; Li, J.; Li, K.; Yu, F.; Ma, J. Highly flexible, self-healable and conductive poly(vinyl alcohol)/$Ti_3C_2T_x$ MXene film and it's application in capacitive deionization. *Chem. Eng. J.* **2021**, *408*, 127256.
(152) Liu, G.; Zou, J.; Tang, Q.; Yang, X.; Zhang, Y.; Zhang, Q.; Huang, W.; Chen, P.; Shao, J.; Dong, X. Surface Modified Ti_3C_2 MXene Nanosheets for Tumor Targeting Photothermal/Photodynamic/Chemo Synergistic Therapy. *ACS Appl. Mater. Interfaces* **2017**, *9* (46), 40077−40086.
(153) Meng, Z.; Li, Z.; Li, Y.; Zhang, C.; Wang, K.; Yu, W.; Wu, D.; Zhu, H.; Li, W. Novel nanofluid based efficient solar vaporization systems with applications in desalination and wastewater treatment. *Energy* **2022**, *247*, 123513.
(154) Bonab, H. B.; Javani, N. Investigation and optimization of solar volumetric absorption systems using nanoparticles. *Sol. Energy Mater. Sol. Cells* **2019**, *194*, 229−234.
(155) Ghafurian, M. M.; Dastjerd, F.; Afsharian, A.; Esfahani, F. R.; Niazmand, H.; Behzadnia, H.; Wongwises, S.; Mahian, O. Low-cost zinc-oxide nanoparticles for solar-powered steam production: Superficial and volumetric approaches. *J. Clean. Prod.* **2021**, *280*, 124261.
(156) Yan, J.; Su, Q.; Xiao, W.; Wu, Z.; Chen, L.; Tang, L.; Zheng, N.; Gao, J.; Xue, H. A review of nanofiber membranes for solar interface evaporation. *Desalination* **2022**, *531*, 115686.
(157) Zhao, L.; Wang, P.; Tian, J.; Wang, J.; Li, L.; Xu, L.; Wang, Y.; Fei, X.; Li, Y. A novel composite hydrogel for solar evaporation enhancement at air-water interface. *Sci. Total Environ.* **2019**, *668*, 153−160.
(158) Zhao, J.; Yang, Y.; Yang, C.; Tian, Y.; Han, Y.; Liu, J.; Yin, X.; Que, W. A hydrophobic surface enabled salt-blocking 2D Ti_3C_2 MXene membrane for efficient and stable solar desalination. *J. Mater. Chem. A* **2018**, *6* (33), 16196−16204.
(159) Fan, X.; Yang, Y.; Shi, X.; Liu, Y.; Li, H.; Liang, J.; Chen, Y. A MXene-Based Hierarchical Design Enabling Highly Efficient and Stable Solar-Water Desalination with Good Salt Resistance. *Adv. Funct. Mater.* **2020**, *30* (52), 2007110.
(160) Li, Z.; Zhang, H.; Han, J.; Chen, Y.; Lin, H.; Yang, T. Surface Nanopore Engineering of 2D MXenes for Targeted and Synergistic Multitherapies of Hepatocellular Carcinoma. *Adv. Mater.* **2018**, *30* (25), 1706981.
(161) Chen, L.; Shi, X.; Yu, N.; Zhang, X.; Du, X.; Lin, J. Measurement and Analysis of Thermal Conductivity of $Ti_3C_2T_x$ MXene Films. *Materials* **2018**, *11* (9), 1701.
(162) Li, K.; Chang, T.-H.; Li, Z.; Yang, H.; Fu, F.; Li, T.; Ho, J. S.; Chen, P.-Y. Biomimetic MXene Textures with Enhanced Light-to-Heat Conversion for Solar Steam Generation and Wearable Thermal Management. *Adv. Energy Mater.* **2019**, *9* (34), 1901687.
(163) Zhou, X.; Zhao, F.; Guo, Y.; Zhang, Y.; Yu, G. A hydrogel-based antifouling solar evaporator for highly efficient water desalination. *Energy Environ. Sci.* **2018**, *11* (8), 1985−1992.
(164) Yu, Z.; Wu, P. Biomimetic MXene-Polyvinyl Alcohol Composite Hydrogel with Vertically Aligned Channels for Highly Efficient Solar Steam Generation. *Adv. Mater. Technol.* **2020**, *5* (6), 2000065.
(165) Li, W.; Li, X.; Chang, W.; Wu, J.; Liu, P.; Wang, J.; Yao, X.; Yu, Z.-Z. Vertically aligned reduced graphene oxide/$Ti_3C_2T_x$ MXene hybrid hydrogel for highly efficient solar steam generation. *Nano Res.* **2020**, *13* (11), 3048−3056.
(166) Jun, B. M.; Park, C. M.; Heo, J.; Yoon, Y. Adsorption of Ba^{2+} and Sr^{2+} on $Ti_3C_2T_x$ MXene in model fracking wastewater. *J. Environ. Manage.* **2020**, *256*, 109940.
(167) Jeon, M.; Jun, B. M.; Kim, S.; Jang, M.; Park, C. M.; Snyder, S. A.; Yoon, Y. A review on MXene-based nanomaterials as adsorbents in aqueous solution. *Chemosphere* **2020**, *261*, 127781.
(168) Peng, Q.; Guo, J.; Zhang, Q.; Xiang, J.; Liu, B.; Zhou, A.; Liu, R.; Tian, Y. Unique lead adsorption behavior of activated hydroxyl group in two-dimensional titanium carbide. *J. Am. Chem. Soc.* **2014**, *136* (11), 4113−4116.
(169) Zhang, G.; Wang, T.; Xu, Z.; Liu, M.; Shen, C.; Meng, Q. Synthesis of amino-functionalized $Ti_3C_2T_x$ MXene by alkalization-grafting modification for efficient lead adsorption. *Chem. Commun.* **2020**, *56* (76), 11283−11286.
(170) Shahzad, A.; Nawaz, M.; Moztahida, M.; Tahir, K.; Kim, J.; Lim, Y.; Kim, B.; Jang, J.; Lee, D. S. Exfoliation of Titanium Aluminum Carbide (211 MAX Phase) to Form Nanofibers and Two-Dimensional Nanosheets and Their Application in Aqueous-Phase Cadmium Sequestration. *ACS Appl. Mater. Interfaces* **2019**, *11* (21), 19156−19166.
(171) Bilal, M.; Ihsanullah, I. What makes MXenes emergent materials for the adsorption of heavy metals from water? A critical review. *J. Water Process. Eng.* **2022**, *49*, 103010.
(172) Peng, C.; Li, X.; Jiang, P.; Peng, W.; Tang, J.; Li, L.; Ye, L.; Pan, S.; Chen, S. Thermoresponsive MXene composite system with high adsorption capacity for quick and simple removal of toxic metal ions from aqueous environment. *J. Hazard. Mater.* **2022**, *440*, 129740.
(173) Far, H. S.; Najafi, M.; Hasanzadeh, M.; Rabbani, M. Self-Supported 3D-Printed Lattices Containing MXene/Metal-Organic Framework (MXOF) Composite as an Efficient Adsorbent for Wastewater Treatment. *ACS Appl. Mater. Interfaces* **2022**, *14* (39), 44488−44497.
(174) Zheng, J.; Tian, J.; Wu, D.; Gu, M.; Xu, W.; Wang, C.; Gao, F.; Engelhard, M. H.; Zhang, J. G.; Liu, J.; Xiao, J. Lewis acid-base interactions between polysulfides and metal organic framework in lithium sulfur batteries. *Nano Lett.* **2014**, *14* (5), 2345−2352.
(175) Cai, C.; Wei, Z.; Huang, Y.; Fu, Y. Wood-inspired superelastic MXene aerogels with superior photothermal conversion and durable superhydrophobicity for clean-up of super-viscous crude oil. *Chem. Eng. J.* **2021**, *421*, 127772.
(176) Shahzad, A.; Nawaz, M.; Moztahida, M.; Jang, J.; Tahir, K.; Kim, J.; Lim, Y.; Vassiliadis, V. S.; Woo, S. H.; Lee, D. S. $Ti_3C_2T_x$ MXene core-shell spheres for ultrahigh removal of mercuric ions. *Chem. Eng. J.* **2019**, *368*, 400−408.

https://doi.org/10.1021/acs.iecr.3c00306
Ind. Eng. Chem. Res. 2023, 62, 7297−7335

(177) He, Z.; Huang, D.; Yue, G.; Zhu, J.; Zhao, P. Ca^{2+} induced 3D porous MXene gel for continuous removal of phosphate and uranium. *Appl. Surf. Sci.* **2021**, *570*, 150804.
(178) Murali, G.; Modigunta, J. K. R.; Park, S.; Lee, S.; Lee, H.; Yeon, J.; Kim, H.; Park, Y. H.; Park, S. Y.; Durrant, J. R.; Cha, H.; An, T. K.; In, I. Enhancing Light Absorption and Prolonging Charge Separation in Carbon Quantum Dots via Cl-Doping for Visible-Light-Driven Photocharge-Transfer Reactions. *ACS Appl. Mater. Interfaces* **2021**, *13* (29), 34648−34657.
(179) Cheriyamundath, S.; Vavilala, S. L. Nanotechnology-based wastewater treatment. *Water Environ. J.* **2021**, *35* (1), 123−132.
(180) Wang, H.; Wu, Y.; Xiao, T.; Yuan, X.; Zeng, G.; Tu, W.; Wu, S.; Lee, H. Y.; Tan, Y. Z.; Chew, J. W. Formation of quasi-core-shell In_2S_3/anatase TiO_2@metallic $Ti_3C_2T_x$ hybrids with favorable charge transfer channels for excellent visible-light-photocatalytic performance. *Appl. Catal., B* **2018**, *233*, 213−225.
(181) Fayyaz, A.; Saravanakumar, K.; Talukdar, K.; Kim, Y.; Yoon, Y.; Park, C. M. Catalytic oxidation of naproxen in cobalt spinel ferrite decorated $Ti_3C_2T_x$ MXene activated persulfate system: Mechanisms and pathways. *Chem. Eng. J.* **2021**, *407*, 127842.
(182) Liu, M.; Li, J.; Bian, R.; Wang, X.; Ji, Y.; Zhang, X.; Tian, J.; Shi, F.; Cui, H. ZnO@Ti_3C_2 MXene interfacial Schottky junction for boosting spatial charge separation in photocatalytic degradation. *J. Alloys Compd.* **2022**, *905*, 164025.
(183) Feng, X.; Yu, Z.; Sun, Y.; Shan, M.; Long, R.; Li, X. 3D MXene/Ag_2S material as Schottky junction catalyst with stable and enhanced photocatalytic activity and photocorrosion resistance. *Sep. Purif. Technol.* **2021**, *266*, 118606.
(184) Wu, Z.; Liang, Y.; Yuan, X.; Zou, D.; Fang, J.; Jiang, L.; Zhang, J.; Yang, H.; Xiao, Z. MXene Ti_3C_2 derived Z−scheme photocatalyst of graphene layers anchored TiO_2/g−C_3N_4 for visible light photocatalytic degradation of refractory organic pollutants. *Chem. Eng. J.* **2020**, *394*, 124921.
(185) Shahzad, A.; Rasool, K.; Nawaz, M.; Miran, W.; Jang, J.; Moztahida, M.; Mahmoud, K. A.; Lee, D. S. Heterostructural TiO_2/$Ti_3C_2T_x$ (MXene) for photocatalytic degradation of antiepileptic drug carbamazepine. *Chem. Eng. J.* **2018**, *349*, 748−755.
(186) Yang, J.; Wang, D.; Han, H.; Li, C. Roles of Cocatalysts in Photocatalysis and Photoelectrocatalysis. *Acc. Chem. Res.* **2013**, *46* (8), 1900−1909.
(187) Zhao, G.; Xu, X. Cocatalysts from types, preparation to applications in the field of photocatalysis. *Nanoscale* **2021**, *13* (24), 10649−10667.
(188) Ran, J.; Jaroniec, M.; Qiao, S. Z. Cocatalysts in Semiconductor-based Photocatalytic CO_2 Reduction: Achievements, Challenges, and Opportunities. *Adv. Mater.* **2018**, *30* (7), 1704649.
(189) Liang, Z.; Shen, R.; Ng, Y. H.; Zhang, P.; Xiang, Q.; Li, X. A review on 2D MoS_2 cocatalysts in photocatalytic H_2 production. *J. Mater. Sci. Technol.* **2020**, *56*, 89−121.
(190) Liu, B.; Yu, L.; Yu, F.; Ma, J. In-situ formation of uniform V_2O_5 nanocuboid from V_2C MXene as electrodes for capacitive deionization with higher structural stability and ion diffusion ability. *Desalination* **2021**, *500*, 114897.
(191) Wu, C.; Zhang, J.; Tong, X.; Yu, P.; Xu, J. Y.; Wu, J.; Wang, Z. M.; Lou, J.; Chueh, Y. L. A Critical Review on Enhancement of Photocatalytic Hydrogen Production by Molybdenum Disulfide: From Growth to Interfacial Activities. *Small* **2019**, *15* (35), 1900578.
(192) Cheng, L.; Li, X.; Zhang, H.; Xiang, Q. Two-Dimensional Transition Metal MXene-Based Photocatalysts for Solar Fuel Generation. *J. Phys. Chem. Lett.* **2019**, *10* (12), 3488−3494.
(193) Jiao, S.; Liu, L. Friction-Induced Enhancements for Photocatalytic Degradation of MoS_2@Ti_3C_2 Nanohybrid. *Ind. Eng. Chem. Res.* **2019**, *58* (39), 18141−18148.
(194) Sherryna, A.; Tahir, M. Role of Ti_3C_2 MXene as Prominent Schottky Barriers in Driving Hydrogen Production through Photo-induced Water Splitting: A Comprehensive Review. *ACS Appl. Energy Mater.* **2021**, *4* (11), 11982−12006.
(195) Ganguly, P.; Harb, M.; Cao, Z.; Cavallo, L.; Breen, A.; Dervin, S.; Dionysiou, D. D.; Pillai, S. C. 2D Nanomaterials for Photocatalytic Hydrogen Production. *ACS Energy Lett.* **2019**, *4* (7), 1687−1709.
(196) Zhan, X.; Si, C.; Zhou, J.; Sun, Z. MXene and MXene-based composites: synthesis, properties and environment-related applications. *Nanoscale Horiz.* **2020**, *5* (2), 235−258.
(197) Li, K.; Zhang, S.; Li, Y.; Fan, J.; Lv, K. MXenes as noble-metal-alternative co-catalysts in photocatalysis. *Chin. J. Catal.* **2021**, *42* (1), 3−14.
(198) Linsebigler, A. L.; Lu, G.; Yates, J. T., Jr. Photocatalysis on TiO_2 Surfaces: Principles, Mechanisms, and Selected Results. *Chem. Rev.* **1995**, *95* (3), 735−758.
(199) Peng, C.; Yang, X.; Li, Y.; Yu, H.; Wang, H.; Peng, F. Hybrids of Two-Dimensional Ti_3C_2 and TiO_2 Exposing 001 Facets toward Enhanced Photocatalytic Activity. *ACS Appl. Mater. Interfaces* **2016**, *8* (9), 6051−6060.
(200) Quyen, V. T.; Ha, L. T. T.; Thanh, D. M.; Le, Q. V.; Viet, N. M.; Nham, N. T.; Thang, P. Q. Advanced synthesis of MXene-derived nanoflower-shaped TiO_2@Ti_3C_2 heterojunction to enhance photocatalytic degradation of Rhodamine B. *Environ. Technol. Innov.* **2021**, *21*, 101286.
(201) Ihsanullah, I. MXenes as next-generation materials for the photocatalytic degradation of pharmaceuticals in water. *J. Environ. Chem. Eng.* **2022**, *10* (3), 107381.
(202) Zeng, G.; Wei, K.; Zhang, H.; Zhang, J.; Lin, Q.; Cheng, X.; Sengupta, A.; Chiao, Y.-H. Ultra-high oil-water separation membrane based on two-dimensional MXene ($Ti_3C_2T_x$) by co-incorporation of halloysite nanotubes and polydopamine. *Appl. Clay Sci.* **2021**, *211*, 106177.
(203) Ma, X.; Wang, A.; Miao, J.; Fan, T. 2D lamellar membrane with MXene hetero-intercalated small sized graphene oxide for harsh environmental wastewater treatment. *Sep. Purif. Technol.* **2023**, *311*, 123248.
(204) Ding, L.; Li, L.; Liu, Y.; Wu, Y.; Lu, Z.; Deng, J.; Wei, Y.; Caro, J.; Wang, H. Effective ion sieving with $Ti_3C_2T_x$ MXene membranes for production of drinking water from seawater. *Nat. Sustain.* **2020**, *3* (4), 296−302.
(205) Lu, Z.; Wei, Y.; Deng, J.; Ding, L.; Li, Z. K.; Wang, H. Self-Crosslinked MXene ($Ti_3C_2T_x$) Membranes with Good Antiswelling Property for Monovalent Metal Ion Exclusion. *ACS Nano* **2019**, *13* (9), 10535−10544.
(206) Zhang, B.; Gu, Q.; Wang, C.; Gao, Q.; Guo, J.; Wong, P. W.; Liu, C. T.; An, A. K. Self-Assembled Hydrophobic/Hydrophilic Porphyrin-$Ti_3C_2T_x$ MXene Janus Membrane for Dual-Functional Enabled Photothermal Desalination. *ACS Appl. Mater. Interfaces* **2021**, *13* (3), 3762−3770.

https://doi.org/10.1021/acs.iecr.3c00306
Ind. Eng. Chem. Res. 2023, 62, 7297−7335